UNIVERSITÉ DE LIÈGE
Faculté des sciences
Département de géographie

Study of the recent disappearance of a tropical glacier in the Bolivian Andes with the help of the high resolution regional climate model MAR

Mémoire présenté par
Chloé SCHOLZEN
en vue de l'obtention du titre de
Master en sciences géographiques
orientation climatologie

Année académique
2014-2015

Membres du jury
Xavier FETTWEIS (Promoteur)
Michel ERPICUM
Louis FRANÇOIS
Geoffrey HOUBRECHTS

En premier lieu je tiens à remercier le promoteur de ce mémoire, Xavier Fettweis, pour sa grande disponibilité et pour ses judicieux conseils. Sa patience, sa confiance et son enthousiasme ont été pour moi une source d'encouragement inestimable.

Merci également à Michel Erpicum, pour nous avoir suivis et guidés tout au long de notre formation, et pour nous avoir fait découvrir les multiples facettes du monde de la climatologie. Chacun de ses enseignements aura contribué à alimenter ma réflexion durant mes recherches.

J'adresse ensuite une reconnaissance toute particulière à mes grands-parents, Thierry et Almuth, pour m'avoir fourni, au moment le plus crucial, l'infrastructure et le calme nécessaires à la réalisation de ce travail. Ils m'ont été d'une aide très précieuse. Merci aussi à Maman pour ses relectures, et surtout pour m'avoir permis d'aller jusqu'au bout de ce parcours universitaire.

Je n'oublie évidemment pas mes amis et collègues climatologues, en particulier Mélody, Coraline et Charlotte. Nos nombreux échanges m'ont souvent apporté l'inspiration et les solutions dans les moments critiques. Enfin, merci à la plus fidèle et inlassable, Aline.

Abstract

This study provides a first evaluation of the MAR (Modèle Atmosphérique Régional) model over the Bolivian tropical Andes. MAR is currently developed at the ULg and allows dynamical downscaling up to 5 km of horizontal resolution. The purpose of this work is to model the recent changes in the climatic parameters which are thought to control the mass and energy balance of mountain glaciers in the outer tropics. We focus on the recently vanished Chacaltaya Glacier (16°S), which by virtue of its location and its environmental context is representative of many small-sized glaciers of the Bolivian Andes.

To evaluate our model, we first examine simulated precipitation and near-surface temperature against in situ observations from ground weather stations. Since observational data is very scarce in this part of the world, we also refer to qualitative information provided by the scientific literature. We compare the performance of the model forced with two different reanalyses, and with several corrections applied to the lateral boundary conditions (LBCs) impacting on temperature and humidity. MAR forced with the ERA-Interim reanalysis yields better results than with the NCEP/NCAR-v2 reanalysis. We then use the best ERA-driven simulation to assess the long-term climate change over 1960-2014 in the region of the Chacaltaya Mountain.

The regional atmospheric circulation is adequately simulated by MAR, which reproduces the prevailing seasonal features of the lower, middle and upper troposphere. The climatic anomalies associated to the El Niño Southern Oscillation (ENSO) events are also properly recreated. Remaining model biases include an overall year-round dry bias over the Altiplano region, due to the strong corrections applied to the LBCs (-15% for humidity). Over the highest elevations of the Andes, both precipitation and cloud cover are probably overestimated by MAR. The sporadic spatial distribution of convective rainfall also suggests numerical instability in the convective parameterization scheme. Modeled temperatures match very well the observations, but the reliability of the observed time series is highly questionable.

Between 1960 and 2014, the most significant trends concern precipitation and cloud cover which both decreased of about 35%. The surface radiation budget also changed as a result of the reduced cloudiness. Near-surface temperature increased by about 1.5°C. Those trends are believed to have been enhanced by the more frequent and more intense El Niño events during the warm Pacific Decadal Oscillation (PDO) phase between 1977 and 1999. The combination of the repeated droughts and the enhanced incoming short-wave radiation due to reduced low-level cloudiness are probably the main factors responsible for the acceleration of the Chacaltaya Glacier recession. Nevertheless, the ENSO signal is not always clear in the Bolivian Andes, because of the interference with strong local climatic processes. Moreover, additional forcings of non climatic nature may also be responsible for the rapid demise of the Chacaltaya Glacier.

Contents

List of Figures

List of Tables

List of abbreviations and acronyms

a.s.l.	above sea-level
BH	Bolivian High
CC	Correlation Coefficient
CIIFEN	Centro Internacional para la Investigación del Fenómeno de El Niño
DJF	December-January-February: summer season in the Southern Hemisphere
ECMWF	European Centre for Medium-Range Weather Forecast
ENSO	El Niño Southern Oscillation
ERA-40	Reanalysis of the ECMWF (1958-1978)
ERA-Interim	Reanalysis of the ECMWF (1979-present)
FLH	Freezing Level Height
GCM	Global Climate Model
GHG	Greenhouse Gas
ITCZ	Inter-Tropical Convergence Zone
JJA	June-July-August: winter season in the Southern Hemisphere
LLJ	Low-Level Jet
LBC	Lateral Boundary Condition
LHF	Latent Heat Flux
LIA	Little Ice Age
LSC	Lateral Surface Condition
LWD	Long-Wave Downward flux
LWU	Long-Wave Upward flux
MAR	Modèle Atmosphérique Régional
MGE	Maximum Glacial Extent
n. s.	Near-surface
NCEP	National Center for Environmental Prediction (US)
NCAR	National Center for Atmospheric Research (US)
OLR	Outgoing Long-wave Radiation
PDO	Pacific Decadal Oscillation
RCM	Regional Climate Model
RMSE	Root Mean Square Error
SACZ	South Atlantic Convergence Zone
SASH	South Atlantic Subtropical High
SEB	Surface Energy Balance
(S)MB	(Surface) Mass Balance
SISVAT	Soil Ice Snow Vegetation Atmosphere Transfer

SEPH	South-East Pacific High
SHF	Sensible Heat Flux
SST	Sea Surface Temperature
STD	Standard Deviation
SWD	Short-Wave Downward flux
SWU	Short-Wave Upward flux
WMO	World Meteorological Organization

1. Introduction

There is growing evidence indicating that dramatic changes in climate and hydrological cycle are occurring in the tropical latitudes (Casassa *et al.*, 2007; Vuille *et al.*, 2008; Soruco *et al.*, 2009a; Rabatel *et al.*, 2013). Since the late 1970s, unprecedented shrinkage of glaciers and ice caps has been observed in South America, threatening the nearby communities who rely on them as freshwater resources and for hydropower production (Coudrain *et al.*, 2005; Chevallier *et al.*, 2011; Rangecroft *et al.*, 2013; Soruco *et al.*, 2015).

A most outstanding example is provided by the iconic Chacaltaya Glacier, located at 16°S latitude in the Bolivian Andes. Perched at about 5,400 meters above sea level (a.s.l.), this 18,000 year-old glacier was originally famous for hosting the highest and the most equatorial ski resort in the world. Nowadays the Chacaltaya Mountain sadly owes its renown to the extremely rapid recession of its glacier, which led to the complete disappearance of the latter in 2009 (WGMS, 2011).

Although global circulation model based experiments suggest that high elevations in the Tropics are particularly sensitive to greenhouse gas induced warming of the troposphere, the changes altering the surface are far from uniform, and the causes of these heterogeneities remain still unclear (Chen *et al.*, 2002; Vuille *et al.*, 2003; Garreaud *et al.*, 2003, 2007). The main source of uncertainty is the inability of global climate models (GCMs) to properly simulate the climate in the Andes mountains. GCMs operate on too coarse resolutions (typically 100-500 km) to resolve the complex topography and the related steep climatic gradients which characterize the Andean region. Therefore, regional climate models (RCMs) with significantly finer spatial grids have been increasingly implemented and evaluated over South America since the late 2000s (e.g. Nicolini *et al.*, 2002; Fernandez *et al.*, 2006; Pesquero *et al.*, 2010). Nevertheless, while RCMs have provided effective added value to climate modeling at higher spatial resolution, several challenging issues remain, most notably concerning the representation of atmosphere and land-surface interactions (Solman, 2013).

In parallel, two decades of monitoring, measurements and documentation on glaciers in Bolivia, including the Chacaltaya (Ramirez *et al.*, 2001; Francou *et al.*, 2003), have provided considerable knowledge about the mass and energy balance of tropical glaciers and their response in relation to climate change (Ribstein *et al.*, 1995, 1999; Wagnon *et al.*, 1999a,b; Soruco *et al.*, 2009b). On the one hand, several authors have emphasized the crucial role played by the large-scale atmospheric and oceanic circulation systems in the interannual variability of glacier mass balance (Vuille, 1999; Wagnon *et al.*, 2001; Francou *et al.*, 2005; Rabatel *et al.*, 2006). The data collected on these glaciers revealed a close link between the more frequent and intense ENSO (El Niño Southern Oscillation) related events since the late 1970s and the recent decline of glaciers in the Bolivian Andes (Francou *et al.*, 2000). On the other hand, a major outcome of these studies is that monthly and daily mass balance fluctuations in glaciers of the outer tropics (Bolivia and Peru) seem to be driven predominantly by changes in air humidity, cloudiness and precipitation, and less by changes in near-surface temperature, in contrast to their temperate and polar counterparts (Kaser, 1999, 2001; Favier *et al.*, 2004). Until recently, these atmospheric parameters had not been linked to glacier evolution, primarily because the Bolivian Andean region is sorely lacking of detailed climatic documentation due to inadequate spatial and temporal data coverage.

These recent advances in tropical glacier and atmosphere observation have brought new prospective targets for regional climate modeling, as well as further motivation to enhance model parameterization related to small-scale processes like sublimation, radiative transfer, convective clouds and cloud microphysics (e.g. Lange *et al.*, 2014). Using such model simulations can not replace observational data, but if model results and observations match, they may provide additional information which could help to attribute local changes in a particular glaciated zone to their causal mechanisms, as well as to perform future projections in the framework of global climate change.

2. Background

2.1. Geographic and climatic context of the Bolivian Andes

2.1.1. General overview

Bolivia is a landlocked country located in the west-central part of South America, and sharing borders with Peru, Brazil, Paraguay, Argentina and Chile. The Andes mountains, which stretch in a broad arc across western Bolivia, divide the country into three main geographic zones: *(i)* the mountains and drier highlands in the west, *(ii)* the semi-tropical Yungas ("warm valleys" in Quechua) which consist of moist broadleaf forests descending the eastern slopes of the Andes, and *(iii)* the green tropical lowlands and grasslands covering the entire eastern half of the country, belonging to the Amazon River Basin. Owing to its unique topographic context, Bolivia is a country of many extremes and notable records. The study area relevant within this work is indicated in Figures 2.2, 2.3 and 2.4.

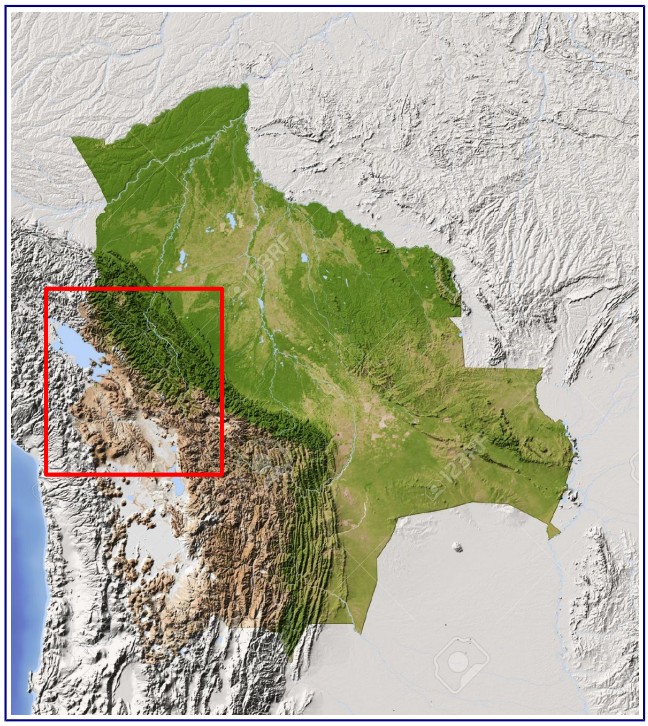

Figure 2.1 (left): Location of Bolivia with respect to the Equator and the world's oceans. Source: *http://www.worldatlas.com/webimage/countrys/samerica/bolivia/boland.htm*

Figure 2.2 (right): Shaded relief of Bolivia, colored according to vegetation. The red rectangle indicates the location of our study area. Source: *NASA Earth Observatory*

The orographic system in Bolivia is dominated by two parallel ranges: the Occidental Cordillera to the west along the borders with Chile, and the Oriental Cordillera to the east next to the Amazon Basin (Figure 2.3). While the western range hosts the country's highest peak Nevado Sajama (6,542 meters a.s.l.), most of Bolivia's glaciers are located in the eastern range. The northern section of the Oriental Cordillera, called the Cordillera Real ("Royal Range" in Spanish), forms a massive line of snow-capped peaks. The presence of many summits reaching above 6,000 meters a.s.l. maintains an average elevation of about 5,500 meters a.s.l. in the Cordillera Real. Among those peaks stands the moderately high Chacaltaya Mountain at some 5,395 meters a.s.l.

Enclosed between the Occidental and the Oriental Cordilleras lies the Altiplano ("High Plateau" in Spanish), an inter-mountain plateau extending through entire Bolivia from north to south (15–24°S), at a height averaging about 3,500 meters a.s.l. (Figure 2.3). The Bolivian Altiplano is mostly famous for hosting the highest navigable body of water in the world, Lake Titicaca (3,810 meters a.s.l.), which also happens to be South America's largest freshwater lake by surface area (8,372 km²).

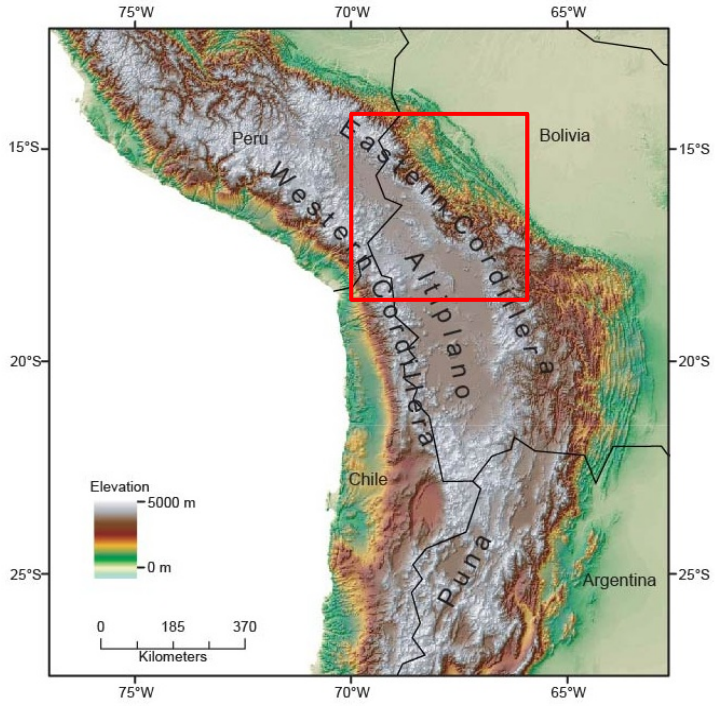

Figure 2.3: The Bolivian Altiplano, surrounded by the Occidental Cordillera to the west and the Oriental Cordillera to the east. The red rectangle indicates the location of our study area.
Source: *http://www.optics.rochester.edu/workgroups/cml/opt307/spr12/nandini/index.html*

Figure 2.4: Topographic profile of Bolivia. The red circle indicates the location of our study area. Source: *http://www.explorebolivia.com/our-country/map-of-bolivia/*

Although less than one third of its territory is covered by the Andes, Bolivia is traditionally regarded as a highland country because almost half its population lives in the Altiplano, where most of the nation's large cities are located. Bolivia also has the highest administrative capital city in the world, La Paz (roughly 3,650 meters a.s.l.), which sits in a valley at the western foot of the Cordillera Real, at about 20 km southwest of the Chacaltaya Mountain.

Mainly due to its latitudinal position and to its complex topography, Bolivia experiences very contrasted climates, both in terms of spatial and temporal variability. A common climatic pattern to all regions in Bolivia is the high seasonality of precipitation. This feature is inherent to the outer tropics, which can be regarded as an intermediate climatic zone between the inner tropics and the subtropics, where alternatively tropical and subtropical conditions prevail (Kaser, 2001). Accordingly, precipitation in Bolivia alternates between a wet period during the austral summer (November–March), and a dry period during the austral winter (May–October).

Another peculiarity of the Bolivian climate is the very low thermal seasonality (< 5°C), with temperatures of the wet season being slightly higher than those of the dry season (Rabatel *et al.*, 2008). Although incident solar radiation is strong all year-round due to the low latitude, its maximum summertime peak occurs during the wet season and is then attenuated by the cloud cover. By contrast, temperatures can differ drastically between day and night, especially during the dry season (Hardy *et al.*, 1998). In the Andean mountainous regions, thermal gradients depend predominately on altitude. Nevertheless, temperature lapse rates undergo seasonal changes in parallel with variations in humidity rates. In some parts of the tropical Andes, the lapse rate ranges from -0.55°C per 100 meters during the wet season, to -0.80°C per 100 meters during the dry season (Lejeune *et al.*, 2003).

2.1.2. Large-scale circulation and mean annual cycles

The well-defined annual cycle in precipitation is primarily related to the annual fluctuations of six large-scale circulation systems.

The Southeast Pacific High (SEPH) Throughout the year, a quasi-stationnary high pressure system prevails over the Southeast Pacific Ocean at subtropical latitudes. Induced by this anticyclonic circulation, a southerly wind blows over the coastal sea surface and generates an oceanic current promoting upwelling of deep cold waters, known as the Humboldt Current (Garreaud *et al.*, 2009). The SEPH and the resulting cold sea-surface temperatures (SSTs) produce dry and stable conditions over the west coast of South America. Moist, cool air from the ocean remains trapped below the subsiding warm air masses at about 900 hPa, preventing moisture to rise along the western slopes of the Andes (Vuille, 1999). This circulation feature is responsible for the extreme aridity which characterizes the Occidental Cordillera and the westernmost parts of the Bolivian Altiplano (Figure 2.5).

The South Atlantic Subtropical High (SASH) and the Inter-tropical Convergence Zone (ITCZ) Another large-scale anticyclonic gyre generates a westward circulation from the tropical Atlantic Ocean to the Amazon Basin. During the austral summer (DJF), this moisture advection is enhanced by the southward shifting of the ITCZ and its associated trade winds that cross the Equator along the northeastern coast of Brazil. As these warm, moist air masses move further inland, they recycle their humidity from water vapor released through evapotranspiration over the Amazonian forest (Roche *et al.*, 1990).

The SASH is less stable than the SEPH, and therefore undergoes more pronounced seasonal shiftings. Its influence over Bolivia's regional climate is stronger during the austral summer, when the anticyclone is larger and moves to the west.

The Low-Level Jet (LLJ) In the west-central part of Bolivia, the low-tropospheric easterly winds that transport moisture of atlantic and amazonian origin are deflected by the Andes mountains, which channel them into a southward Low-Level Jet (Vera *et al.*, 2006; Insel *et al.*; 2010; Seiler, 2013). The LLJ is responsible for heavy, orographically induced precipitation along the windward eastern slopes of the Andes (location of the Yungas), while the downwind interandean valleys and the western slopes benefit from the residues of the eastern moisture.

The Bolivian High (BH) During the austral summer (DJF), an upper-tropospheric anticyclone develops over the Bolivian Altiplano. This high pressure system is generated through the combination of sensible heat release from intense solar heating of the Altiplano surface, and latent heat release from strong convective activity over the Amazon Basin (Lenters & Cook, 1997; Vuille, 1999; Vuille *et al.*, 2000). The Bolivian High induces deep convection which associates to the moisture advected from the east to trigger typically convective precipitation over the Bolivian western highlands.

Several studies suggested that summertime precipitation over the Altiplano is higher (resp. lower) when the BH is strengthened (resp. weakened) and shifted south (resp. north) of its climatological mean position (Lenters & Cook, 1999; Vuille, 1999).

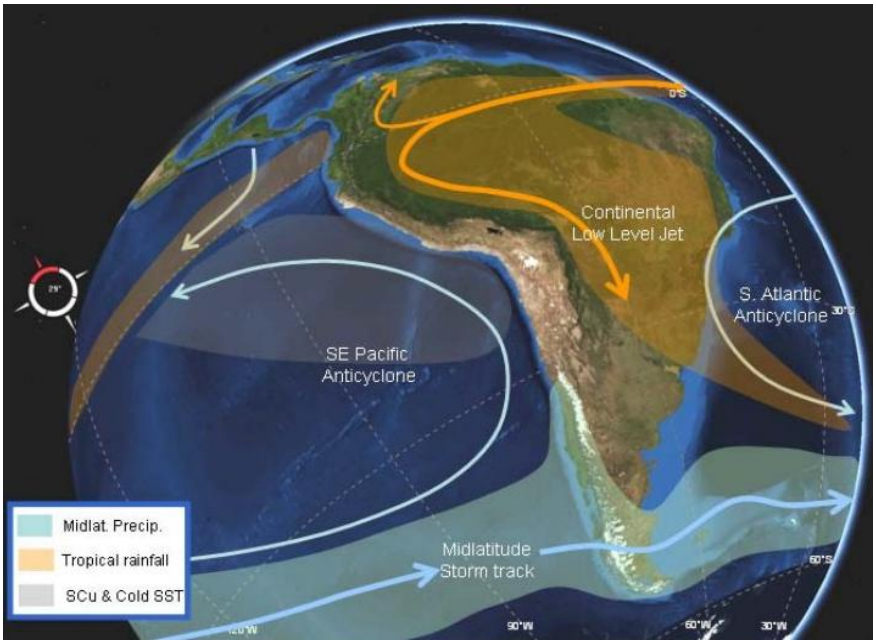

Figure 2.5: Main components of the low-level atmospheric circulation around the Andes Cordillera. Source: Garreaud *et al.* (2009)

The South Atlantic Convergence Zone (SACZ) The position and intensity of the BH are intimately related to fluctuations in the South Atlantic Convergence Zone, a region of high cloudiness and precipitation that stretches diagonally from the northwestern part of the Amazon Basin to the southeast coast of South America (Liebmann *et al.*, 1999; Todd *et al.*, 2003). The SACZ is a quasi-permanent feature of the low-level circulation, which forms as warm, moist air flowing from the SASH converges with the northwesterly LLJ advecting warm, moist, unstable air from the Amazon Basin. The upper-tropospheric response to the westward/eastward displacements of the SACZ are the corresponding southward/northward shiftings of the BH (Lenters & Cook, 1999).

The Subtropical Jet Stream and the polar surges During the austral winter months (JJA), as the tropospheric temperature gradient between the Tropics and the midlatitudes increases, the subtropical jet stream reaches its maximum of intensity and its northernmost position. Consequently, westerly winds prevail in the middle and upper-level circulation over Bolivia, thereby preventing moisture advection from the east (Garreaud *et al.*, 2003).

The westerly jet stream is occasionally interrupted by polar outbreaks originating at high latitudes over the South Pacific Ocean (Vuille, 1999). During those surges, cold air masses move northward, sometimes even as far as near-equatorial latitudes when they are channelled on the eastern side of the Andes. In contrast, on the western side of the Andes these active cold fronts only reach the subtropical latitudes at best, and rarely proceed up to the Bolivian Altiplano (Garreaud, 2000). Unseasonably moist and unusually cold conditions accompany those polar surges, causing heavy mountain snowfalls and very low daytime temperatures.

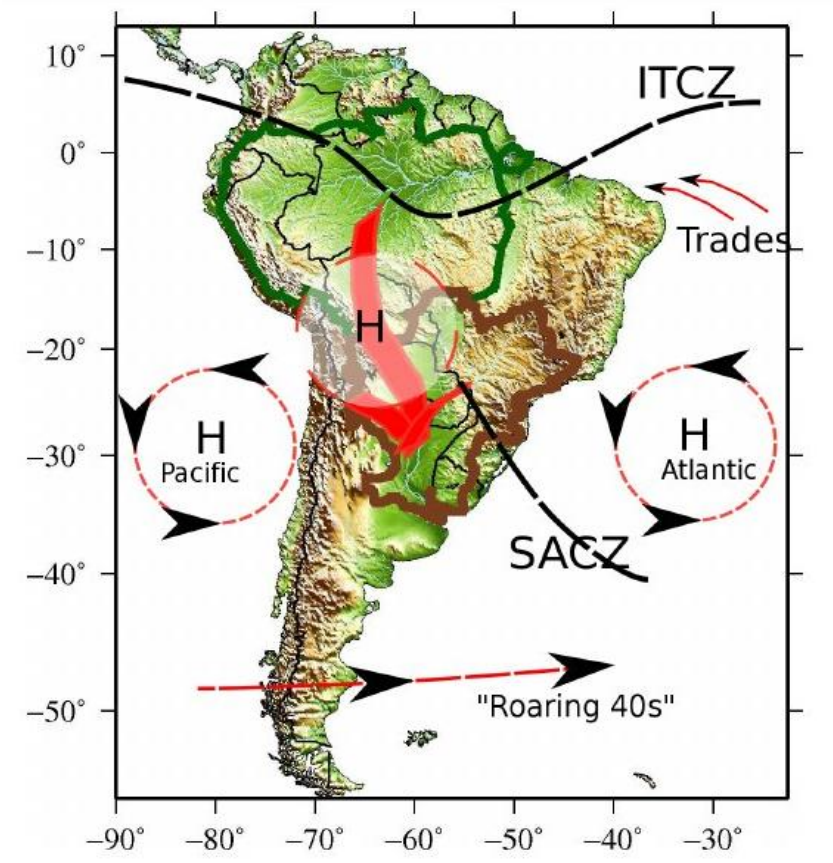

Figure 2.6: Main features of the main upper- and lower-level atmospheric circulation over the South American continent. The Bolivian High (light grey) is depicted aloft the Low-Level Jet (bold red arrow). Source: Remedio (2013)

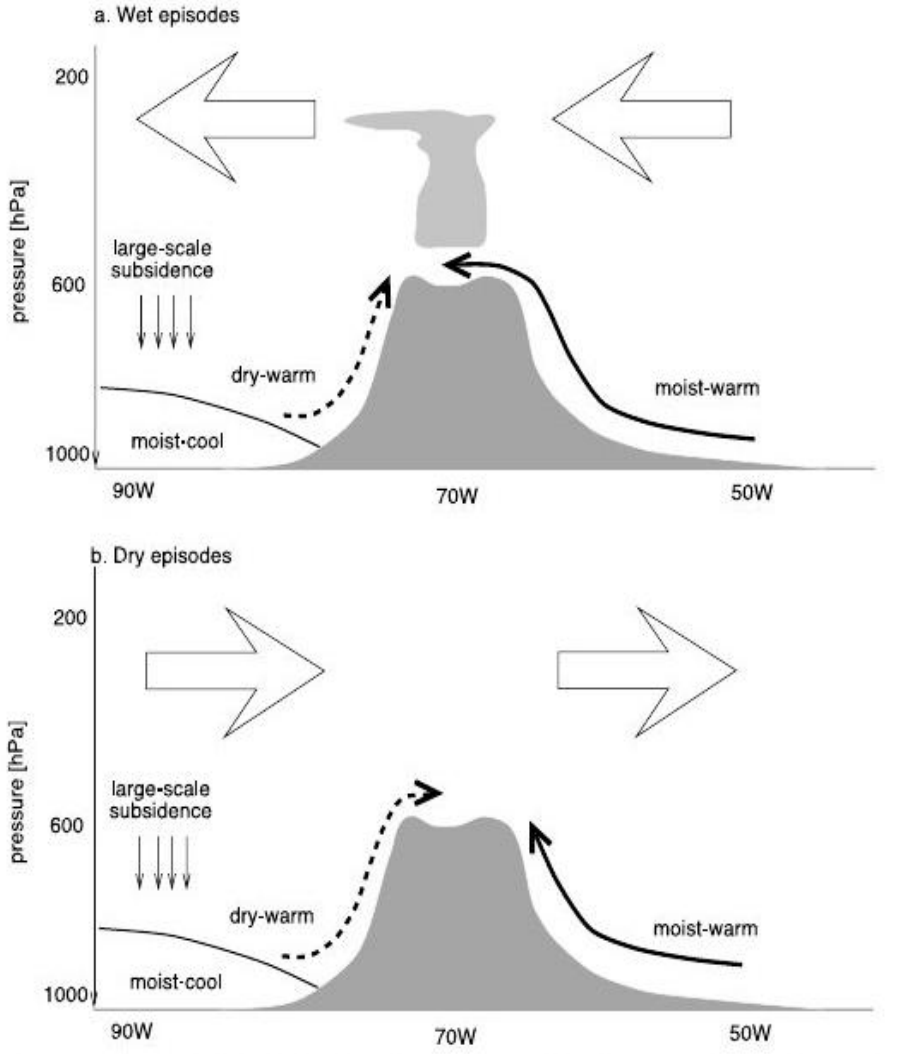

Figure 2.7: Prevailing circulation patterns and different air masses over the Bolivian Andes, in a vertical-longitude section at the latitudes of the Altiplano, for **(a)** wet conditions, and **(b)** dry conditions. Large, open arrows indicate the direction of the upper-level, large-scale flow. Solid (dashed) arrows represent the transport of moist (dry) air by the regional circulation over the Andean slopes. Thin vertical arrows represent the large-scale subsidence associated to the high pressure system over the Southeast Pacific Ocean. Source: Garreaud *et al.* (2003)

Summary

In short, the high spatial variability of precipitation in Bolivia is primarily related to the dynamics of sharply contrasting air masses that prevail over the South American continent. Besides, the large-scale atmospheric circulation is greatly affected by the Andes mountains which act as a physical separation between the cool, dry air from the Pacific Ocean and the warm, moist air advected from the Amazon Basin. As a result, a strong zonal climate gradient characterizes the

tropical and subtropical latitudes (5°S–30°S) in South America, with annual precipitation amounts varying from more than 2,000 mm over the northeastern slopes of the Andes, to less than 200 mm in the southwestern part of the Altiplano (Seiler *et al.*, 2013). At a smaller scale, the spatial heterogeneity of climate is further emphasized by orographic effects which focus precipitation along the eastern flanks of the Andes, with a maximum rainfall amount situated between 1,500–2,000 meters a.s.l. (Wagnon, 1999). In the highest elevations, intense solar radiation induces convective precipitation at a very localized scale, while in the northern Bolivian Andes large valleys open to the northeasterly winds and receive more moisture than the sheltered valleys. Therefore, no general relationship exists between precipitation and altitude in this part of the world (Roche *et al*., 1990).

2.1.3. Local climate in the Cordillera Real and the Bolivian Altiplano

2.1.3.1. Temperature and wind regime

Broadly speaking, the Bolivian Altiplano experiences arid, chilly climatic conditions as this plateau is swept by strong, cold winds throughout the year. By virtue of its altitude, the Altiplano is characterized by a high radiative input and a low air density, which cause daily temperature to vary considerably. Average temperatures during the day range from about 7°C to 12°C, but in the summer sun maxima they may occasionally exceed 25°C (according to daily observational data from LACA&D, 2015). After nightfall, temperatures rapidly drop and in winter they may fall far below freezing level. As a result, the mean daily amplitude in air temperature is generally greater than the annual range in mean monthly temperature (Kaser, 1999). The austral winter months (JJA) are those of greatest diurnal thermal variability, because humidity is at its lowest rate at that time of the year. It is not uncommon for relative humidity to remain below 20% for several consecutive days during the dry season, especially in the highest and southernmost locations of the Altiplano (Hardy *et al.*, 1998).

Meteorologic and climatic conditions in the Cordillera Real, especially for temperature, are poorly documented, like in many other glaciated regions of the Andes mountains. It is assumed though, that owing to its higher elevation, the Cordillera Real has an overall colder climate than the Altiplano. Wind speed is on average lower than in the large, flat-floured Altiplano, since it strongly depends upon the geometry of the site. On the moutain tops and along the steep slopes, two typical wind regimes can be observed: at night radiative cooling favors descending katabatic winds, whereas by day, advected air masses invade the mountains slopes from downward. Night katabatic winds are slightly stronger during the dry season, since nocturnal cloudiness is always zero at that time of the year, and hence radiative cooling is higher (Wagnon *et al.*, 1999b).

2.1.3.2. Precipitation regime

Precipitation systems in both the Cordillera Real and the Bolivian Altiplano are mainly driven by moisture supply from the Amazon Basin, the position of the BH, and the presence of Lake Titicaca. Like most parts of Bolivia, these regions have a well-marked summer precipitation regime, with 70% to 80% of the annual amount falling between December and February (Garreaud *et al.*, 2003; Lejeune *et al.*, 2003). According to their convective nature, summertime precipitation

events typically occur in episodic thunderstorms (showers, hail, snow) rather than in continuous rain or snow (Lenters & Cook, 1999). As in the tropical Andes the 0°C isotherm is located around 5,000 meters a.s.l. and undergoes only little altitude variation throughout the year, precipitation falls exclusively as snow in most parts of the Cordillera Real (Wagnon *et al.*, 1999a). Wet days tend to cluster in short sequences of about a week in duration, and are usually followed by dry episodes of similar length (Garreaud *et al.*, 2003). Moreover, as it is mainly convective, precipitation also exhibits a clear diurnal cycle, being most frequent in the afternoon and in the evening, with a peak between 18.00h and 22.00h (Vuille *et al.*, 2001). Wintertime precipitation is a rather rare phenomena, which represents less than 10% of the annual amount of precipitation (Lejeune *et al.*, 2003). These sporadic events always occur in the form of snow storms originating from polar outbreaks, and are associated with high humidity, high wind speeds and low air temperature (Hardy *et al.*, 1998). Most of the time however, the austral winter months are characterized by cloudless skies and remarkably clear air.

The Bolivian Altiplano is drier than the Cordillera Real, due to the sheltering effect of the latter which intercepts the moist trade winds from the east. In La Paz, located at the eastern edge of the Altiplano just at the rim of the Cordillera, the mean annual amount of precipitation is about 540 mm (Figure 2.8). Nevertheless, the northern part of the Altiplano benefits from substantially higher precipitation rates than the southern part, according to the moderating influence of Lake Titicaca (Garreaud *et al.*, 2009). Owing to its considerable size, Lake Titicaca generates indeed enough amounts of humidity by evaporation to produce precipitation in its immediate vicinity throughout the year, with a maximum during the austral summer (Martinez *et al.*, 2011). Annual amounts of precipitation decrease from 1,200 mm in the center of the lake to about 700 mm within a few tens of kilometers away from its shores (Roche *et al.*, 1990).

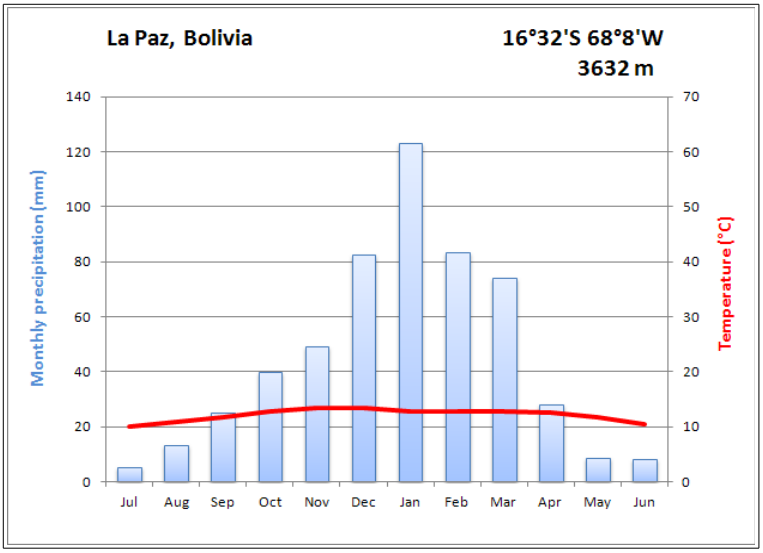

Figure 2.8: Mean annual cycle of temperature and rainfall in La Paz, Bolivia.
Data source: LACA&D

2.2. Andean glaciers of the outer tropics

2.2.1. Definition

Glaciers of the tropical latitudes currently represent less than 5% of the mountain glaciers in the world, and altogether cover an area comparable to the glaciers of the Alps (Francou *et al.*, 2000). Although scattered over three continents (America, Africa and Indonesia), 99% of the world's remaining tropical glaciers are concentrated in the Andes mountains, distributed between Peru (70%), Bolivia (22%), and the rest (8%) in Ecuador, Colombia and Venezuela (Chevallier *et al.*, 2011).

A glaciological definition of the Tropics has been provided by Kaser (1999), who delimited the tropical zone on the basis of three criteria. Tropical glaciers are those that lie within: *(i)* the astronomical tropics (between the Tropics of Cancer and Capricorn), characterized by intense solar radiation throughout the year; *(ii)* the zone with no major thermal seasonality, where daily amplitudes in air temperature exceed annual variations; and *(iii)* the oscillation zone of the Intertropical Convergence Zone (ITCZ), responsible for either humid or dry conditions according to its meridional position. The resulting delimitations for tropical glaciers and their worldwide distribution are shown in Figure 2.9.

Within these boundaries, the outer tropical zone can be distinguished from the inner tropical zone; while the former has a contrasted precipitation regime alternating between a wet and a dry season, the latter experiences more or less continuous precipitation throughout the year. Following this definition, the glaciers of Bolivia's Cordillera Real belong to the outer tropics.

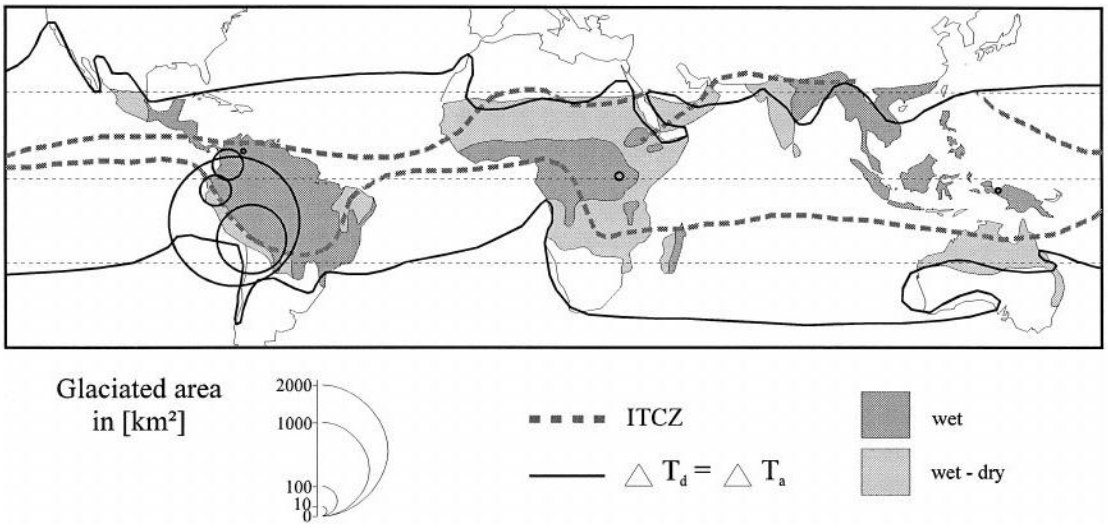

Figure 2.9: Delimitation of the Tropics from a glaciological point of view, and the worldwide distribution of the contemporary tropical glaciers. ΔTd is the daily amplitude in air temperature, and ΔTy is the annual amplitude in air temperature. Light grey zones correspond to the outer tropics; dark grey zones are for the inner tropics. Source: Kaser (1999)

2.2.2. Mass balance

Glaciers gain mass in transforming solid water (snow, hail, frost) into ice, and lose mass in restoring water either to vapor form by evaporation or sublimation, or to liquid form by melting, thus contributing to meltwater runoff through their emissary torrent (Jeschke, 2009).

The net difference between mass gain (accumulation) and mass loss (ablation) of a glacier is referred to as its surface mass balance (MB). The intra-annual mass variations of a glacier depend intrinsically upon the climatic conditions the glacier experiences throughout the year. Hence, glaciers of the outer tropics behave differently compared to glaciers of the inner tropics or glaciers of the mid- and high-latitudes. The difference is most obvious for three main features: *(i)* the duration of the ablation period, *(ii)* the duration of the accumulation period, and *(iii)* the ratio of melting to sublimation (Kaser, 2001).

(i) Tropical glaciers (both of the inner and the outer tropics) undergo ablation all year round in their lowest part, as opposed to extratropical glaciers (in temperate and polar latitudes) which experience one long accumulation period during winter and one short ablation period during summer (Coudrain *et al.*, 2005).

(ii) In the inner tropics, constant humidity conditions cause accumulation and ablation to occur simultaneously throughout the year. In the outer tropics, where climate is defined by a pronounced seasonality of precipitation, accumulation is confined to the wet season (Kaser, 2001).

(iii) Extratropical glaciers undergo ablation almost exclusively through melting. Sublimation is most important for glaciers of the outer tropics, because the dryness of the troposphere in these regions allows only little melting during the austral winter (Kaser, 2001). Therefore, in the Bolivian Andes melting is at its highest rate during the austral summer, when the maximum of humidity coincides with the maximum of precipitation (Coudrain *et al.*, 2005). Since to melt snow requires about eight times less energy than to sublimate it, melting leads to higher ablation rates than sublimation. As a result, the season of accumulation in the outer tropics is also a period of enhanced ablation.

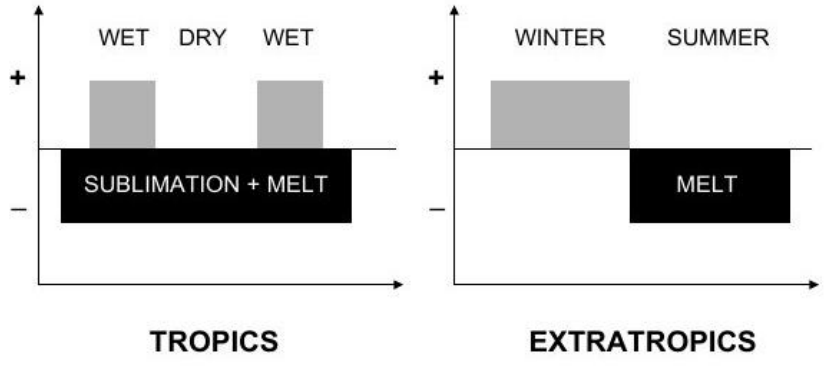

Figure 2.10: Accumulation (grey) and ablation (black, with its dominant components) regimes in relation with climate seasonality, for mountain glaciers of the tropical latitudes **(left)** and glaciers of the mid- and high-latitudes **(right)**. Source: Mölg (2009)

Glaciers of tropical latitudes are generally smaller than their counterparts in temperate or polar zones, and respond thus more rapidly to any environmental forcing. As a result, tropical glaciers are often described as highly sensitive indicators for large-scale climatic changes, such as the ongoing global warming (Kaser, 2001; Vuille *et al.*, 2003). On interannual timescales, significant correlations between mass balance and air temperature have indeed been observed (Francou *et al.*, 2003). However, on daily and monthly timescales, temperature is also correlated with almost every energy flux (Jomelli, 2009). Therefore, these results should not be regarded as an evidence that temperature is the primary factor controlling glacier ablation in the Tropics. The link between temperature and ice shrinkage is usually indirect and hides other underlying mechanisms inherent to tropical glaciers.

2.2.3. Energy balance

In contrast to extratropical latitudes, seasonal temperature variations in the Tropics are small, and climate seasonality is mainly driven by changes in atmospheric moisture and precipitation. As a consequence, tropical glaciers are sensitive to a broad range of variables beyond temperature, and especially to humidity-related variables, which include mainly air specific humidity, cloudiness, precipitation, albedo and wind. As depicted in Figure 2.11, these variables play a major role in the surface energy balance (SEB) of tropical glaciers, since they control the heat fluxes occurring at the interface between the atmosphere and the glacier surface (Coudrain *et al.*, 2005; Mark, 2008).

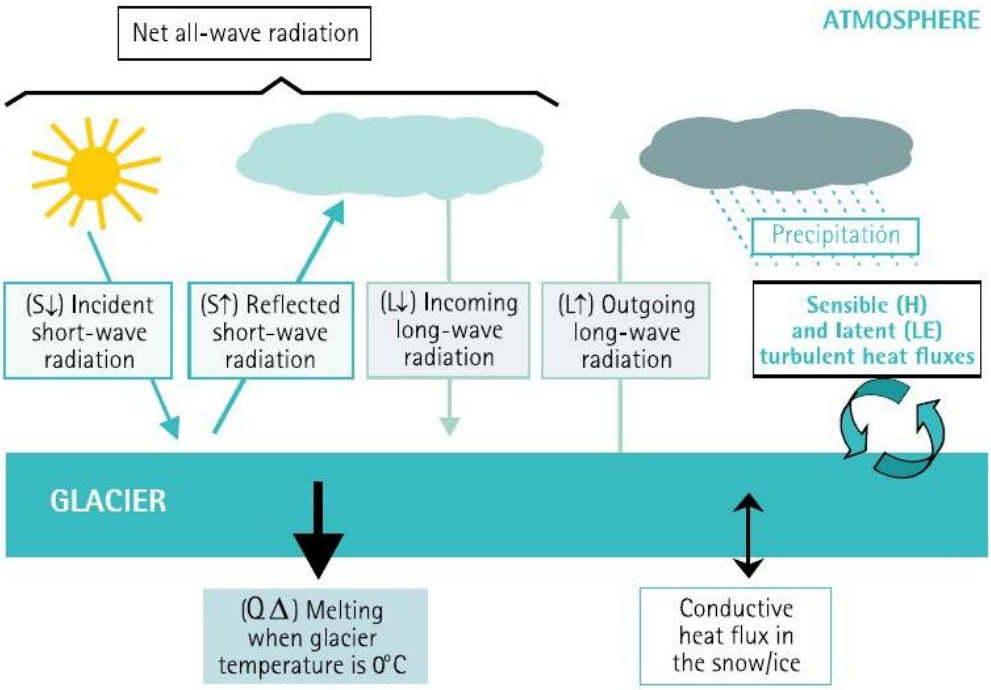

Figure 2.11: Surface energy balance (SEB) on a tropical glacier, with main atmospheric and radiative inputs/outputs controlling the glacier mass balance (MB). Source: Jeschke (2009)

The SEB of a melting glacier is given by Wagnon *et al.* (1999a):

$$R_n + SHF + LHF + Q_G + Q_P = Q_M$$

where R_n is the net all-wave radiation, H is the sensible heat flux, LE is the latent heat flux, Q_G is the conductive heat transfer into snow/ice, Q_P is the heat supplied by precipitation, and Q_M is the energy available for the melting. Energy fluxes are defined as positive when they are directed toward the surface, and negative when they are directed away from the surface.

Net all-wave radiation (R_n) Net all-wave radiation corresponds to the balance between the incident and reflected short-wave radiation, and the incident and emitted long-wave radiation. In the Tropics, where about 50% of the extraterrestrial solar radiation reaches the surface, against barely 25% in the temperate latitudes (Oerlemans, 2001), R_n is the main source of energy for the glacier surface (Wagnon *et al.*, 1999b).

$$R_n = SWD + LWD - LWU - SWU$$

$$R_n = (1 - AL) * SWD + LWD - LWU$$

where R_n is the net all-wave radiation, SWD and SWU are the incident and the reflected short-wave radiation respectively, LWD and LWU are the incident and the emitted long-wave radiation respectively, AL is the short-wave albedo of the snow/ice surface, and SHF and LHF are the sensible and the latent heat flux respectively.

Since extraterrestrial solar radiation is fairly constant in the Tropics, glaciers of these latitudes receive the same amount of net all-wave radiation throughout the year. Nevertheless, atmospheric moisture alters the incoming solar radiation in various ways.

Short-wave radiation (SWD – SWU) Solar radiation is the major source of energy for the melting of the glacier surface, and thus controls the variability of the glacier SEB. In the outer tropics, the short-wave radiation budget is closely related to surface albedo (Jomelli *et al.*, 2009). Albedo values are thus higher during the wet season, as fresh snow accumulates on the glacier almost every day. During the dry season, albedo decreases as the fresh snowpack is not renewed by precipitation and old snow turns progressively into bare ice. Lower albedo values imply enhanced absorption of solar radiation and thus increased melting.

According to its positive feedback on albedo, solid precipitation is thus considered as a key meteorological parameter in MB variability of Andean tropical glaciers (Wagnon *et al.*, 1999a,b; Favier *et al.*, 2004; Vincent *et al.*, 2005). Besides, albedo values also decrease when impurities, such as atmospheric dust and aerosols, are present on the glacier surface. In very dry environments such as the Andes mountains, dust deposit is frequently observed, especially during the dry season (Ribstein, 2002). Finally, as near-surface air temperature controls precipitation phase (liquid or solid), surface albedo is also indirectly linked to air temperature during precipitation events (Sicart *et al.*, 2008).

Long-wave radiation (LWD – LWU) The infrared radiation of the earth's surface, atmosphere, clouds and greenhouse gases (GHG), referred to as the long-wave radiation, directly affects near-surface air temperature. On the one hand, clouds and aerosols absorb the reflected short-wave radiation and release it as long-wave radiation toward the glacier surface (LWD). On the other hand, the thus heated glacier surface then releases its own long-wave radiation (LWU) which, if not intercepted by clouds, GHG or aerosols, represents a greater energy loss for the glacier. Consequently, since cloudiness increases near-surface air temperature by intercepting the long-wave radiation, and since temperature in turn controls precipitation phase which affects surface albedo, an indirect link exists between cloudiness and albedo.

The annual seasonality of long-wave radiation is highly pronounced in the outer tropics: the net budget is negative during the dry winter months due to a very reduced cloudiness, and slightly positive or near-zero during the wet summer months due to significant cloud cover (Vincent *et al.*, 2005). As a result, during the dry season, the more negative long-wave radiation partly counterbalances the more positive short-wave radiation (Wagnon *et al.*, 1999b), and the net all-wave radiation budget is thus close to equilibrium. During the wet season however, the R_n is clearly dominated by the strongly negative short-wave radiation (Favier *et al.*, 2004). This explains why variations in the long-wave radiation are less consequent for the SEB than the short-wave radiation, and why the variability of the latter has a greater impact on tropical glaciers during the wet season (DJF).

Latent heat flux (LHF) The turbulent latent heat flux depends on air humidity, which is limited by saturated specific humidity, which in turn is a function of air temperature (Sicart *et al.*, 2008), since at saturation warm air contains more water vapor than cold air.

While of minor importance in temperate or polar conditions, the latent heat flux is a key parameter to explain the high seasonality of melting under tropical conditions. As aforementioned, the high dryness of the air during the austral winter months is favorable for intense sublimation from the glacier surface, thus consuming most of the available energy and leaving only very little left for melting. The situation reverses during the wet summer months, when high air humidity causes low sublimation rates, so that most of the available energy is used for melting. As a result, latent heat flux is permanently negative in the outer tropics, and exhibits its lowest values during the austral summer (Wagnon *et al.*, 1999a).

Since melting is much more efficient than sublimation for the ablation process, more humidity in the near-surface levels would lead to considerable higher ablation rates (Kaser, 1999). Accordingly, the impact on glacier mass balance of an increased humidity in the outer tropics is likely to be much more dramatic than an increase in temperature in the extratropics, where melting is already high.

Sensible heat flux (SHF) The turbulent sensible heat flux occurs at the glacier/atmosphere interface and provides generally a positive gain of energy to the glacier surface. This energy flux depends primiraly on the temperature gradient between ice and air (Sicart *et al.*, 2008), and is also influenced by wind speed. Given the absence of major thermal seasonality, the low air density, and the light winds which characterize the Andean mountains of the outer tropics, glaciers in these regions are only little influenced by sensible heat flux (Ribstein, 2002).

Therefore, although the sensible heat flux remains positive all year-round, the sum of the turbulent heat fluxes (LHF + SHF) always represents a heat sink (Vincent *et al.*, 2005).

Conductive energy flux in snow/ice (Q_G) The conductive heat transfer within the snowpack or the ice is small during the wet season, but is responsible for a non-negligible upward flux (ice fusion) during the dry season. Nevertheless, conductive fluxes remain less important than radiative and turbulent heat fluxes (Wagnon *et al.*, 1999b).

Heat supplied by precipitation (Q_P) This energy flux remains relatively negligible as compared to the other terms of the SEB equation, because precipitation is always snow in the vicinity of the equilibrium line, and snowfall intensities are usually weak in the outer tropics.

Summary

In conclusion, seasonality in mass balance of tropical glaciers is controlled by the share between sublimation and melting in the year-round ablation process. In the outer tropics more particularly, air humidity is the main factor governing ablation seasonality, since it modulates the energy transfer from melting to sublimation, which is characterized by the latent heat flux. Precipitation is also a key factor in mass balance variability, firstly through accumulation in the upper-part of the glacier, and secondly due to its feedback effect on albedo, especially in the core of the wet season (DJF) which coincides with the period of highest ablation. Net all-wave radiation also plays an important role, and is mainly ruled by short-wave radiation via albedo, while long-wave radiation is controlled by cloudiness. Finally, since in the low latitudes sensible heat flux undergoes only little variations throughout the year, tropical glaciers are less sensitive to temperature variations than their counterparts in higher latitudes.

In the context of the ongoing climate change, the key diagnostic variables that should hence be investigated to understand tropical glacier recession are: *(i)* air specific humidity, *(ii)* precipitation, *(iii*) cloudiness, *(iv)* albedo or reflected short-wave radiation, and *(v)* incoming long-wave radiation. Nevertheless, as all these meteorological variables are strongly interconnected, they should not be treated separately.

Besides, the apparent correlation between temperature and mass balance is only a consequence to the fact that temperature integrates all the aforementioned fluxes. Therefore, temperature alone does not reflect the real physical processes occurring at the glacier surface (Francou *et al.*, 2003).

2.2.4. Influence of the glacier geometry

In addition to the climatic conditions experienced by glaciers, the morphological context is another key aspect of the glacier environment to consider when studying deglacierization of mountain regions on very long timescales.

Altitude Altitude is a critical parameter upon which the MB and the SEB of tropical glaciers are strongly dependent, since these glaciers are highly sensitive to the precipitation phase. Indeed, glaciers of the outer tropics usually end where solid precipitation becomes liquid, which coincides with the mean annual position of the free air 0°C isotherm (Bradley *et al.*, 2009). Recent studies

revealed that glaciers located at (relatively speaking) low elevations have been retreating at a more pronounced rate than glaciers at higher elevations, because the former are more exposed to ablation than the latter, and are thus less able to maintain a permanent accumulation zone.

Rabatel *et al.* (2013) studied the cumulative annual mass balance of eight glaciers between Colombia and Bolivia (Figure 2.12). They concluded that glaciers with a maximum elevation lower than 5,400 meters a.s.l. are more unbalanced than glaciers with a higher maximum elevation, and that many of the low-elevated glaciers would probably completely disappear in one or two decades.

Size Since the freezing level height (FLH) is always higher in the Tropics than in the temperate and polar latitudes, tropical glaciers are strictly restricted to the highest elevations of mountainous regions (Soruco, 2008). In the Bolivian Andes, the inferior limit of most glaciers ranges between 4,900 and 5,000 meters a.s.l. (Jeschke, 2009). As a result, glaciers of the tropical Andes have a very limited extension (0.5-2.5 km²) in comparison to Alpine glaciers (5-10 km²) or Himalayan glaciers (10-20 km²) (Soruco, 2008), and are therefore more sensitive to environmental forcing at short timescales.

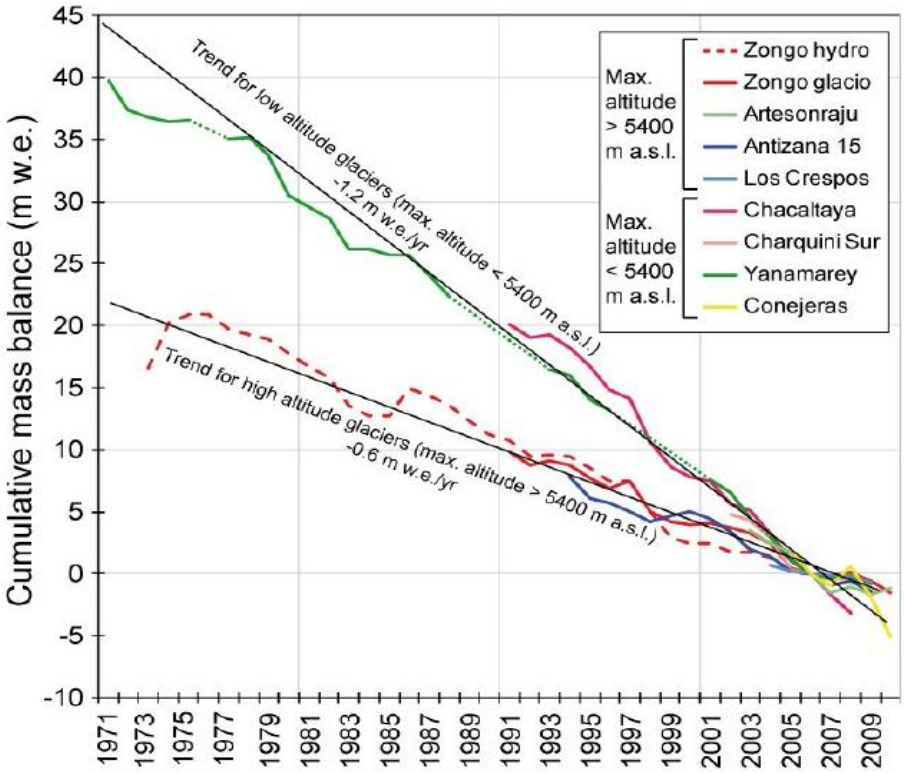

Figure 2.12: Cumulative annual mass balance series computed for eight glaciers in the tropical Andes. Source: Rabatel *et al.* (2013)

Exposure Glacier exposure to solar irradiance depends primiraly on latitude. In the Southern Hemisphere the trend is reversed in comparison with the Northern Hemisphere: glaciers are preferably well-developed on the southern slopes where they are less exposed to radiative energy than on the northern slopes. The relationship between glacier geometry and exposure is very clear in the Cordillera Real, where most glaciers are located on the southern, southwestern and southeastern slopes (Soruco, 2008), as shown in Figures 2.13 and 2.14. Besides, in the outer tropics cloudiness also contributes to some extent to an asymmetric extension of glaciers. The slopes oriented eastward are typically less glaciated since they receive stronger solar radiation from the more direct morning sun, as skies are usually cloud-free during the first half of the day. The western slopes are often more glaciated because during the wet season, convective clouds obstruct the sun irradiance in the afternoon hours (Hastenrath, 1991). This feature is also manifest in the Cordillera Real, though not very marked, but still significant (Figure 2.13).

Slope steepness Finally, the degree of slope steepness may also influence the extent of glacier development in mountainous regions. The steeper the slope, the less extended the glacier will be. In the Cordillera Real (Figure 2.13), glaciers that belong to the Altiplano basin are better developed than those belonging to the Amazon Basin, although being on the lee-side of the dominant moist winds (Soruco, 2008).

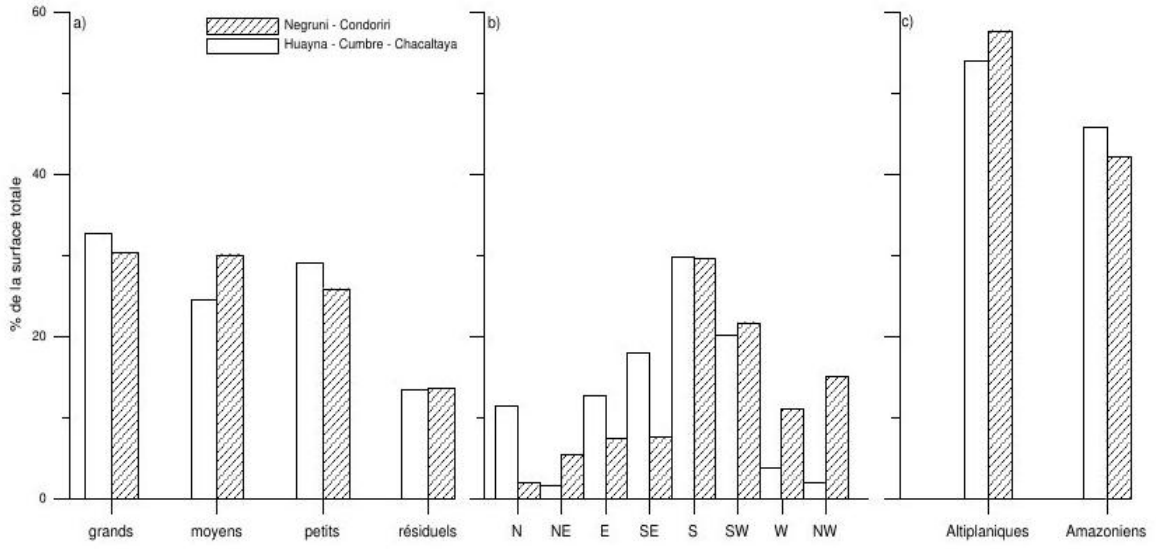

Figure 2.13: Differenciation of a set of selected glaciers in the regions of Negruni – Condoriri and Huayna Potosi – Cumbre – Chacaltaya (Cordillera Real, Bolivia) according to their size **(a)**, their orientation **(b)** and their drainage basin belonging **(c)**. Source: Soruco (2008)

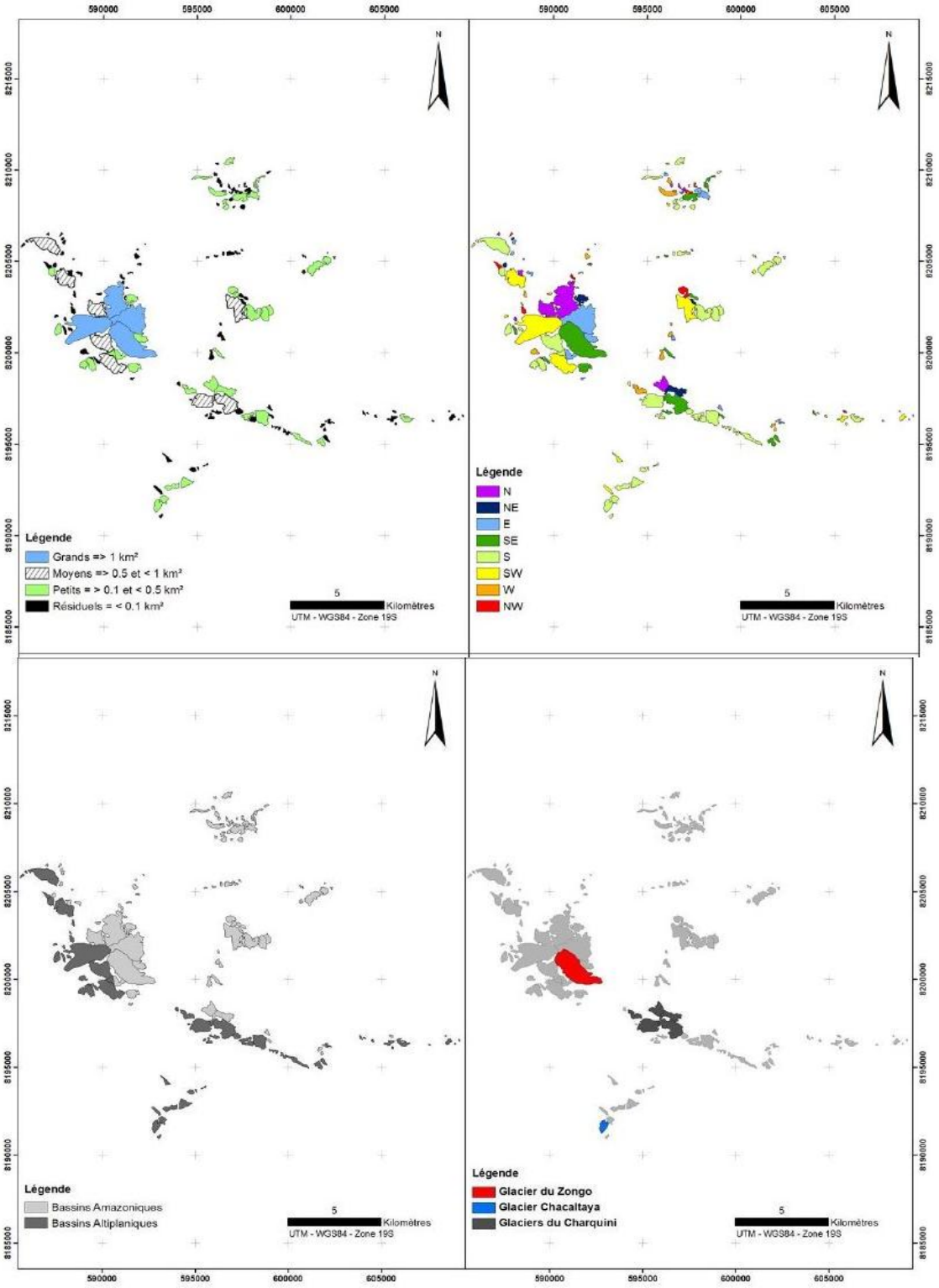

Figure 2.14: Differenciation of a set of selected glaciers in the region of Huayna Potosi – Cumbre – Chacaltaya (Cordillera Real, Bolivia) according to their size **(upper left)**, their orientation **(upper right)** and their drainage basin belonging **(lower left)**. The Chacaltaya Glacier is depicted in blue **(lower right)**. Source: Soruco (2008)

2.3. Past and current glacier fluctuations in the Bolivian Andes

The significance of the contemporary changes observed in tropical climate and glaciers can only be appreciated when placed in the perspective of a longer time frame. Unfortunately, instrumental records are scarce in South America, and of the three Andean countries (Ecuador, Peru, Bolivia), Bolivia is where glaciers have been the least documented until the early 1990s (Rabatel, 2005; Rabatel *et al.*, 2006, 2008; Jomelli *et al.*, 2009). Therefore, paleoclimatic reconstruction relies on proxy records such as ice cores, glacial moraines, pollens and tree-rings. Furthermore, historical written documents can provide a valuable and complementary source of information about past climate conditions. As a matter of fact, the Andes have been fairly well-documented since the Spanish colonial conquest in the 16th century (Gioda & Prieto, 1999). Nevertheless, the collected documents mainly focus either on the Southern-Central Andes (south of 35°S), or on the Northern Andes (Venezuela and Colombia), so that very little is known about the Cordillera Real in Bolivia.

2.3.1. Evolution over the last millenium

There is plenty evidence that glaciers in the tropical Andes were once much more extensive than today. Over the last millenium, three major glacier fluctuations have been identified across the world's mountains: an early advance ending around 1350, a maximum glacial extent ending between the 17th and 18th centuries, and a phase of global deglaciation interrupted by only minor glacial advances (Jomelli *et al.*, 2009).

The early glacial advance Although the early glaciation phase at the beginning of the last millenium has not been unanimously evidenced in the tropical Andes, moraines relative to three different glaciers in the Cordillera Real (Bolivia) have been interpreted as corresponding to this 14th century glacial stage. Nevertheless, the absence of similar evidence in most valley glaciers suggests that younger glacial advances extended once further than those that occurred in the 14th century (Jomelli *et al.*, 2009).

The maximum glacial extent The maximum glacial extent (MGE) is defined as the furtherest down valley extent recorded synchronously by most of the Andean glaciers (Jomelli *et al.*, 2009). This major glacial advance, commonly referred to as the Little Ice Age (LIA), has been observed in many other mountain regions throughout the world (Rabatel *et al.*, 2008), and has left its mark in various historical records (narrative, paintings, engravings). Figure 2.15 displays the approximate period of the LIA maximum dated for various locations across the world. In the outer tropics, the MGE occurred around 1630-1680, which coincides with the Maunder Minimum of solar activity (1645-1715). Consequently, it has been assumed that solar energy modulation was responsible for this worldwide glacier expansion, by inducing a global atmospheric cooling (Jomelli *et al.*, 2009). In the Bolivian Andes, the LIA was probably triggered both by cooler and wetter climatic conditions than today, but the cause of the presumed enhanced precipitation remains still unknown. More precisely, glacier–climate models could reproduce the LIA maximum in the outer tropics either with a decrease in temperature of 1.1–1.2°C and a simultaneous increase in precipitation by 20–30% (compared to present conditions), or with an increase in cloudiness of

about 10-20% (Rabatel, 2005; Rabatel *et al.*, 2006, 2008). However, written documents collected from libraries in Bolivia and Spain report that the LIA was accompagnied by significant dryness in the Potosi region, situated several hundreds of kilometers southwest of the Cordillera Real in Bolivia (Gioda & Prieto, 1999). These outcomes suggest that changes in precipitation occurred not uniformly in Bolivia, but were on the contrary very contrasted from one region to another.

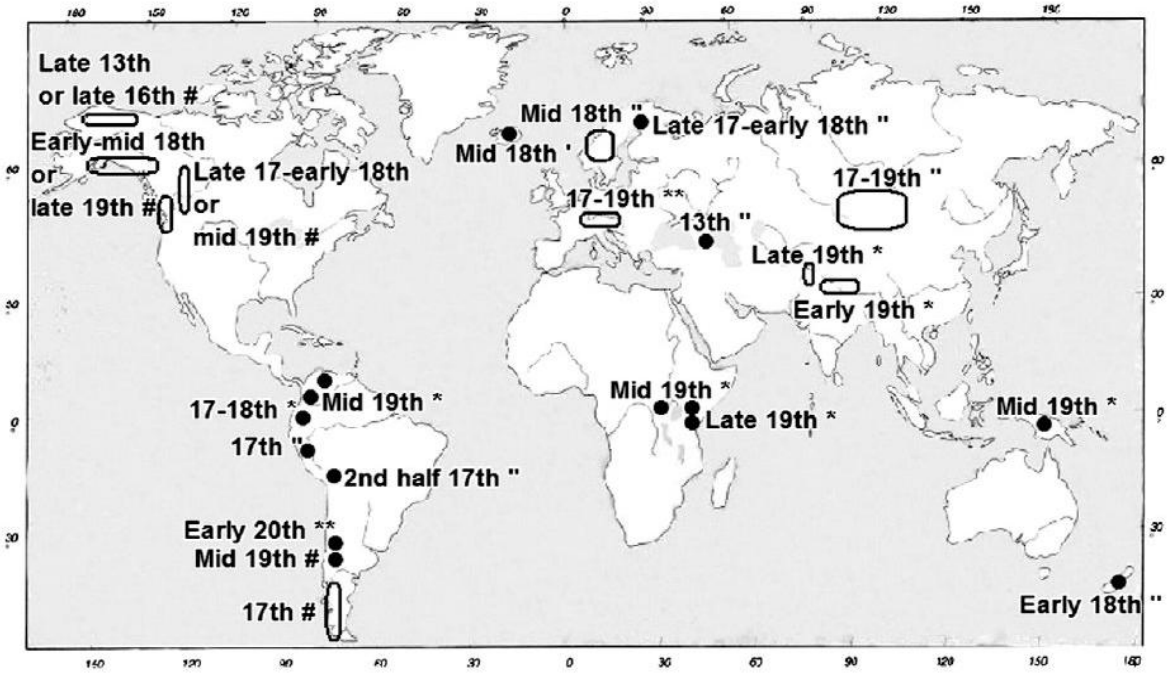

Figure 2.15: Dating of the LIA maximum throughout the world, based on different methods (e.g. lichenometry, historical documents, dendrochronology, tephrochronology, etc.).

Source: Rabatel *et al.* (2008)

The deglaciation phase The progressive glacier decline following the MGE began at the end of the 17th century in the tropical Andes, and more precisely after 1740 in the Bolivian Andes (Rabatel, 2005). In contrast to Europe and to other parts of the Northern Hemisphere, there is no evidence suggesting that temperature increased during the 18th century (Jomelli, 2009). Consequently, it has been assumed that glacier retreat after 1740 was a consequence of a climate change toward gradually drier conditions, with a significant drop in precipitation of about 20% (Rabatel *et al.*, 2008).

While glacier recession was moderate between the 17th and the 18th centuries, it became more pronounced after 1870 (Jomelli *et al.*, 2009), which definitely put an end to the LIA in the tropical Andes. The glacier shrinkage observed in Bolivia during the 18th and 19th centuries is specific for the outer tropical region, since it was not observed on mid-latitude glaciers (Rabatel *et al.*, 2008). This general receding trend was disrupted by only minor readvances, which occurred around 1730, 1760, 1800, 1850 and 1870 (Jomelli *et al.*, 2009).

Since the 20th century however, glacial recession has become a worldwide pattern. In the Bolivian Andes, the deglaciation occurred in three stages: *(I)* a major retreat starting in the late 19th century; *(II)* a relative slowdown between the 1910s and the 1930s followed by a marked glacial retreat after the 1940s; and *(III)* a very strong retreat during the 1980s and 1990s (Rabatel *et al.*, 2006). The rapid glacier shrinkage over these past decades is clearly depicted in Figure 2.16, which shows the evolution in terms of surface area of eight glaciers in the Cordillera Real since the MGE.

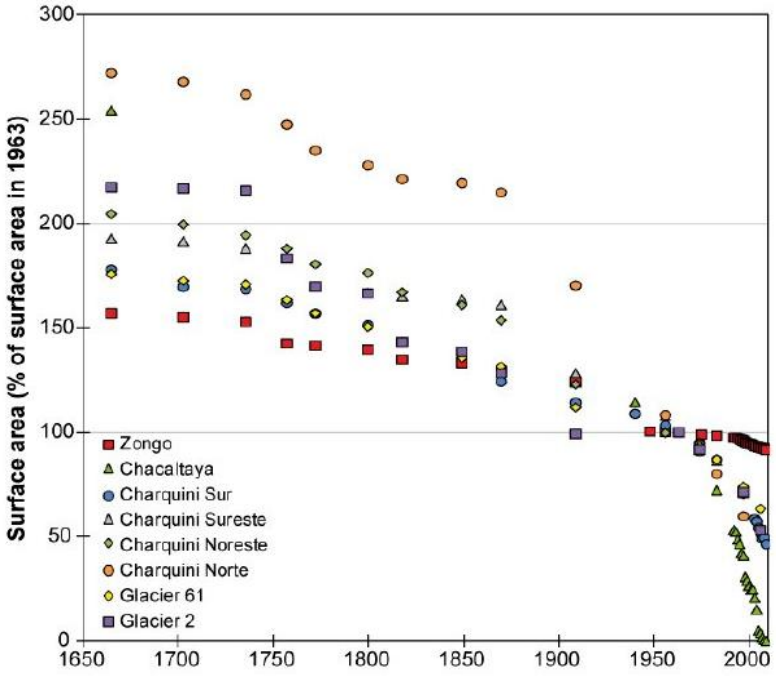

Figure 2.16: Changes in the surface area of eight glaciers in the Cordillera Real, Bolivia, since the LIA maximum, reconstructed from moraine stages (LIA maximum and before 1940) and aerial photographs (1940 and after). 1963 was chosen as the common reference.

Source: Rabatel *et al.* (2013)

To conclude, the reconstructed chronology of paleoclimatic conditions and past glacier fluctuations corroborates the results of the recent studies performed on contemporary glaciers in the tropical Andes, suggesting that glacier response in the outer tropics is driven rather by regional changes in precipitation than by changes in global temperature.

2.3.2. Accelerated glacier retreat and climate change over the last decades

Throughout the second half of the 20th century, the retreat of glaciers in the tropical Andes has considerably accelerated. For the glaciers in the Cordillera Real, Bolivia, recession rates have increased by a factor 4 over the last decades (Vuille *et al.*, 2008). While all glaciers in Bolivia are currently in imbalance, the small-sized glaciers located at the lowest elevations are those exhibiting the most negative mass balances.

This sustained glacial shrinkage occurs conjointly with increasing climatic and environmental changes. However, attributing glacier retreat to a particular climate forcing is one of the greatest issues in climatology. This task is even more challenging as direct meteorological observations indicate that changes in climatic parameters exhibit considerable regional heterogeinity. Western Bolivia is precisely one of these regions which seems to respond differently than its surrounding areas.

Temperature In most instances, glacier retreat has been attributed to a warming of the global troposphere, leading to increased melting and a negative mass balance. Such a warming has been confirmed in the tropical Andes (Vuille & Bradley, 2000) and even throughout most of the Bolivian regions, where temperature has increased by approximately 0.10°C/decade (Vuille *et al.*, 2008). The temperature increase over the last 70 years is evident in Figure 2.17, which shows an analysis of near-surface air temperature trends based on a compilation of 279 station records between the 1°N and 23°S. On the other hand, it has been observed that the rate of the warming varies markedly between the eastern and the western slopes of the Andes, with a much larger increase to the west (Vuille *et al.*, 2003). This suggests that changes in temperature are more complex at a regional scale.

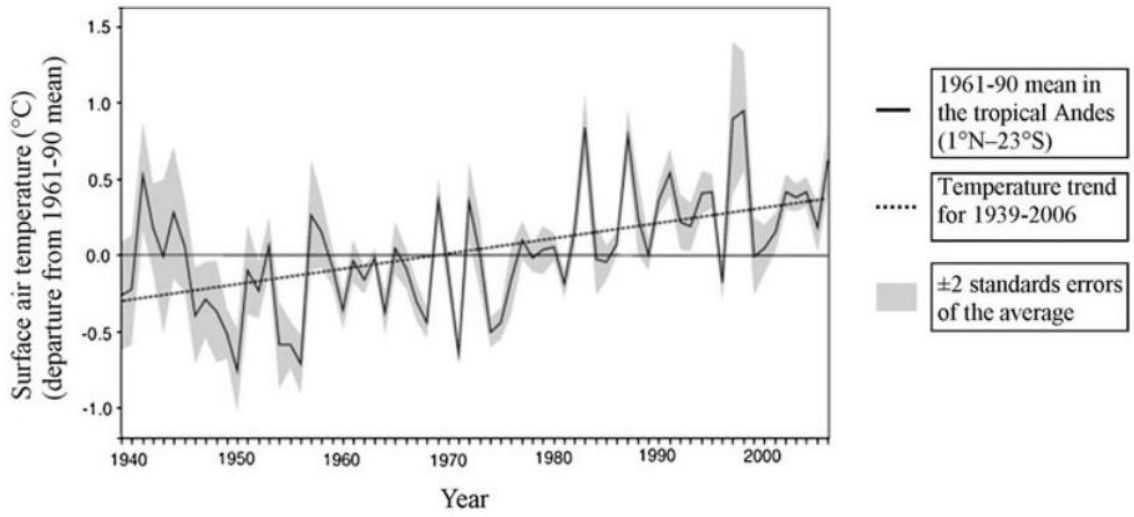

Figure 2.17: Annual temperature deviation from the 1961-1990 average in the tropical Andes (1°N–23°S) between 1939 and 2006, based on a compilation of 279 station records. Grey shading indicates ± 2 standards errors of the mean. Black line shows long-term warming trend (+0.10°C/decade) based on ordinary least square regression. Adapted from Vuille *et al.* (2008)

Precipitation Observations reveal that while changes in precipitation are minor in most tropical regions, Peru and western Bolivia exhibit a general tendency toward slightly drier conditions (Vuille *et al.*, 2003). There is indeed a constrast between the inner and the outer tropics, as precipitation has increased in the former and decreased in the latter.

Humidity In the Andes, long-term and in situ records of humidity are non-existent. Remote sensing data sets of tropospheric water vapor are currently used to document these changes, but they suffer from low spatial resolution and are still too short to be used in trend analyses (Vuille *et al.*, 2008). However, it is assumed that given the significant increase in atmospheric temperature, specific humidity of saturated air has increased throughout the Andes as well.

Convective cloud cover In the tropical Andes, assessment of convectice cloud cover is based on measurements of the outgoing long-wave radiation (OLR) emitted by the earth's surface and the overlying atmosphere. Since 1974, OLR is permanently monitored by polar orbiting satellites. The presence of deep convective clouds is detected by the satellite sensor which measures radiation emitted from the top of the clouds, which are high in the atmosphere and thus cold, leading to low OLR values. In the absence of convective clouds, OLR values are high (Vuille *et al.*, 2008).

Satellite-based observations reveal that since 1974 convective activity and clouds have increased in the inner tropics, but have decreased in the outer tropics, which is consistent with the observed changes in precipitation.

Large-scale atmospheric circulation The general pattern of moistening in the inner tropics and drying in the outer tropical Andes suggests an alteration of the mean tropical atmospheric circulation (Vuille *et al.*, 2008). More precisely, these changes could be explained by an intensification of the regional Hadley circulation (Figure 2.18). A strengthened meridional overturning circulation would indeed result in enhanced vertical ascent and convective activity in the inner tropics (10°N–10°S), whereas in the subtropics (10°S–30°S) stronger descending motion would lead to drier conditions (Vuille *et al.*, 2008). Such changes were reported, among others, by Chen *et al.* (2002) who used satellite observations.

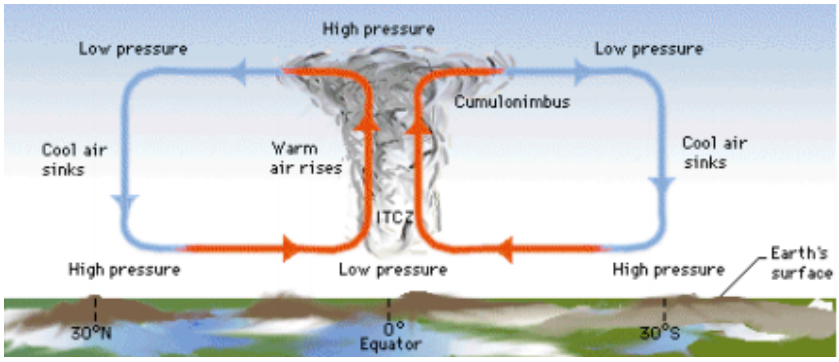

Figure 2.18: The meridional overturning Hadley circulation.
Source: *http://blogs.swa-jkt.com/swa/11029/2013/10/02/hum-unit-1-assessment-task-2/*

On the other hand, climate models suggest a weakening of the mean tropical atmospheric circulation, as a response to the increasing greenhouse gas induced warming (Vuille *et al.*, 2008). The component affected by this weakening is preferentially the zonal (east-west) asymmetric Walker circulation rather than the meridional (north-south) Hadley circulation (Vecchi *et al.*, 2006; Vecchi & Soden, 2007). The Walker circulation is driven by convection to the west in the Pacific Ocean and subsidence to the east along the South American continent (Figure 2.19). The simulated relaxation in the tropical overturning circulation is supported by observations reported by Curtis & Hastenrath (1999), who showed that SLP increased in the western and decreased in the eastern tropical Pacific Ocean throughout the 20th century. These observed changes in atmospheric and oceanic circulation over the tropical Pacific lead to a shift of the mean conditions toward a more El Niño-like state (Vecchi *et al.*, 2006; Vecchi & Soden, 2007), which is described in the next section.

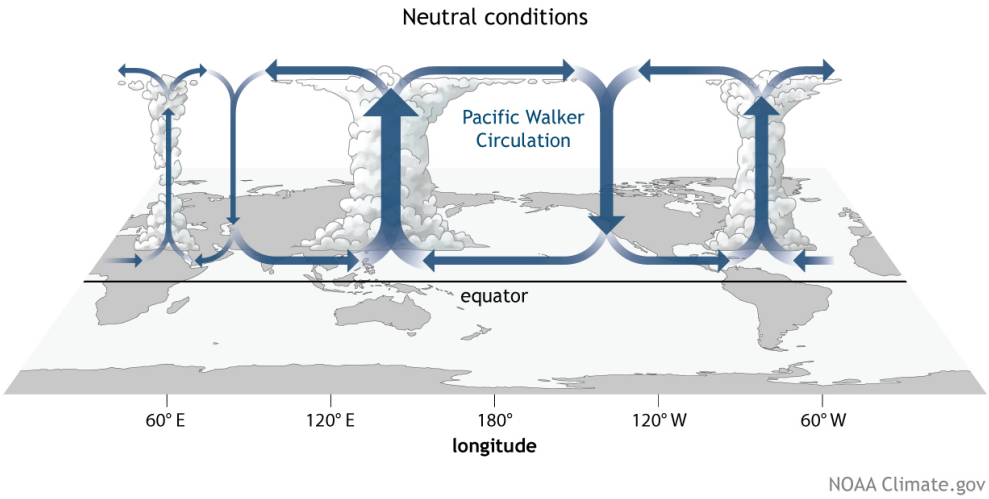

Figure 2.19: The zonal overturning Walker circulation. Source: *https://www.climate.gov*

2.3.3. Mechanisms of interannual and interdecadal climate variability

Superimposed on the general trend of receding glaciers, are interannual glacier fluctuations which alternate between phases of advance and recession. In recent decades, these short-term oscillations coincide with recurrent anomalies in the sea surface temperature (SST) of the tropical Pacific Ocean, which were identified as El Niño Southern Oscillation (ENSO) events.

2.3.3.1. The El Niño Southern Oscillation (ENSO)

The El Niño Southern Oscillation (ENSO) is a cyclic fluctuation in temperature between the ocean and atmosphere in the east-central equatorial Pacific. This naturally occurring phenomenon oscillates between two states: the warm oceanic phase (El Niño) and the cold oceanic phase (La Niña). The changes in SST in the tropical Pacific are related to changes in the zonal atmospheric Walker circulation. An El Niño phase occurs when the Walker circulation weakens or reverses, whereas a strengthened Walker circulation leads to a La Niña phase.

These events are accompagnied by changes in precipitation and temperature, and have a significant impact on the Altiplano climate, especially during the austral summer (DJF). The strong linkage that exists between tropical Andean glaciers and the tropical Pacific is mainly due to the fact that the associated response in the continental climate to SST anomalies is either a warm/dry signal (El Niño) or a cold/wet signal (La Niña), but seldom a warm/wet or a cold/dry signal (Vuille, 1999; Vuille & Bradley, 2000). As a result, the impact is amplified since La Niña (El Niño) events act in favor of (against) a positive glacier mass balance.

El Niño El Niño phases result in significantly higher temperatures and specific humidity, and in deficient precipitation during the austral summer (DJF), which delays snow cover (Wagnon *et al.*, 2001). The consequence for the glaciated areas in the Bolivian Andes is an increase in the melting of the glacier surface above 5,300 meters a.s.l., which results in strongly negative glacier mass balance (Wagnon *et al.*, 2001). These dry events are due to an enhanced westerly flow in the upper troposphere, which prevents the concurrent moist easterly flow from reaching the Bolivian Altiplano. The prevailing westerlies are associated with a northward displaced and weakened Bolivian High (Vuille, 1999). On average, near-surface summer temperatures are 0.7–1.3 °C higher during El Niño as compared to La Niña, and precipitation decreases by 10–30% (Vuille *et al.*, 2000).

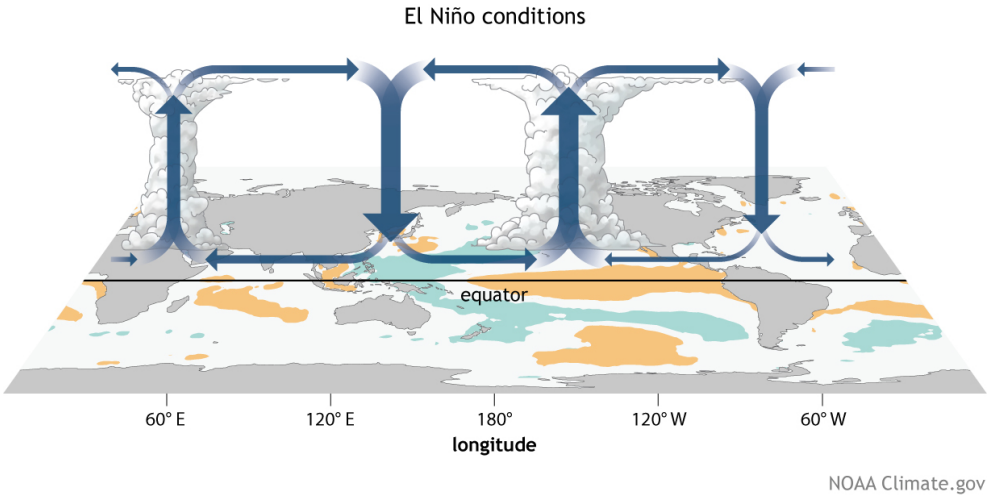

Figure 2.20: Modified zonal atmospheric circulation during El Niño conditions.
Source: *https://www.climate.gov*

La Niña By contrast, La Niña phases are characterized by regular snowfall, increased cloudiness and lower temperatures, all conditions which are favorable to maintain snow cover on glaciers during the entire summertime season. As a result, glacier mass balance is generally close to equilibrium or slightly positive. Wet summers during La Niña events are related to weaker upper-level westerlies, which results in an increased moisture influx from the interior of the continent. During those periods, the Bolivian High is intensified and displaced southward (Vuille, 1999).

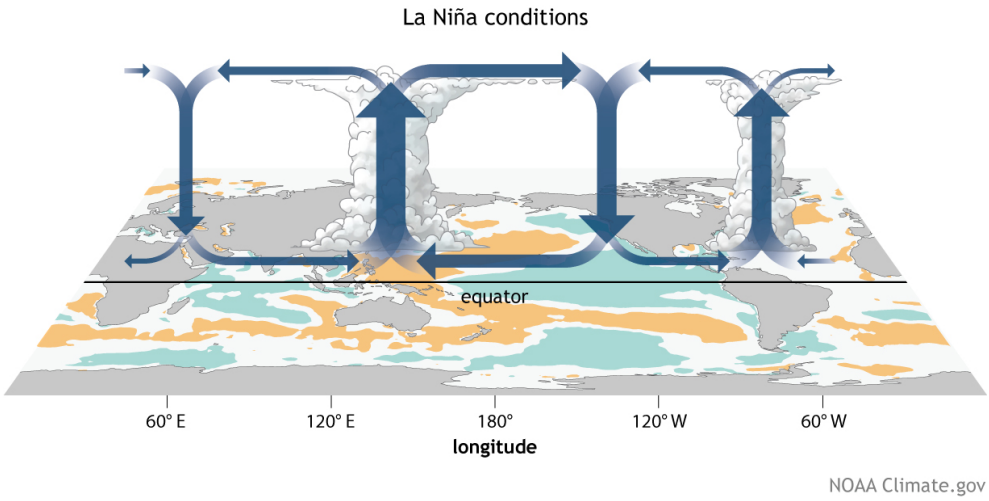

Figure 2.21: Modified zonal atmospheric circulation during La Niña conditions. Source: *https://www.climate.gov*

It is important to mention that, although the general pattern of precipitation anomalies during the El Niño and La Niña phases is the same in almost all regions throughout the tropical Andes, the ENSO signal is modified in certain parts of the Bolivian Altiplano. Vuille *et al.* (2000) found that over the eastern part of the Altiplano, correlations of atmospheric changes with ENSO are weaker. They explained this particular behavior by the convective nature of precipitation in this part of the Bolivian Andes, which ENSO-induced westerly wind disturbances can not modulate. By contrast, the western part of the Altiplano is more sensitive to ENSO-induced circulation anomalies because this region is located further away from the moisture source, i.e. the Amazon Basin, and is thus more affected by the lowered moist air advection from the east during El Niño periods.

Nevertheless, during the most severe ENSO events, the correlations are significant even for glaciers in the eastern Bolivian Andes. The three last decades were marked by several particularly strong El Niño phases, which occurred during the following years (in the chronological order):

1982-1983, 1987-1988, 1991-1992, 1994-1995, 1997-1998, 2002-2003, 2009-2010.

The most remarkable of these events were the two mega El Niño phases which occurred in 1982-1983 and 1997-1998 (Figure 2.22). Both warm phases produced exceptionally high SST anomalies in the tropical Pacific Ocean, and thereby induced strongly negative mass balances for all glaciers in the entire outer tropical region, and also in the inner tropics and the mid-latitudes. These events are among the most extreme El Niño phases of the 20th century.

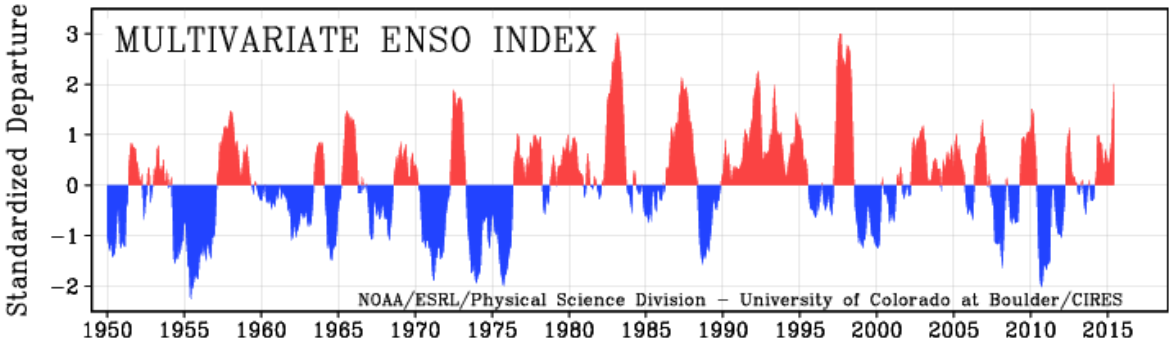

Figure 2.22: Multivariate ENSO Index (MEI) from 1950 onward. Positive values (red) represent El Niño phases, and negative values (blue) represent La Niña phases.

Source: *http://www.esrl.noaa.gov/psd/enso/mei/*

The 1990s was the decade the most affected by warm ENSO phases. In Figure 2.23, mass balance records from Bolivia (outer tropics) and Ecuador (inner tropics) show a very similar evolution for all four glaciers between 1992 and 2005, characterized by a generally negative trend (a). When analysing the specific mass balance fluctuations (b), ENSO phases can be easily detected. The only positive mass balance recorded on all four glaciers during the 1990s decade was during the hydrological year 1992-1993. This period constitutes a notable exception, because although it was part of an El Niño phase, it experienced anomalously cold climatic conditions (Francou *et al.*, 2003). This anomaly was most probably caused by the volcanic eruption of Mount Pinatubo in June 1991, which created an enormous stratospheric cloud and thereby cooled the lower and mid-troposphere throughout the Tropics for several months.

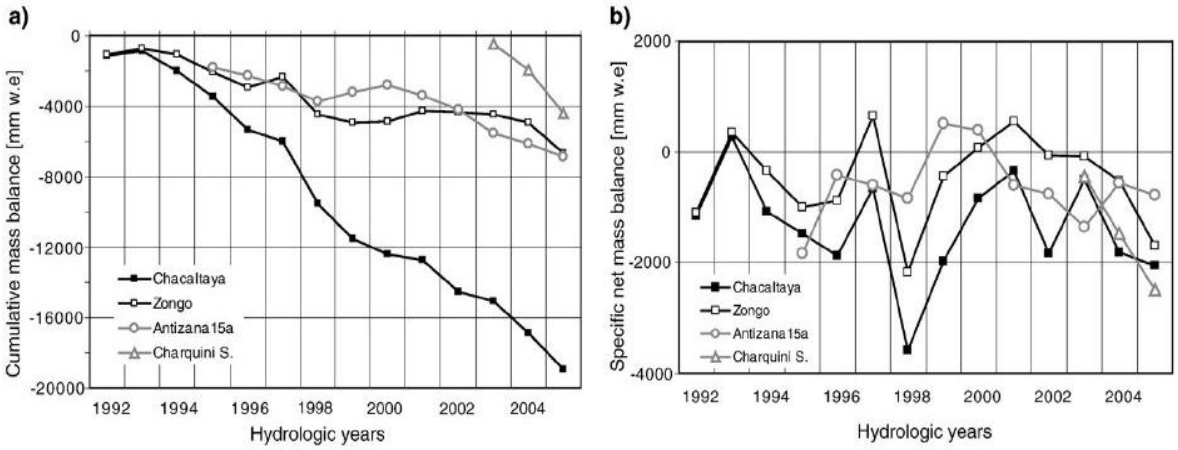

Figure 2.23: Cumulative **(a)** and annual **(b)** mass balance on glaciers of the outer tropics in Bolivia (Chacaltaya, Zongo) and of the inner tropics in Ecuador (Antizana 15a, Charquini S.). The hydrological year is September–August in Bolivia. Source: Vuille *et al.* (2008)

2.3.3.2. The Pacific Decadal Oscillation (PDO)

Long time series of ENSO exhibit a regime shift around 1976-1977 (Zhang *et al.*, 1997). This break in the long-lived Pacific climate regime has been identified as a reversal in the prevailing polarity of the Pacific Decadal Oscillation (PDO). Like the ENSO phenomenon, the PDO is a recurrent pattern of the Pacific climate variability, but which varies over much longer timescales. Indeed, while ENSO phases last only 6 to 18 months, the PDO cycle can persist for 20 to 30 years. The mode of variation, however, is the same for ENSO and PDO indexes, as both alternate between warm (positive) and cold (negative) phases. Although PDO-induced SST anomalies concern mainly the extratropical North Pacific Ocean, extreme shifts have significant implications for climate at the global scale. As can be seen in Figure 2.24, evidence was found for only three complete PDO phases throughout the 20th century, and the shifts occurred around 1925, 1947, and 1977.

It is believed that ENSO and PDO affect each other in the sense that, when they both are in the same phase, the El Niño and La Niña impacts are magnified. Conversely, when ENSO and PDO are out of phase, they offset one another, which significantly minimizes the ENSO impacts.

Since the great Pacific Shift of 1976-1977, it has been observed that El Niño phases have become both more frequent and more intense. Since then, SST anomalies in the eastern equatorial Pacific Ocean have been consistently higher during the austral summer season, and the glacier retreat in the tropical Andes has synchronously increased (Francou *et al.*, 2003). The PDO values remained positive until the late 1990s; after that, negative PDO values have generally been observed, suggesting that the current phase is a cold one. Nevertheless, the 22 years long positive phase between 1977 and 1999 generated several harsh El Niño events, which brought many tropical glaciers out of balance.

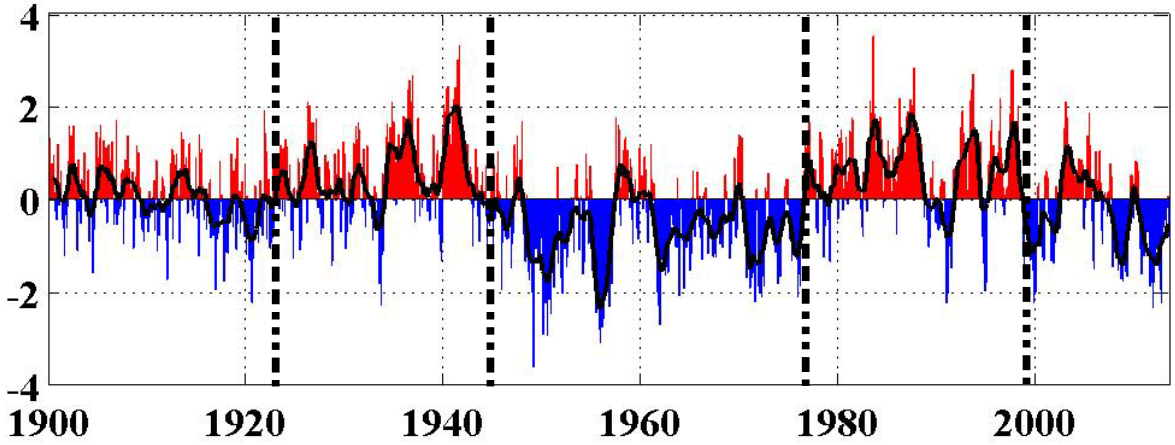

Figure 2.24: Mean annual values of the Pacific Decadal Oscillation Index from 1900 to 2013. Source: *http://research.jisao.washington.edu/pdo/PDO.latest*

2.4. The Chacaltaya Glacier

2.4.1. Morphological features and climatic context

The Chacaltaya Mountain (16°21'S, 68°07'W) is located in the Cordillera Real range which shapes the northernmost and highest part of the Bolivian Cordillera Oriental. With its summit culminating at 5,359 meters a.s.l., this mountain is relatively low-elevated as compared to other neighboring peaks.

The late Chacaltaya was a south facing cirque glacier which presumably formed 18,000 years ago. Before completely vanishing in 2009 (WGMS, 2011), the glacier was frequently visited since it served as Bolivia's sole ski resort. The glacier was also notorious for being the highest lift-served ski area in the world. Despite the alarming rate of its shrinkage, the Chacaltaya still functioned as a ski resort in the early 1990s (Ramirez *et al.*, 2001).

Its proximity to La Paz (approximately 20 km northeast of the capital city, accessible by road) made the glacier very opportune for long-term monitoring, and is thus very well documented. Between 1953 and 1998, the mean annual temperature was -1.1°C, with average monthly values ranging between -0.3°C in November and -2.5°C in July (Ramirez *et al.*, 2001). The climate of the Chacaltaya Mountain is semi-desertic: from the annual precipitation total amount of 680 mm, about 50% occurs during the austral summer season (according to the *Chacaltaya GAW Station* website). The accumulation period is also when ablation is at its highest rates: during these months, high humidity levels allow melting to be distinctly predominant over sublimation, which in turn prevails during the dry austral winter season.

By virtue of its very small size and its low elevation, the Chacaltaya Glacier is representative of many glaciers located in the outer tropics. Therefore, the diagnosis of this one glacier can be extended to the glacier recession in the entire Cordillera Real of Bolivia, where 80% of the glaciers are less than 0.5 km² in size (Ramirez *et al.*, 2001; Francou *et al.*, 2000, 2003).

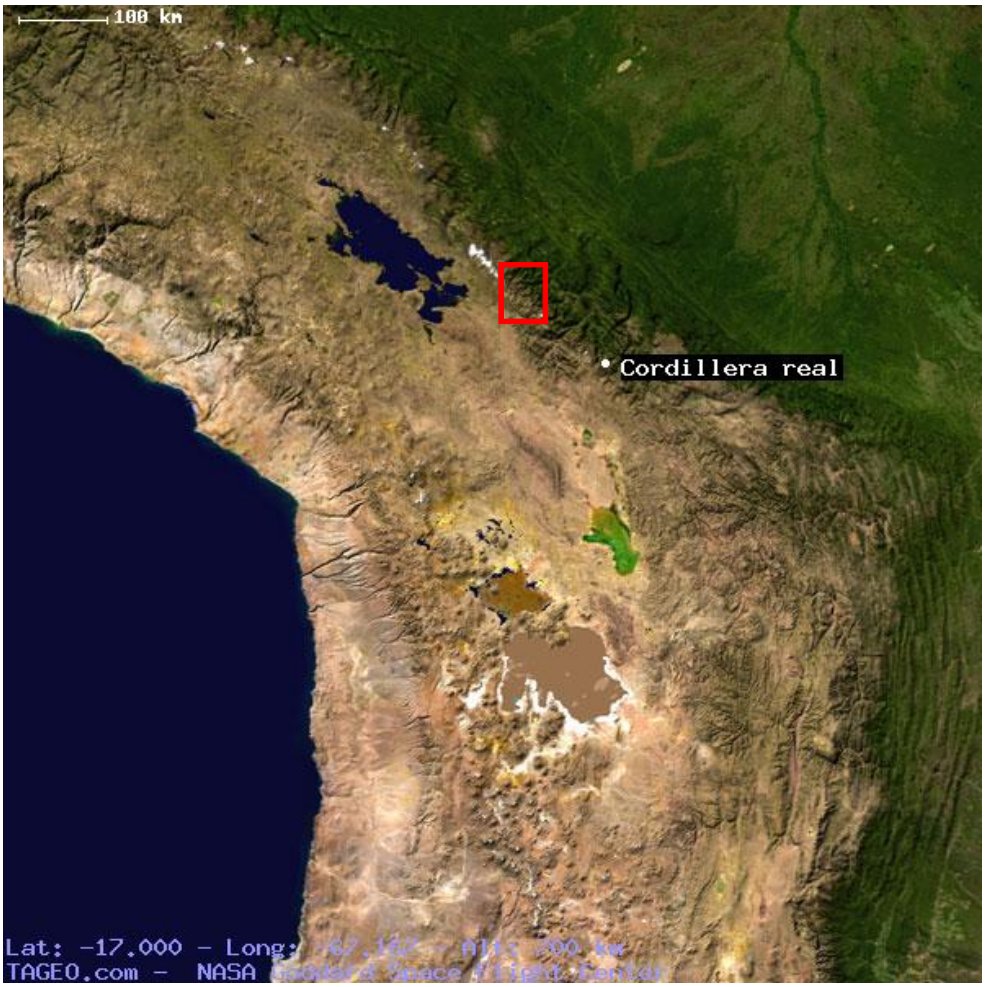

Figure 2.25: Location of the Chacaltaya Glacier. The red rectangle indicates the area of interest detailed in Figure 2.24. Source: *NASA Earth Observatory*

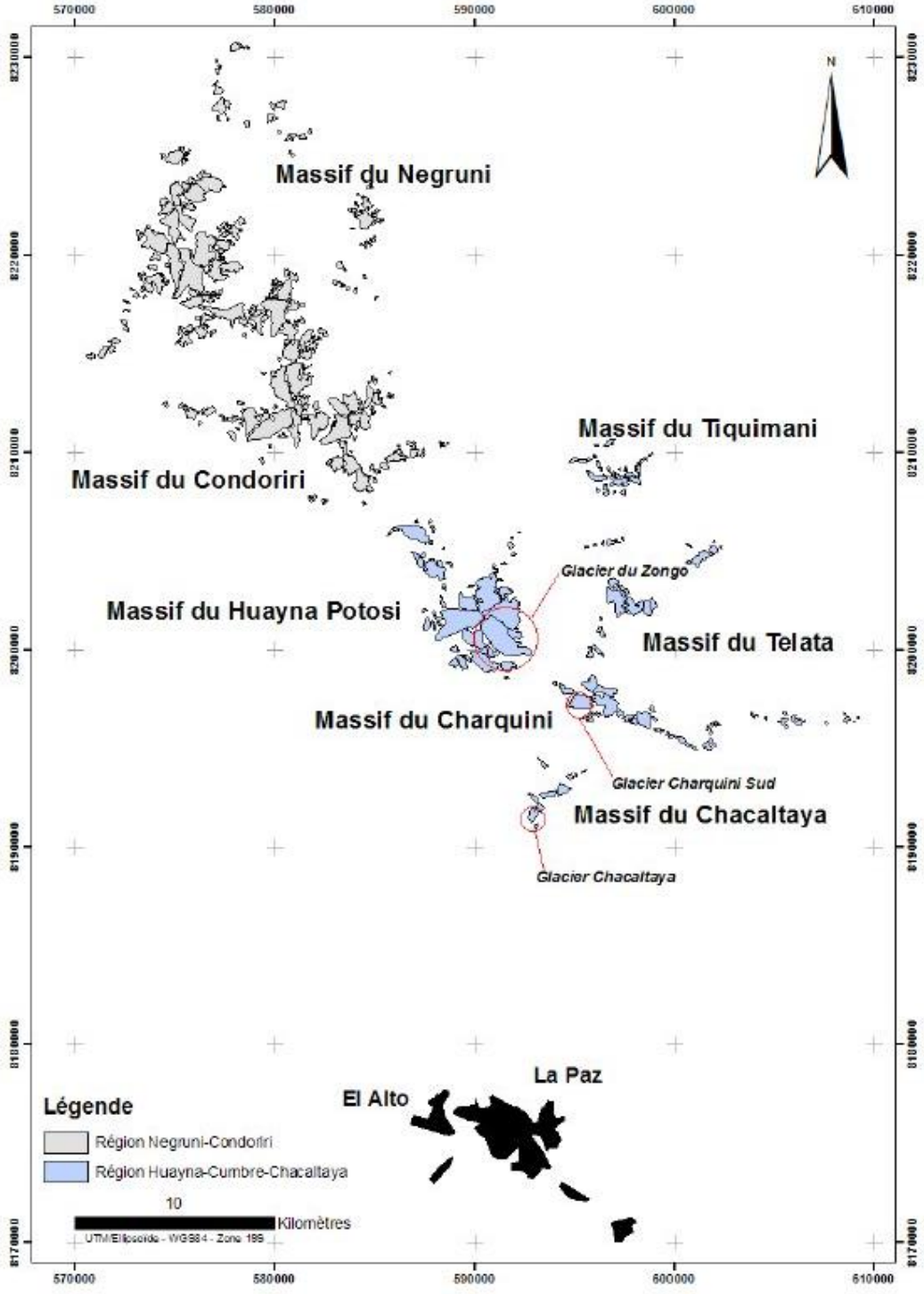

Figure 2.26: Detailed map of the different massifs in the vicinity of the Chacaltaya Glacier and the city of La Paz, Bolivia. All glaciers belong to the Cordillera Real range. Source: Soruco (2008)

2.4.2. Evolution from 1940 to 2009

The Chacaltaya is one of the rare glaciers of the tropical Andes to have undergone a long-term monitoring of its evolution (Ramirez *et al.*, 2001). Under the initiative of the IRD (Institut de Recherche pour le Développement, France) and several South American partners, mass balance has been continuously surveyed on the Chacaltaya by monthly direct records since September 1991 (Francou *et al.*, 2003).

The past areas and volumes of the glacier over the last six decades were reconstructed by means of several methods involving: *(i)* topographic measurements since 1992, *(ii)* stereo-photogrammetric analysis of aerial photographs taken in 1940, 1963 and 1983, and *(iii)* reconstruction of the LIA maximum using the well-preserved external moraines and a ground-penetrating radar (GPR) survey in 1998 (Ramirez *et al.*, 2001). The different stages of the glacier since the LIA are mapped in Figure 2.27. Figure 2.28 resumes the observed and reconstructed evolution of the Chacaltaya.

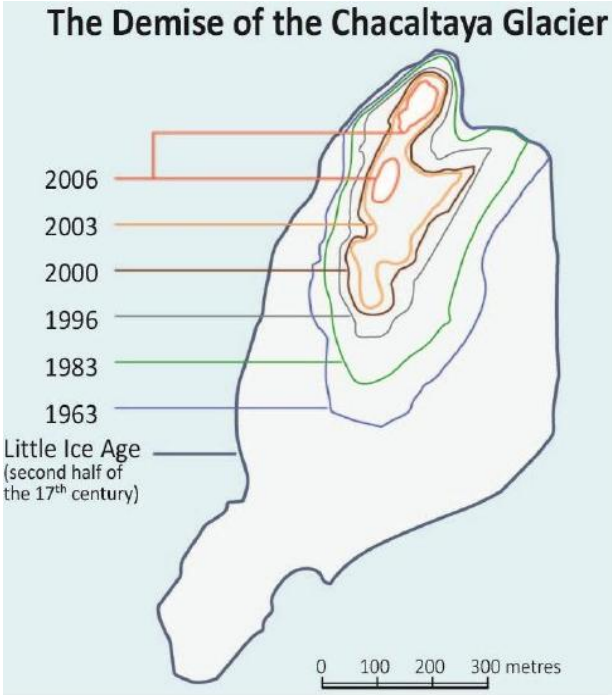

Figure 2.27: Changes in size of the Chacaltaya Glacier. Source: UNEP (2013)

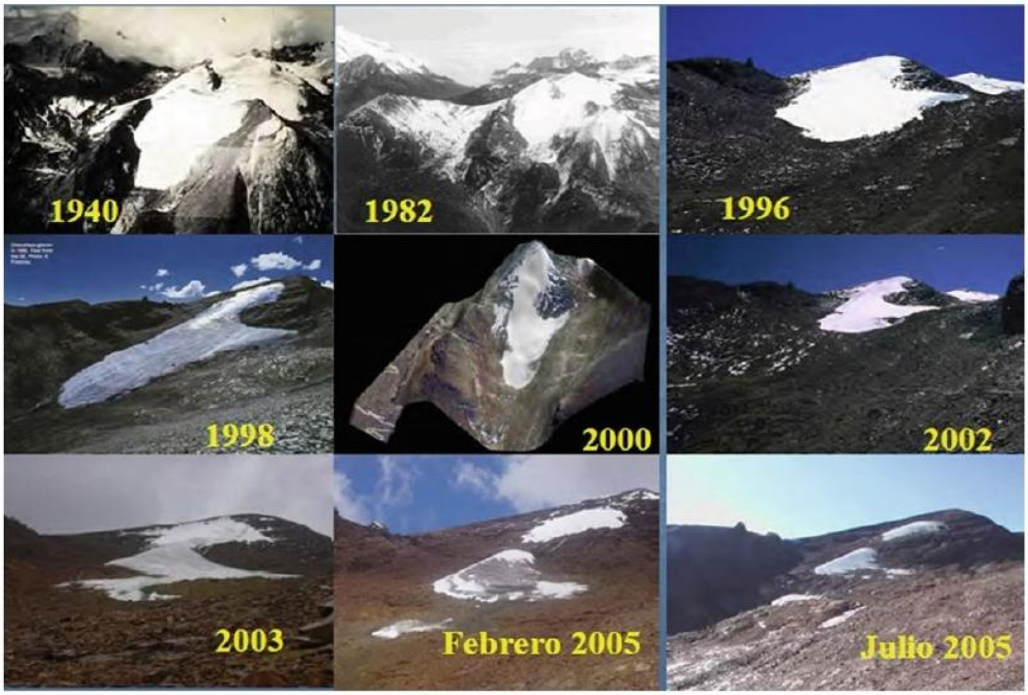

Figure 2.28: Visual documented disappearance of the Chacaltaya Glacier since 1940 through photography and modeling. Source: Rangecroft *et al.* (2013)

The observed and reconstructed data revealed that the retreat of the Chacaltaya Glacier had been continuous since the 1940s, and had accelerated since the late 1970s. The average loss of ice volume during the 1983-1998 period was twice the amount of the moderate loss during the 1940-1963 period.

Throughout the 1990s decade, the yearly net mass balance of the glacier was almost permanently negative (Ramirez *et al.*, 2001). The negative trend was interrupted briefly in 1992-1993, when the Pinatubo volcanic eruption induced a slightly positive mass balance. From 1992 to 1998, the Chacaltaya lost in only six years 2/3 of its total volume, and its thickness was reduced by more than 40% (Ramirez *et al.*, 2001). As a result, in 1998 the remaining surface area of the glacier was only 0.01 km², or 7% of its extent in 1940 (0.22 km²) (Francou *et al.*, 2000). Also in 1998, the glacier had an altitudinal extension ranging from 5,360 to 5,140 meters a.s.l., with a maximum width of 230 meters (Ramirez *et al.*, 2001).

The mass balance deficit of the Chacaltaya was greatly amplified during the El Niño Southern Oscillation (ENSO) events. During the whole period of observation, the Chacaltaya Glacier underwent three major ablation peaks, which all occurred during the 1990s decade: one very strong in September 1997 – February 1999, and two others in September 1994 – December 1995 and September 1991 – April 1992. As can be seen in Figure 2.29, the impact of the period 1997-1999 was exceptionally strong, since during 18 months the glacier lost 6 meters of water equivalent, or one third of its entire ice volume (Francou *et al.*, 2003).

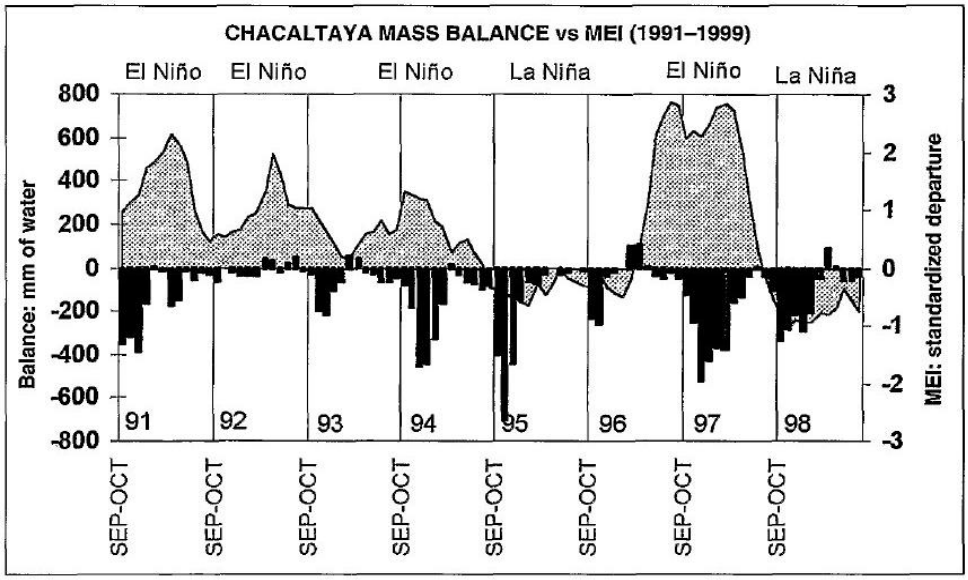

Figure 2.29: Monthly evolution of the net mass balance of the Chacaltaya Glacier at 5,170 meters a.s.1. (bars), and Multivariate ENSO Index (MEI) (line) from September – October 1991 to July – August 1999. Source: Francou *et al.* (2000)

In the early 2000s, scientists predicted that the Chacaltaya would completely disappear within the next 10-15 years (Ramirez *et al.*, 2001; Francou *et al.*, 2003). In 2005 however, the glacier had essentially disintegrated into a few small stagnant ice fields (Coudrain *et al.*, 2005), and in 2009 it was completely gone.

3. Objectives

This study aims to provide a climatological analysis of the current evolution of tropical glaciers in the Bolivian Andes, by integrating both global and local aspects of the ongoing climate change. We focus on the case of the Chacaltaya Glacier, which is a representative specimen of many other endangered glaciers located in this part of the world.

For this purpose, we will reconstruct the atmospheric conditions during the past 55 years over the area of interest with the help of the regional climate model MAR, developed at the ULg.

Before analysing the simulation outputs, we will submit our model to a necessary stage of validation where its performance to reproduce the peculiar climate of the tropical Andes will be assessed.

In the following interpretation phase, our results will first be integrated into a meso-scale context by analysing the behavior of the medium and upper troposphere, both on the long-term and during the recent ENSO events, with the objective of characterizing the relationships between glaciers and ocean-atmosphere dynamics.

Furthermore, we will examine our results in terms of surface energy budget, with a view to better understanding the physical response of glaciers to short-term changes in local climate conditions. We expect the model to highlight the underlying mechanisms (other than temperature) which control the mass balance variability of tropical Andean glaciers.

4. Methodology

4.1. Regional climate modeling

Global climate models (GCMs) are models which generate global-scale climate simulations but at a relatively coarse spatial resolution (~100 km). Conversely, regional climate models (RCMs) are run over a limited area of the planet, which allows them to perform results at a comparatively higher resolution (~10 km), yet at affordable computational cost. Another major advantage of using RCMs is that they can be parameterized for a specific climatic context.

It is well known that at the regional scale climate may be significantly influenced by local topographic features. Global models are not able to account for these local effects, due to their coarse resolution. The Andes, with their steep slopes and their associated rainfall and temperature gradients, provide a typical example of a complex orographic and climatic domain which GCMs can not resolve (Figure 4.1). Figure 4.2 illustrates a portion of the Andes Cordillera simulated at a 1.125° resolution (about 125x125 km). The orographic features are so strongly smoothed away that the Cordillera Real, which is the mountain range that hosts Mount Chacaltaya, does not even exist.

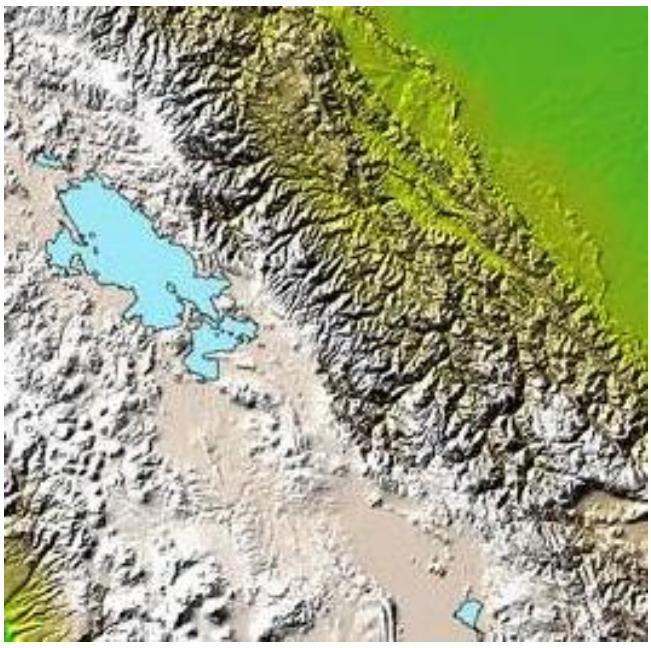

Figure 4.1: Topography of the study area generated by radar observation.
Source: *NASA Earth Observatory*

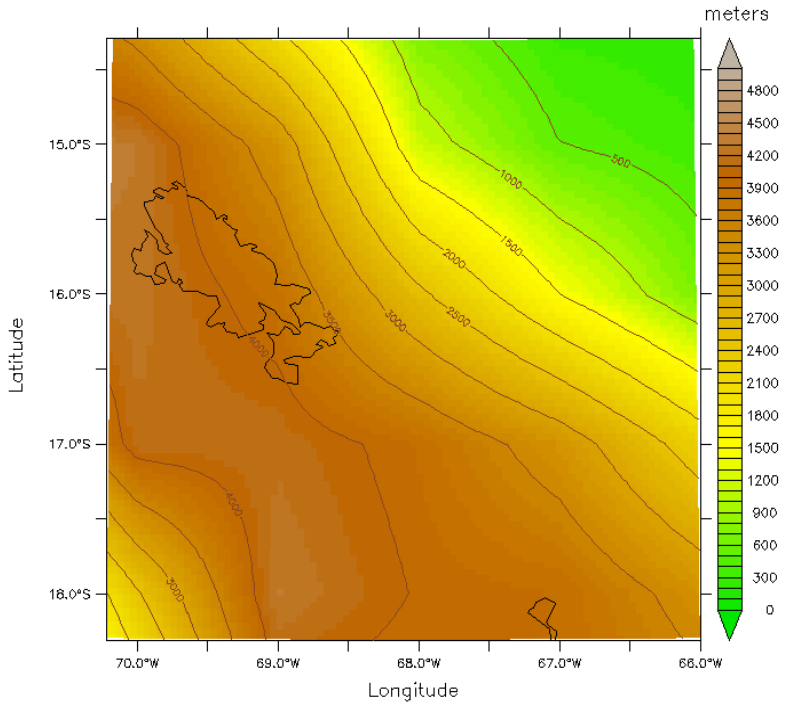

Figure 4.2: Topography of the study area simulated at the resolution (1.125°) of the ECMWF-ERA40 reanalysis. The dark lines stand for the contours of lakes, and the brown lines are the lines of equal altitude.

When studying climate at local scales, it is thus much preferable to work with regional models. In addition to the gain in spatial resolution, RCMs can be calibrated and developed for specific climates (by using specific parametrizations) while GCMs need to work well over all the climates. However, a common issue with RCMs is that the simulation domain, though limited to a specific area, has to be large enough to include all the terrain characteristics that are believed to locally influence the circulation of air masses over the studied area (Soriano *et al.*, 2002). Some of these forcing mechanisms may be far away from the area of interest. Yet extending the simulation to a larger domain while maintaining a very high resolution would require excessive time and computational costs.

A solution to this issue is to embed the regional model in a global model by a technique called “model nesting”. Spatial resolution is thereby increased only in the inner domain (RCM) where the small-scale phenomena might occur, while in the outer domain (GCM) the resolution remains coarse. This technique ensures the introduction of large-scale forcings modeled by the GCM into the highly resolved area of interest modeled by the RCM (Soriano *et al.*, 2002).

The nesting of a RCM within a GCM can be used either in one-way mode or in two-way mode, each of which respectively allowing unidirectional or bidirectional interaction between the inner and the outer domain. In a one-way nesting (as used in this work), no feedback is provided from the RCM to the encompassing GCM because inner and outer domains are run separately. The one-way nesting is applied for most of the GCM-forced RCM simulations. The outer coarser domain (GCM) is run first, then its output fields are interpolated in space to 6-hourly supply the embedded RCM as inputs at its lateral boundaries. By contrast, in a two-way nesting both inner

and outer domains ought to be run simultaneously, so that they interact and complement each other. Therefore, two-way nesting is generally believed to yield better results than one-way nesting (Soriano *et al.*, 2002).

Nevertheless, even two-way nested RCMs can not thoroughly compensate the errors that may exist in the large-scale circulation fields modeled by GCMs. As a consequence, these errors, once transmitted to the RCM through its lateral boundaries, propagate into the RCM domain and cause both models to produce unrealistic results (Zhong *et al.*, 2010). Hence, for a successful RCM simulation it is critical that the lateral boundary conditions (LBCs) be of good quality (Giorgi, 2011).

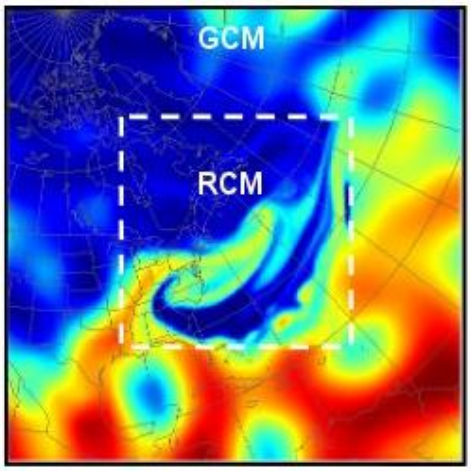

Figure 4.3: Illustration of the nesting technique.

4.2. The regional climate model MAR

4.2.1. Description

The regional climate model used in this study is the MAR (for Modèle Atmosphérique Régional in French) model, described by Fettweis (2006) and which is developed in part at the Laboratory of Climatology from ULg. MAR consists of a three-dimensional atmospheric module coupled with a 1D land-surface module called SISVAT (Soil Ice Snow Vegetation Atmosphere Transfer).

The atmospheric part of MAR, fully detailed in Gallée & Schayes (1994), is a hydrostatic model that solves the primitive equations of fluid dynamics. The vertical coordinate is the sigma coordinate, i.e. the terrain-following reduced pressure:

$$\sigma = (p - p_t)/(p_s - p_t)$$

where p, p_s and p_t being respectively the pressure at the considered level, the surface pressure and the constant model top pressure. This coordinate system is well-suited for climatological applications since it allows easy inclusion of topography.

Parameterization is performed to include physical subgrid-scale processes, i.e. the processes that are smaller than the spatial resolution of the model. The radiative (solar and infrared) transfer scheme is parameterized following Morcrette (2002) and is the one used in the ECMWF-ERA40 reanalysis (see section 4.2.2.1.). The vertical fluxes in the near-surface boundary layer are computed with the turbulence closure model of Duynkerke (1988), while the convective scheme is based on Bechtold's (2001) parameterization. The representation of the hydrological cycle includes a cloud microphysical model that also requires parameterization. This model allows to account for cloud droplet, cloud ice crystal, raindrop and snow flake concentrations (Gallée, 1995).

The SISVAT scheme, explained by De Ridder & Gallée (1998) and Lefebre *et al.* (2003, 2005), simulates mass and energy fluxes occurring in the surface-atmosphere system. SISVAT is a vertical one-dimensional multi-layered model which incorporates both a soil-vegetation module, and a snow-ice module. While the former module works out the heat and moisture fluxes between the snow-uncovered land and the atmosphere, the latter module deals with the exchanges between the snow-covered land, the ice sheet surface, the sea-ice, and the atmosphere (Lang, 2011).

The snow-ice part of SISVAT is based on the snow model CROCUS (Brun *et al.*, 1992; Lejeune *et al.*, 2007), developed at the CEN (Centre d'Etudes de la Neige). CROCUS itself consists of a thermodynamic module, a water balance module, a turbulence module, a snow metamorphism module, a snow/ice discretization module, and an integrated surface albedo module (Fettweis, 2007). These various modules allow the model to take into account specific processes, such as the melting and the sublimation of snow and ice, the evaporation and the refreezing of meltwater, as well as all kinds of heat and radiative fluxes (upward and downward) occurring near the surface.

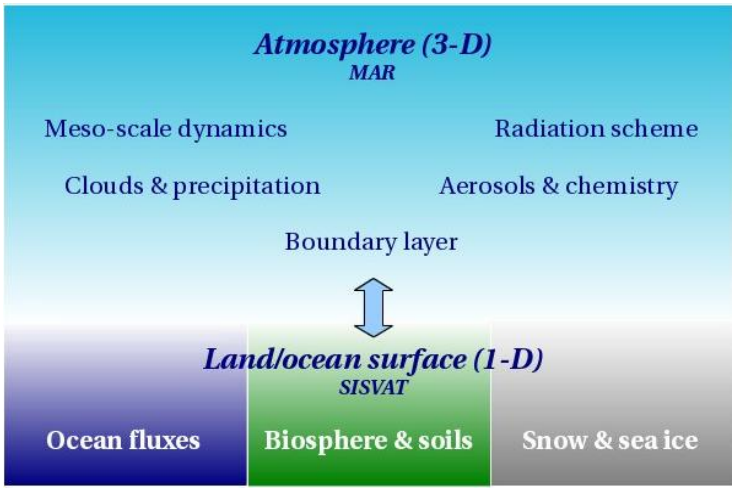

Figure 4.4: Composition of the MAR model and its parameterizations.

The MAR model was initially developed to study polar regions (Greenland and Antarctica). However, the model has since been adapted and applied to many other regions of the globe such as West Africa, Himalaya, the Alps, Belgium, or even Israël and Sahel (Ménégoz *et al.*, 2014).

4.2.2. Experimental setup

The preprocessing tool of the MAR model is called NESTOR (for NESTing Organization for the preparation of meteorological and surface fields in Regional models). The preprocessor is where all the initial conditions must be entered before launching a MAR simulation. Inputs include the time-varying large-scale forcing fields (i.e. the LBCs) and the invariant surface features data (topography, vegetation and soil type). NESTOR is also where the size and grid of the RCM integration domain are defined.

4.2.2.1. Lateral Boundary Conditions

The lateral boundary conditions (LBCs) that are used to force a nested RCM can be provided either by a GCM or by a reanalysis dataset (Marbaix *et al.*, 2003). Reanalyses are more reliable than direct GCM outputs because meteorological data (temperature, humidity, wind and surface pressure) are assimilated every 6 hours into the global model. These correctional observations stem from multiple sources, including radiosondes, satellites, ships, and aircraft (Yu *et al.*, 2010).

In this study, the one-way nested MAR model was forced every 6 hours at its lateral boundaries with the following forcing fields: humidity, temperature and wind at each vertical level, and sea surface temperature (SST) above the ocean. The forcings fields were provided by two different reanalysis datasets:

- the ERA reanalysis from the European Centre for Medium-Range Weather Forecast (ECMWF);
- the NCEP/NCAR reanalysis from the National Center for Environmental Prediction (NCEP) and the National Center for Atmospheric Research (NCAR).

Between 1960 and 1978 we used the ERA-40 reanalysis, which is available from September 1957 to August 2002 with a regular horizontal grid resolution of 1.125° in latitude/longitude (about 125x125 km). From 1979 onwards, we used the ERA-Interim reanalysis, which spatial resolution is 0.75° (about 80x80 km). For further information about ECMWF reanalyses, we refer to Dee *et al.*, 2011.

The reanalysis 2 of NCEP/NCAR used in this study has a coarser spatial resolution of 2.5° (about 280x280 km). Its temporal coverage starts January 1979 and extends to the present day. This is because NCEP/NCAR-v2 is an improved version of NCEP/NCAR-v1 thanks to the assimilation of observational satellite data, which started only in 1979 (Yu *et al.*, 2010).

There are two purposes for using two different reanalyses in this work. The first is to assess the reliability of each reanalysis, as the ERA and the NCEP/NCAR each have their strengths and weaknesses. The ECMWF reanalysis has the advantage of being produced at a higher spatial resolution than the NCEP/NCAR reanalysis. However, the introduction since 1979 of satellite based observational corrections on the ECMWF data strongly affects the homogeneity of the time series. The second reason we used both ERA and NCEP/NCAR reanalyses is linked to the evaluation of the MAR model. Indeed, if the MAR yields similar results in terms of tendencies of temperature or precipitation with both reanalyses, this will support the model validation in this area where the reanalyses are poorly constrained by observations.

4.2.2.2. Domain size and resolution

The choice of the most suitable domain for the nested RCM is constrained by three main conditions.

(i) On the one hand, it is desirable to select a spatial domain that differs significantly from GCMs in terms of spatial resolution, so that RCMs can capture the relevant small-scale processes. This is precisely what provides the added value to the regional simulation by comparison with the global simulation (Marbaix *et al.*, 2003; Giorgi, 2011). This purpose needs a domain that is not too large though, otherwise it would require too much computational time and memory.

(ii) On the other hand, the domain should be large enough to allow the RCM to fully develop its own internal circulation dynamics (Giorgi, 2011; Alves & Marengo, 2010). For instance, if the domain is too small, the model will fail simulating enough precipitation. Indeed, large-scale driven precipitation will not be forced at the boundaries of the domain, but will only be produced by the model's inherent cloud scheme which uses specific humidity as a forcing (Lang, 2011). Therefore, both size and location of the domain should depend on the dominant large-scale circulation pattern.

The choice of the domain size is an important issue in the model setup process, because domain size is partly responsible for the internal variability of the RCM, which may be misinterpreted as a real signal (Giorgi, 2011). For this reason it is recommended to run several test simulations with different integration domain sizes until the model results stop varying as a function of domain size in our area of interest.

(iii) Finally, strong local forcing, such as the presence of high topographic features for instance, ought to be avoided near the lateral boundaries, because this could lead to severe inconsistencies between the RCM and the GCM flow fields (Marbaix *et al.*, 2003). These artefacts occur when the atmospheric part of the RCM is represented in a hydrostatic system, which is the case of the MAR model. In such a coordinate system, the vertical layers of the atmosphere follow the topography and have thus different thicknesses, the layers closer to the surface being thinner than the higher ones.

In short, a compromise has to be reached between domain size and resolution. Since no well-defined strategy nor rule exist, the choice of the model's configuration is left to the discretion of the modeler, provided that the dependence of the model results toward the model configuration is made as minimal as possible (Giorgi, 2011).

Results

(i) Considering the first of these conditions, the domain in our simulations was set at a horizontal resolution of 5 km, which is the finest resolution at which the MAR model can reliably be run as it uses the hydrostatic hypothesis. As stated earlier in the introduction, this aspect of the study is quite original since to date no regional climate model has been implemented or assessed over the Bolivian Andes at such a high resolution. A 5 km resolution modeling is expected to help better understanding the regional climate of the Bolivian Andes by resolving small-scale climatic

processes such as orographically-induced precipitation, cloudiness, elevation-related temperature and humidity gradients, etc. Unfortunately, in the specific case of the very small-sized Chacaltaya Glacier, a 5 km resolution is still to coarse to study the former glacier's mass balance. For this reason, we referred to several well-documented works which present mass balance evolution results from monitoring campaigns performed throughout the 30 last years on the Chacaltaya Glacier (Francou *et al.*, 2000, 2003; Ramirez *et al.*, 2001).

(ii) Regarding the second condition, the approximate location of the domain was firstly determined by analysing the large-scale circulation pattern at low- and at high-level over the South American continent (Figures 4.5 and 4.6). Knowing that the Bolivian climate is dominated by two seasons in terms of pluviometry, we studied the mean general circulation patterns for January and July, these months being in the middle of the wet and the dry season respectively.

Moisture and precipitation distribution across the tropical Andes are mainly driven by two different air masses associated respectively with two large-scale anticyclonic gyres that frame the South American continent: the subtropical high over the Southeast Pacific Ocean to the west, and the subtropical high over the South Atlantic Ocean to the east. As can be observed in Figure 4.6, the Andes mountains have a powerful dividing effect on the low-level atmospheric circulation, as they form a physical barrier between the dry Pacific air to the west, and the moist Atlantic air to the east.

During the austral summer (January), the high-level circulation over the tropical Andes is dominated by the Bolivian High (BH), a quasi-stationary anticyclone centered approximately at 18°S, 68°W over the Bolivian Altiplano, as illustrated in Figure 4.5. This high pressure system results from the intense convective latent heat release over the Amazon Basin, and from the intense solar heating of the Altiplano surface. At low levels, moist air is advected from the Atlantic Ocean toward the northwestern part of the continent by the northeasterly trade winds. While flowing westward over the continent, these air masses lose some of their moisture through precipitation, but also regain large amounts of water vapor through the intense evapotranspiration of the Amazonian rainforest. Further inland, the Andes mountains curve and channel the trade winds toward the south into a northwesterly Low-Level Jet (LLJ), which is well represented in Figure 4.6. This low-level flow is responsible for heavy precipitation over the eastern slope of the Andes. A small part of the moisture transported by the LLJ yet overflows the eastern peaks of the Andes Cordillera and provides just enough water vapor to develop, combined with the BH, convective clouds and precipitation over the highest elevations of the Bolivian Altiplano.

During the austral winter (July), as the easterly trade winds retreat northward with the Intertropical Convergence Zone (ITCZ), and as the South Atlantic High moves to the east (Figure 4.6), the South American continent receives less moisture from the ocean. The low-level atmospheric circulation is hence dominated by the more stable Southeast Pacific High and its associated cold oceanic Humboldt Current, which define very dry conditions over the western part of the tropical Andes. In the upper levels (Figure 4.5), the northward shift of the subtropical jet stream makes a strong westerly flow prevail over the tropical latitudes.

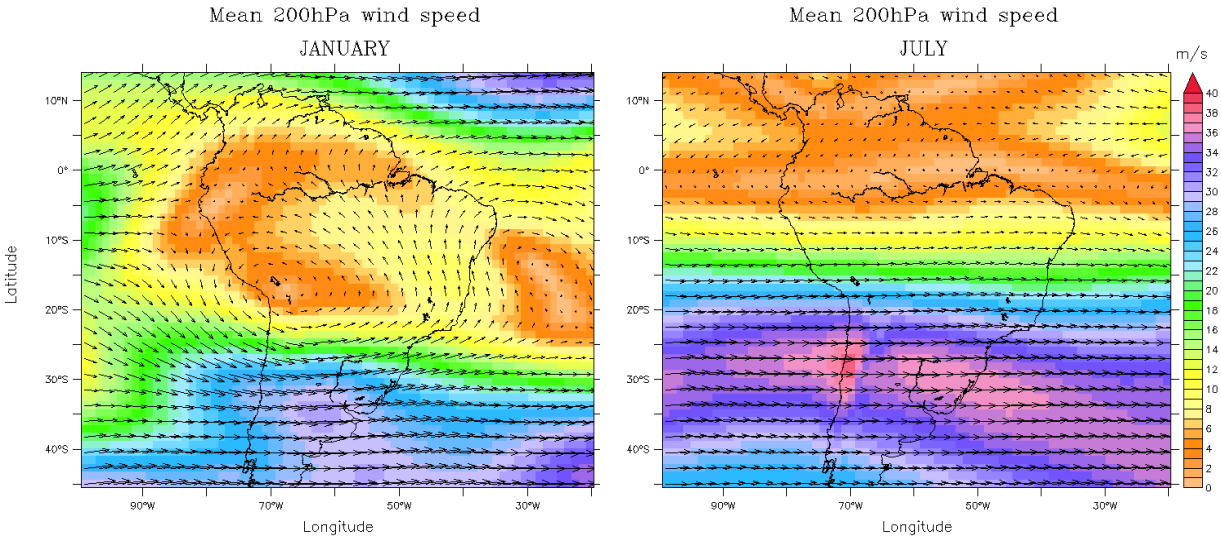

Figure 4.5: Mean (1980-2009) 200 hPa wind speed (m/s) in January and July from ERA-Interim. Arrows indicate wind direction.

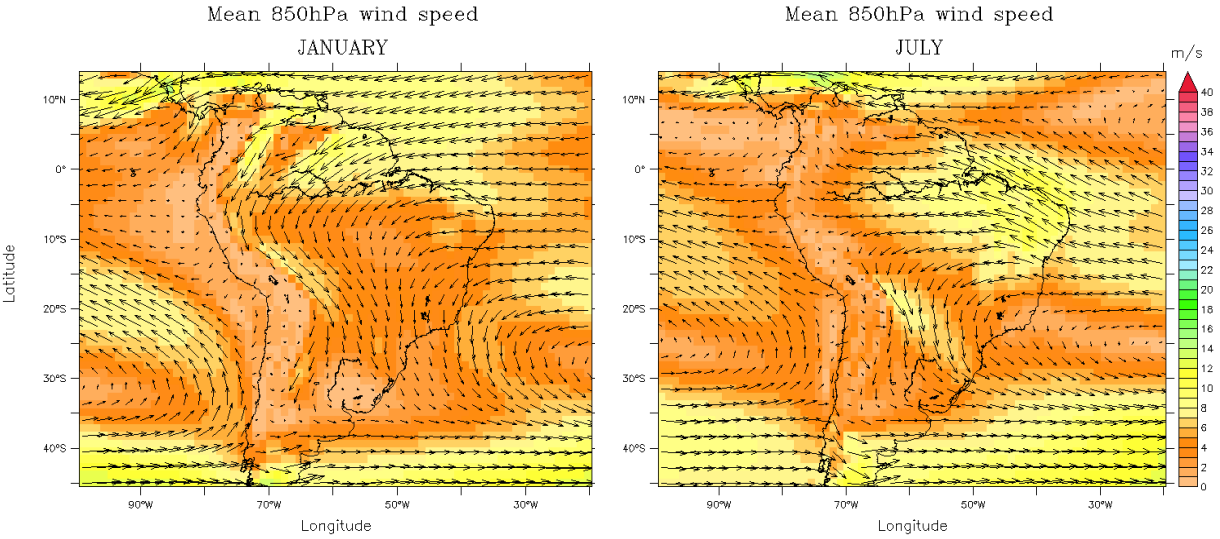

Figure 4.6: Mean (1980-2009) 850 hPa wind speed (m/s) in January and July from ERA-Interim. Arrows indicate wind direction.

Considering these circulational features, our domain ought to be large enough to include both sides of the Andes Cordillera, so as to account for the two major antagonist atmospheric influences, i.e. the Pacific air masses and the Atlantico-amazonian air masses.

Thereafter, in order to fix the domain size, we compared by pairs simulated amounts of precipitation at different domain sizes. The test simulations were performed for January of year 2000; the choice of the year was random, but the month was chosen because it is situated in the middle of the rainy season. We started calculating the total amount of precipitation only from the eleventh day of the month, in order to remove the spin-up time of the atmosphere, which is about ten days. Table 4.1 summarizes the size (in pixels) of the five tested domains.

Domain	A	B	C	D	E
Size (pixels)	60x60	70x70	80x80	90x90	100x100

Table 4.1: Size (in pixels) of the different tested domains.

As can be seen in Figure 4.7, which shows the precipitation difference (mm) over Domains A to D with respect to Domain E, the anomaly in precipitation is the most attenuated in pair D-E. Therefore, we decided to work with Domain D. The grid resolution being 5 km, the domain is thus 450x450 km wide.

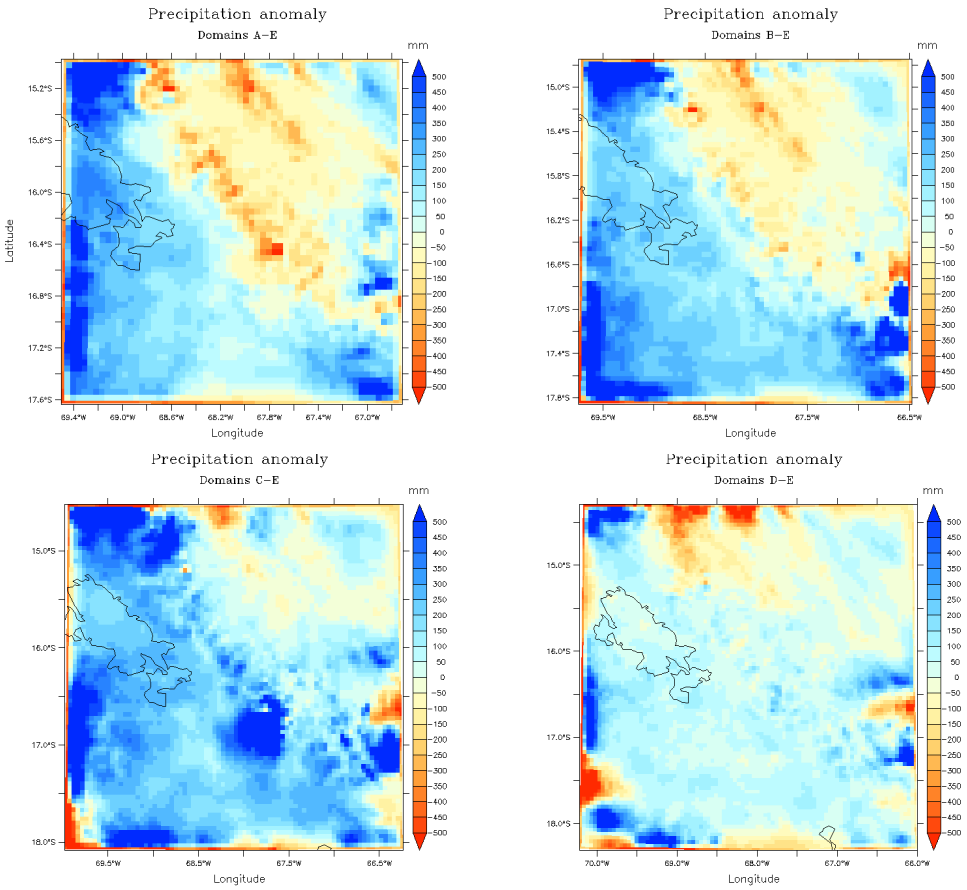

Figure 4.7: Precipitation difference between domains of different sizes (Domains A to D) with respect to the largest (Domain E).

(iii) Eventually, according to the third condition, the definite location of the domain was fixed so as to place the highest part of the Oriental Cordillera in the center of the studied area, thereby avoiding a maximum of the edge effects due to elevation gradients in the MAR lateral boundaries. Nonetheless, because of its extraordinary length, the Andean range still crosses the northern and the southern boundaries of our integration domain. Consequently, when discussing the model results, attention must be paid to the potential inconsistencies that may originate from this unavoidable issue.

The chosen domain is centered on the Chacaltaya Mountain (Cordillera Real) and extends from about 18.3°S to 14.3°S and 70.2°W to 66.0°W.

4.2.2.3. Relaxation schemes

The lateral boundary between a nested RCM and its encompassing GCM is referred to as the "relaxation zone". In this zone distorsions in mass and energy fluxes often arise because of the abrupt change in grid spacing and wind direction between the RCM and the GCM. Several relaxation functions can be applied to smooth the blending between the large-scale lateral boundary conditions (LBCs) and the highly resolved RCM domain (Zhong *et al.*, 2010). The size of the relaxation zone generally varies depending on the size of the model domain. In the MAR model, the relaxation zone is fixed at a width of 7 grid cells (pixels). However, this makes a too short transition from the LBCs to the model solution, so that errors might persist close to the edges of the RCM domain. Therefore, an additional buffer zone is delimited around the model domain, in which data should not be used. In this study, as our domain is rather small, a buffer zone of 10 pixels wide is applied.

Once the buffer zone removed, the final domain extends from about 17.9°S to 14.8°S and 69.8°W to 66.5°W.

Relaxation schemes also have a time component. The spin-up time is the duration time the model needs to be run so as to become independent of its initial conditions. The results yielded by the model during the spin-up time are thus unusable. In our study, one simulation of two years was run for each individual year, and the first year of each simulation was excluded in order to avoid spin-up problems. For example, for running year 1985 we started the simulation the 1st January 1984, so that 1984 was the unusable spin-up year, while 1985 could be used as final result. The strategy of running all years simultaneously allowed to gain considerable computation time, since MAR can simultaneously use 8 CPU maximum, and we had access to several hundreds of CPU on the supercomputer NIC3 from ULg.

4.2.2.4. Surface features data

NESTOR prepares the topographic fields for MAR from ETOPO1, a 1 arc-minute global relief model of the earth's surface. If we compare the MAR topography (Figure 4.8) with the ERA reanalysis topography (Figure 4.2), it plainly appears how much better MAR resolves the orographic features of the study area.

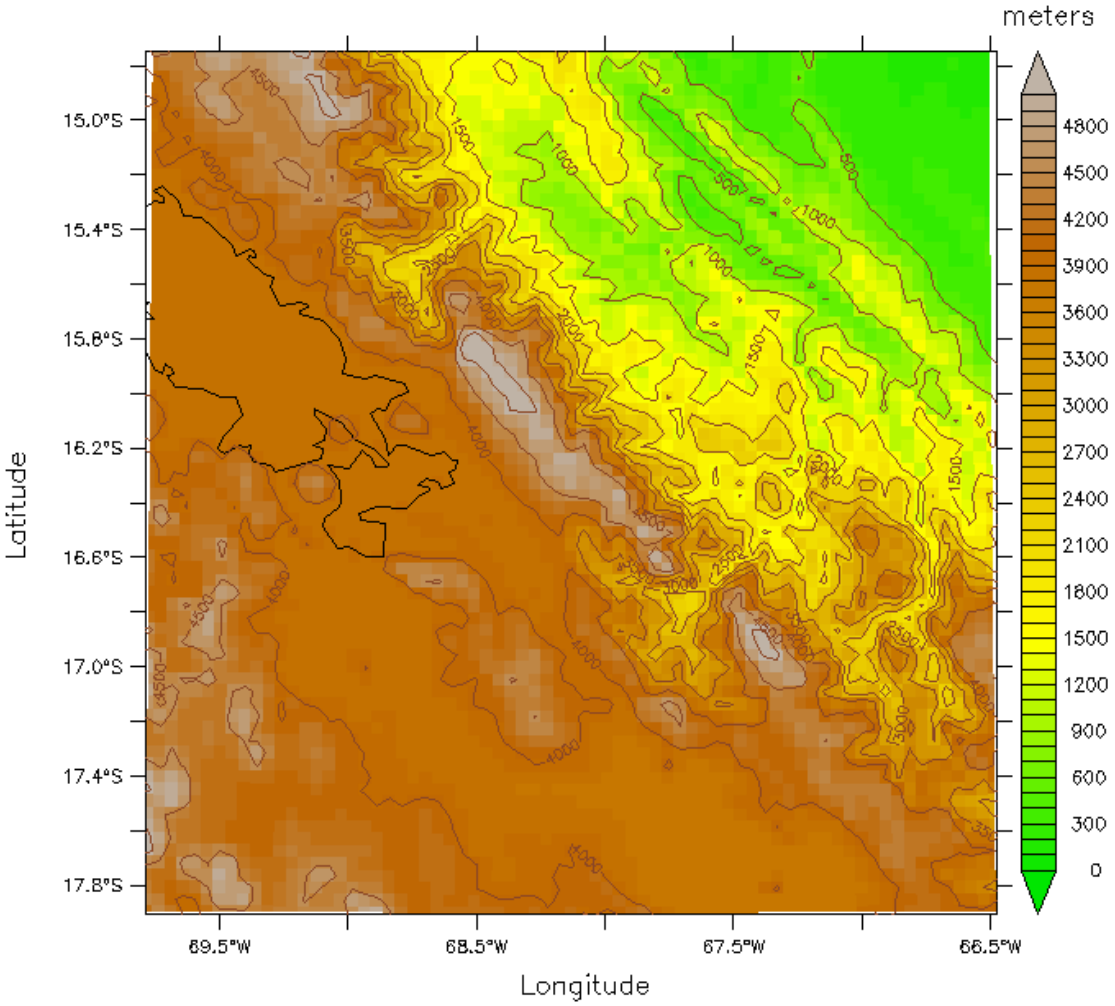

Figure 4.8: Topography of the final domain used by MAR at 5 km resolution. The brown lines are the lines of equal altitude.

Besides the topographic field, MAR also includes a soil type field, in which four different soil types are defined: land, sea, permanent ice (ice sheet), and sea ice. However, Lake Titicaca was represented in the MAR model as a land surface. This had to be rectified because the lake has a strong influence on the regional climate. Indeed, with a surface area covering more than 8,300 km², Lake Titicaca could not be overlooked. Therefore, a mask was created in order to assign the "sea" surface type to the lake (Figure 4.9).

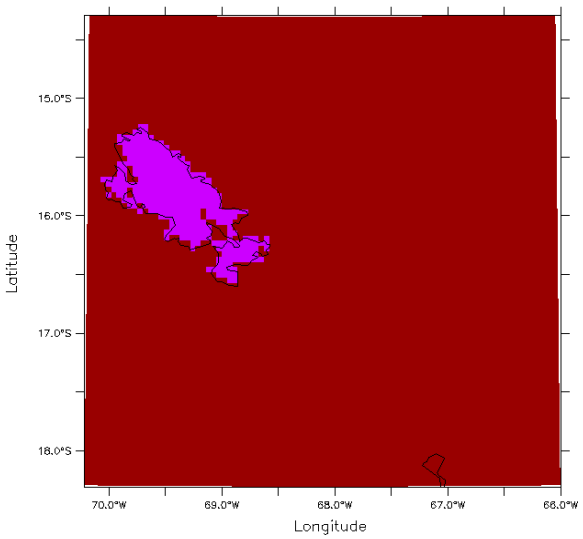

Figure 4.9: Land-sea mask created by NESTOR. In red, the land surface; in pink, the sea area.

4.2.2.5. Model calibration

Model calibration or model tuning is the last step of the model configuration process, wherein selected numerical or physical parameters are adjusted so as to better match the model results with the available in situ observations. Comparing model outputs to observational data is the common way to judge the model's ability in reproducing the climate of a studied area.

In practice, model calibration follows no objective procedure: it is often subjectively performed in manually adjusting one or several parameters of the model, such as wind and pressure fields, sea-ice volume, or cloud properties. By doing so, problems may arise if one omits considering parameter interaction (Bellprat *et al.*, 2012). For instance, adjusting the near-surface air temperature field inevitably leads to a modification of evaporation and precipitation, both parameters which depend non-linearly on temperature. Hence it has always to be remembered that no parameter can be tuned without altering other variables of the climatic system.

Furthermore, care has to be taken to ensure that calibration is not a way of artificially masking the deficiencies of the model (Bellprat *et al.*, 2012). When tuning a model so as it fits observations in a particular context (region or period), the probability is high that the model will no more be effective once applied to another context. In this study for instance, the MAR lateral boundaries were corrected in order to reproduce with MAR the coolness and the dryness which characterizes the climate in the highest elevations of the Andes (> 4000 meters a.s.l.). As a consequence, in the less elevated portions of the domain, like on the edges of the Andean Cordillera or in the valleys, the model yielded less satisfactory results (see section 5.3). While this did not invalidate the model for the conditions for which it was calibrated, it yet revealed its lack of robustness.

Therefore it is essential to be utterly transparent about the model calibration procedure, so that when ulteriorly comparing the model results to other models, it can be assessed whether the model performance actually reflects an improved modeling structure, or whether it only derives from skillful tuning efforts (Bellprat *et al.*, 2012).

In our case, some corrections were applied to the MAR lateral boundaries only because our MAR domain is small (< 500 km) and is thus strongly constrained by the LBCs. However, since very few observations are assimilated into the reanalyses in this part of the world, the reanalyses are consequently a lot of less reliable over this area than over Europe for example. As MAR works well over Europe and the polar regions when using the same forcing (LBC), we can reasonably assume that a large part of the discrepancies between MAR and the observations may be related to the reanalysis based forcing itself. Besides, when we first tested MAR without applying any LBC corrections, the model did not work well at all, which supports our assumption.

Table 4.2 resumes the different tunings tested with the ERA and the NCEP/NCAR reanalyses used as LBCs. Three parameters were calibrated: air specific humidity, air temperature and MAR topography in the relaxation zone.

In Test 4, we forced a constant topography at the boundaries of the MAR domain so as to check if the crossing of the Andes mountain range in the northern and the southern boundaries affected our simulations by introducing artefacts, as mentioned in section 4.2.2.2.

Test	Reanalysis	Simulation period	Calibrated parameters		
			Humidity	Temperature	LSC
Test 1	ERA-Interim	1 Jan 1960 – 31 Dec 2014	-10%	+ 3°C	-
Test 2	NCEP2	1 Jan 1980 – 31 Dec 1989	-10%	+ 3°C	-
Test 3	NCEP2	1 Jan 1980 – 31 Dec 1989	-15%	+ 3°C	-
Test 4	NCEP2	1 Jan 1980 – 31 Dec 1989	-15%	+ 3°C	Topography constant at boundaries
Test 5	NCEP2	1 Jan 1980 – 31 Dec 1989	-15%	+ 4°C	-

Table 4.2: Different tunings tested for air relative humidity, air temperature and lateral surface condition (LSC), with the ERA-Interim and the NCEP/NCAR-v2 reanalyses.

Actually, four other tunings were tested with the ERA reanalysis, but we present here only the one that yielded the best results. The other tests performed with the NCEP/NCAR-v2 reanalysis are only showed in this study to demonstrate their inefficiency when applied to our study area, as will be discussed in the next chapter (section 5.2).

4.2.3. Outputs

The MAR model outputs are annual (1-January to 31-December) NetCDF files containing a daily mean value for each pixel and for a list of simulated variables. Table 4.3 resumes the variables that were selected and used in this study.

Modeled variable	Unit
Model surface height (topography)	m
Near-surface temperature: daily average, minimum and maximum	°C
Total amount of rainfall	mm/day
Total amount of snowfall	mm/day
Total amount of convective precipitation	mm/day
Surface pressure	hPa
Wind speed	m/s
Relative humidity	%
Specific humidity	g/kg
Short-wave fluxes: upward and downward	W/m^2
Long-wave fluxes: upward and downward	W/m^2
Sensible heat flux	W/m^2
Latent heat flux	W/m^2
Albedo	-
Cloud cover: total, upper, middle and lower	-
Cloud optical depth	-
Geopotential height of each pressure level	m
Temperature at pressure levels	°C
Specific humidity at pressure levels	g/kg
Wind speed at pressure levels	m/s

Table 4.3: List of the variables simulated by MAR and used in this study.

All variables excepting the last four listed in Table 4.3 were simulated in a sigma-coordinate system (see section 4.2.1). In the chapter of results, we present the surface and near-surface variables for the first vertical atmospheric level, which is set at about 3 meters above the ground.

The last four variables listed in Table 4.3 were simulated in a non-normalized pressure coordinate system. Each of these variables could be displayed for seven distinct pressure levels, ranging from 925 hPa to 300 hPa.

5. Evaluation of the MAR model

The evaluation of a RCM is performed by running the model for some period in the past and by checking its ability to reproduce the climate over this period. The performance of the model is then assessed by comparing the model outputs with meteorological observations (reference data).

At this point, it is important to remember that models operate on grid cells, while observational data stem from measurements at individual stations. Model outputs thus need to be interpreted as mean values over each grid area (in our case 5 km^2), which inevitably implies a spatial smoothing of local extremes (Kotlarski, 2014).

This is why modelers generally prefer using gridded reference data. These can be obtained by interpolating single-station measurements onto a regular grid, but this process is subject to strong uncertainties. Moreover, as will be detailed in the next section 5.1.1., the study area of this work, i.e. the Bolivian Andes, has a very low station density. Interpolating data would hence lead to considerable smoothing of spatial variability. Another way to get gridded reference data is by using reanalysis products or remote-sensing products. However, both products involve models and hence approximations which increase data uncertainty. Besides, those products can not achieve the high spatial resolution of the MAR model, so the issue of scale mismatch between the MAR outputs and reference data remains. Accordingly, we chose to not look at gridded reference data, and we used exclusively station-based observations, even if they are spatially scarce.

5.1. Observational data

5.1.1. Source and availability of data

The observational data used as reference data in this study are provided by LACA&D (Latin American Climate Assessment & Dataset). LACA&D is the result of a collaboration between several meteorological institutes throughout Latin America, as well as the Royal Netherlands Meteorological Institute KNMI, and the CIIFEN, the international center for research on the El Niño phenomenon. The LACA dataset consists of daily observation series obtained from meteorological stations which are maintained by observatories and research centers. For Bolivia, the data provider is the SENAMHI (Servicio Nacional de Meteorologia e Hidrologia), a state decentralized technical agency whose mission is to collect and to disseminate (agro)-meteorological and hydrological information.

The Andes and particularly the Bolivian Andes have a very low density of weather stations. Inside our study area, only six stations have been identified, and five of them are located in the Altiplano. The only station which lies in the Cordillera Real is Huarina Cota Cota. Furthermore, the temporal coverage of the time series is rather limited, and only monthly data are available. One positive point at least is that the longest data series stems from the city of La Paz, the capital of Bolivia, which is located less than 30 km from the Chacaltaya, just at the rim of the Cordillera.

An exception is made for one station, La Paz / El Alto, whose data series does not stem from the LACA&D but from the WMO (World Meteorological Organization) dataset. Actually, La Paz / El Alto is the only station of our study area which is registered by WMO, and it has the advantage to provide surface pressure data, which is not the case of the LACA&D series.

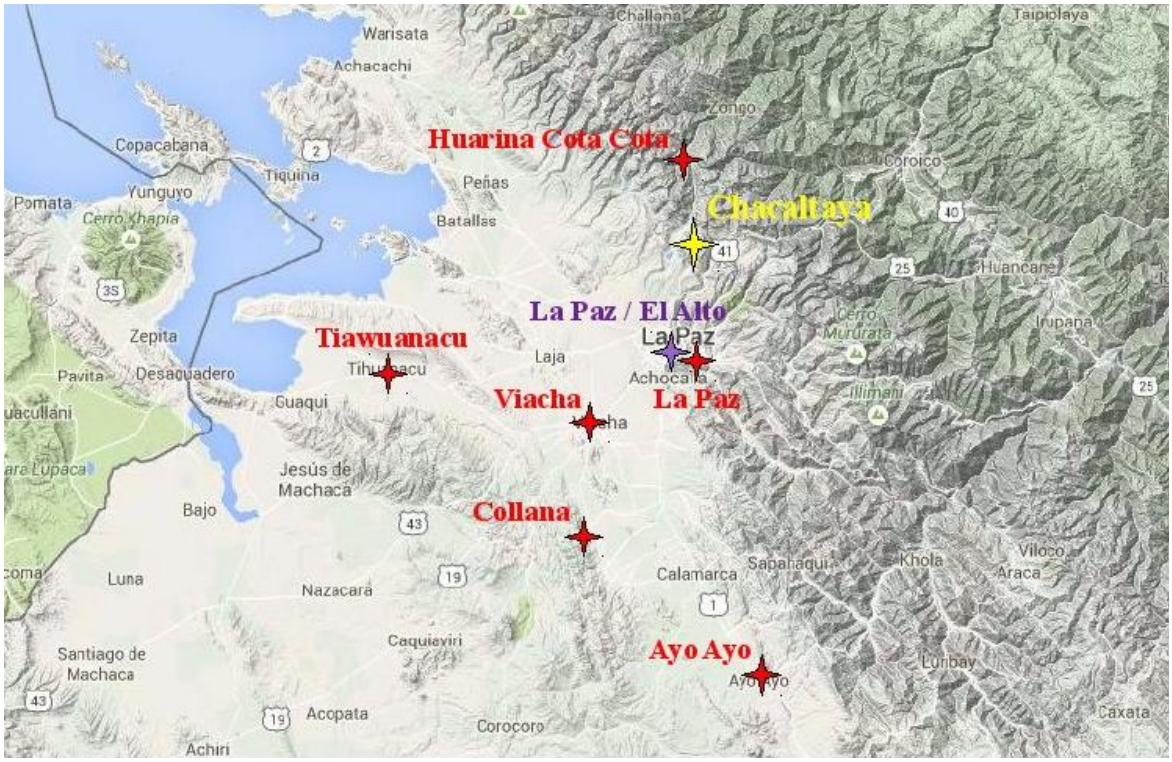

Figure 5.1: Location of the seven stations whose series were used as reference data in the MAR evaluation process. In red, the LACA&D stations. In purple, the WMO station. In yellow, the Chacaltaya Mountain. The water body in the upper left corner is the lake Titicaca.

5.1.2. Reliability of data

The series collected by LACA&D are submitted to quality controls as well as homogeneity tests. The quality control procedure leads to the assignation of three possible flags to individual daily data: “valid”, “suspect” or “missing”. However, some errors may remain undetected, and the risk is greatest for recent data that stem from synoptic messages, because these series did not undergo the validation process.

Besides, changes in observation device may have introduced artefacts of non-climatic origin in long-time series. Also, stations may have been moved in the past to another location whose site characteristics differ from the previous location. Elevation, orientation and localization of the stations with respect to the site configuration are all aspects which significantly impact on climatic conditions measured at the micro-local scale. It is especially true for high mountainous regions such as the Andes, where the steep slopes create strong gradients in temperature and precipitation,

while also being responsible for shadowing effects. As regards the instrumental part of observation device, errors can also result from a bad calibration or from the installation of new instrumentation whose improved technology allows better measurements. Unfortunately, information about site characteristics and measurement device most often lack in weather and climate databases, so that there is no mean to assess how much they contribute to the errors.

This is why the data series collected by LACA&D undergo a homogeneity evaluation. Several common tests are applied to assess homogeneity in both temperature and precipitation series (for more information about these tests, we refer to the *Algorithm Theoretical Basis Document*). Then, the series are classified according to the following flags: “useful”, “doubtful”, “suspect” and “not enough data”. The results of the homogeneity tests are only informative though, since the series are not homogenized in the sense that values are changed. Still, it provides precious information about the reliability of the data.

As can be seen in Table 5.1, observational data is more reliable for precipitation than for temperature. However, both precipitation and temperature series will be used as reference data to evaluate the MAR model, because they are the only observational data we have. Nevertheless, the information provided by the homogeneity tests will help us to think critically when comparing the model outputs to these data series.

Isolated missing values were replaced by interpolation. If more than three consecutive months were missing, the gap was left unchanged and the corresponding values were not taken into account in our calculations.

Station	Temperature series		Precipitation series	
	Length	Homogeneity	Length	Homogeneity
Ayo Ayo	1958-1978	not enough data	1953-1978	suspect
	1979-2006	suspect	1979-2006	useful
Collana	1973-1978	not enough data	1973-1978	not enough data
	1979-2006	useful	1979-2006	useful
Huarina Cota	1973-2006	not enough data	1973-1978	not enough data
			1979-2006	useful
La Paz	1952-1978	not enough data	1952-2009	useful
	1979-2009	suspect		
Tiawuanacu	1974-2006	not enough data	1974-1978	not enough data
			1979-2006	useful
Viacha	1987-2006	not enough data	1987-2006	not enough data

Table 5.1: Availability and homogeneity of the data series used for our model evaluation. Data series that are tagged as “useful” are shaded in green and are the most reliable series.

5.2. Test simulations

5.2.1. Surface pressure and surface height

Before assessing the ability of the model to properly simulate precipitation and temperature variability, one has first to account for surface height biases between the weather station and the MAR pixel representing this weather station. This is particularly relevant for regions characterized by a complex topography like the Andes. Indeed, even with a resolution of 5 km, the MAR model can not resolve the details of its domain's orography.

At first, we had to select the corresponding MAR pixel for each reference station. This required a compromise between two criteria. The first condition was to choose the closest pixel to each station: this was done by comparing the distance in latitude/longitude between the station and the center of the nearest MAR pixels. The second condition was to minimize the surface height deviation between the station and the closest pixel.

Station	Latitude (°S)		Longitude (°W)		Distance (km)	Elevation (m)		
	Station	Pixel	Station	Pixel	Pixel-Station	Station	Pixel	Δ(m)
Ayo Ayo	17.08	17.09	68.00	67.99	2.2	3880	3915	+35
Collana	16.85	16.87	68.33	68.36	4.4	3940	4115	+175
Huarina Cota	16.20	16.20	68.13	68.13	0.0	3825	4343	+518
La Paz	16.53	16.55	68.13	68.13	2.2	3632	3628	-4
Tiawuanacu	16.55	16.55	68.68	68.68	0.0	3629	3871	+242
Viacha	16.65	16.64	68.30	68.32	2.2	3850	3875	+25
La Paz / El Alto*	16.50	16.50	68.18	68.18	0.0	4050	4016	-34
	16.51		68.18		2.2	4071		-55

Table 5.2: Reference stations used for the evaluation of MAR, with station coordinates, coordinates of the corresponding pixel in the MAR model, elevation of the station, elevation of the pixel in the MAR model. Elevation is expressed in meters above sea level.

* Note that La Paz / El Alto station changed location in the course of March 1985, so that its elevation also changed from 4050 meters to 4071 meters, increasing thus the deviation to the modeled surface height.

As can be seen in Table 5.2, MAR overestimates surface height for all stations except La Paz and La Paz / El Alto. This bias will have to be taken into account when comparing the model outputs to the observations, especially for the stations where the deviation exceeds 100 meters. Indeed, a difference in surface height directly influences surface pressure, temperature and precipitation.

For example, the surface pressure simulated by MAR forced with the ERA reanalysis (Test 1 in Table 4.2) over 1980-1989 at La Paz / El Alto is on average about 4.5 hPa higher than the measured surface pressure, although the elevation bias between MAR and the observation is less than 100 meters. Consequently, considering the fact that the station was moved to another location in the middle of the analysed period, causing the elevation bias to change from -34 meters to -55 meters, which makes an average bias of -45 meters, we can assess that the surface pressure gradient with respect to an increase of altitude is of – 1 hPa every 10 meters.

In order to investigate the reasons behind the bias between the modeled and the observed surface pressure, we also analysed the pressure fields from the ERA reanalysis itself. The surface pressure at La Paz / El Alto is on average (1980-1989) about 35 hPa higher in the ERA reanalysis than in the observations. We finally included the NCEP2 reanalysis in our comparison study and found out that the NCEP2 surface pressure fields are even worse than those from the ERA-Interim, i.e. About 85 hPa higher than the observed values. However, as can be seen in Figure 5.2, the temporal variability of the surface pressure is properly reproduced by both reanalyses. These outcomings provide the first evidence of the poor reliability of the reanalyses over our study area, which is due to their coarse horizontal resolution.

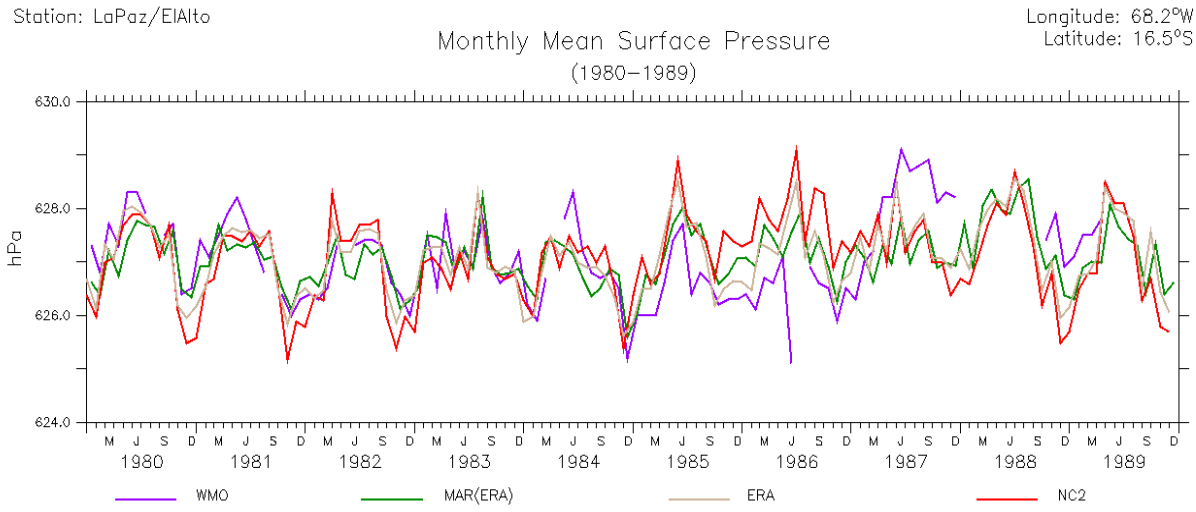

Figure 5.2: Monthly surface pressure (hPa) over the 1980-1989 period for La Paz / El Alto. The mean bias was substracted from the ERA and NCEP2 values. Purple is for the observations (WMO), dark green is for MAR forced with ERA-Interim, grey is for the ERA-Interim reanalysis, and red is for the NCEP2 reanalysis. The discontinuities in the observed values are due to missing data.

5.2.2. Precipitation and temperature

5.2.2.1. MAR forced with several reanalyses

For each LACA&D station and for each calibration, we calculated the mean annual bias and the correlation coefficient between the MAR outputs and the observational data, using the five different corrections of the LBCs that were tested with the ERA and the NCEP/NCAR reanalyses. The corrections and the reanalysis used for each test are detailed in Table 4.2.

It seems appropriate to mention that the correlations were calculated over 10 years but from the monthly values, i.e. a total of 120 values for each station, which gives statistically relevant results.

First of all, it is important to observe that Test 4, wherein we forced a constant topography at the boundaries, provides no better results than those of the other tests, which demonstrates that the crossing of the Andes mountain range at the boundaries of the MAR domain does not affect our simulations.

Figures 5.3 and 5.4 illustrate the monthly evolution of precipitation and temperature over the 1980-1989 period. At first glance, it appears that all tests reproduce reasonably well the annual cycle of precipitation and temperature, with maximum precipitation and temperature occuring during the austral summer (DJF), and minimum precipitation and temperature during the austral winter (JJA). A closer look however reveals that all four tests performed with the NCEP2 reanalysis fail to adequately recreate the interannual variability of precipitation. More precisely, the droughts of years 1982-1983 and 1988-1989, linked to major El Niño events, are totally omitted by MAR when forced with the NCEP2 reanalysis. It is yet crucial that these extreme events be properly simulated by the model, since they are currently acknowledged to have played an important role in the accelerated retreat of tropical glaciers in South America. When forced with the ERA reanalysis, MAR is able to simulate the climate variability associated to these extreme ENSO events. Table 5.4 shows that while NCEP2-forced MAR barely achieves correlations of 0.60 at best, ERA-forced MAR exhibits correlation coefficients ranging from about 0.70 to 0.80.

Regarding near-surface air temperature, the results are all very satisfactory, with correlation coefficients almost all higher than 0.80 and often near 0.95, and no test being significantly better than the others.

Given these results, and as precipitation data is more reliable in observations than temperature data (see Table 5.1), we decided to study here the outputs of the simulation that provides the best results for precipitation, which is the one forced with the ERA reanalysis (Test 1).

Precipitation

Station	Δ(%)					STD (%)
	Test 1	Test 2	Test 3	Test 4	Test 5	Obs
Ayo Ayo	-52.9	+130.7	+65.8	+64.2	-6.8	106.5
Collana	-56.2	+101.0	+42.9	+41.2	-14.7	103.1
Huarina Cota	+60.3	+237.5	+64.5	+142.7	+64.5	108.6
La Paz	-50.8	+22.9	-14.5	-16.3	-50.4	103.3
Tiawuanacu	-64.1	+39.7	-4.0	-3.5	-44.6	96.9

Table 5.3: Mean differences (Δ) over 1980-1989 between the modeled monthly precipitation rates and the corresponding observations. Units are given is percent of the monthly mean observed precipitation rate. Monthly variability (gauged by the standard deviation of the monthly values) is listed in the last row.

Station	CC				
	Test 1	Test 2	Test 3	Test 4	Test 5
Ayo Ayo	0.80	0.59	0.64	0.62	0.59
Collana	0.83	0.61	0.62	0.61	0.57
Huarina Cota	0.70	0.61	0.53	0.59	0.53
La Paz	0.80	0.48	0.55	0.55	0.54
Tiawuanacu	0.74	0.55	0.58	0.57	0.59

Table 5.4: Correlation coefficients (CC) over 1980-1989 between the modeled monthly precipitation rates and the corresponding observations. Values in green show the most satisfactory correlation coefficients.

Near-surface air temperature

Station	Δ(°C)				
	Test 1	Test 2	Test 3	Test 4	Test 5
Ayo Ayo	+1.8	+0.5	+0.3	+0.3	+1.1
Collana	-0.7	-1.7	-1.9	-1.9	-1.0
Huarina Cota	-1.5	-2.4	-1.7	-2.5	-1.7
La Paz	+0.4	-1.0	-1.0	-1.0	0.0
Tiawuanacu	+2.6	+0.9	+0.6	+0.6	+1.5

Table 5.5: Mean differences (Δ) over 1980-1989 between the modeled monthly near-surface air temperatures and the corresponding observations.

Station	CC				
	Test 1	Test 2	Test 3	Test 4	Test 5
Ayo Ayo	0.95	0.94	0.94	0.94	0.94
Collana	0.96	0.96	0.96	0.96	0.96
Huarina Cota	0.81	0.79	0.81	0.80	0.81
La Paz	0.91	0.89	0.90	0.90	0.89
Tiawuanacu	0.86	0.87	0.87	0.87	0.87

Table 5.6: Correlation coefficients (CC) over 1980-1989 between the modeled monthly near-surface air temperatures and the corresponding observations.

a)

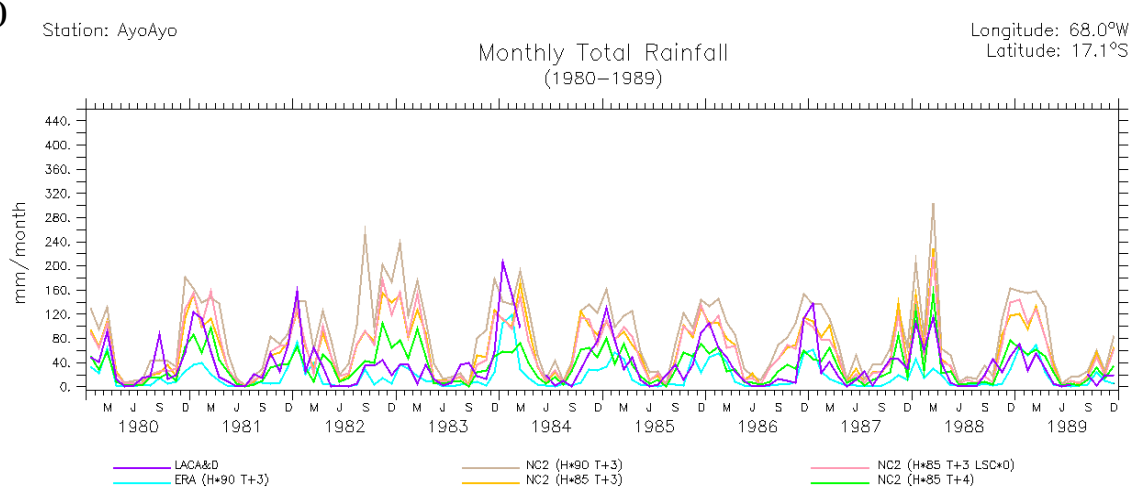
Station: AyoAyo
Longitude: 68.0°W
Latitude: 17.1°S
Monthly Total Rainfall
(1980–1989)
mm/month
440.
400.
360.
320.
280.
240.
200.
160.
120.
80.
40.
0.
M J S D M J S D M J S D M J S D M J S D M J S D M J S D M J S D M J S D
1980 1981 1982 1983 1984 1985 1986 1987 1988 1989
LACA&D
ERA (H*90 T+3)
NC2 (H*90 T+3)
NC2 (H*85 T+3)
NC2 (H*85 T+3 LSC*0)
NC2 (H*85 T+4)

b)

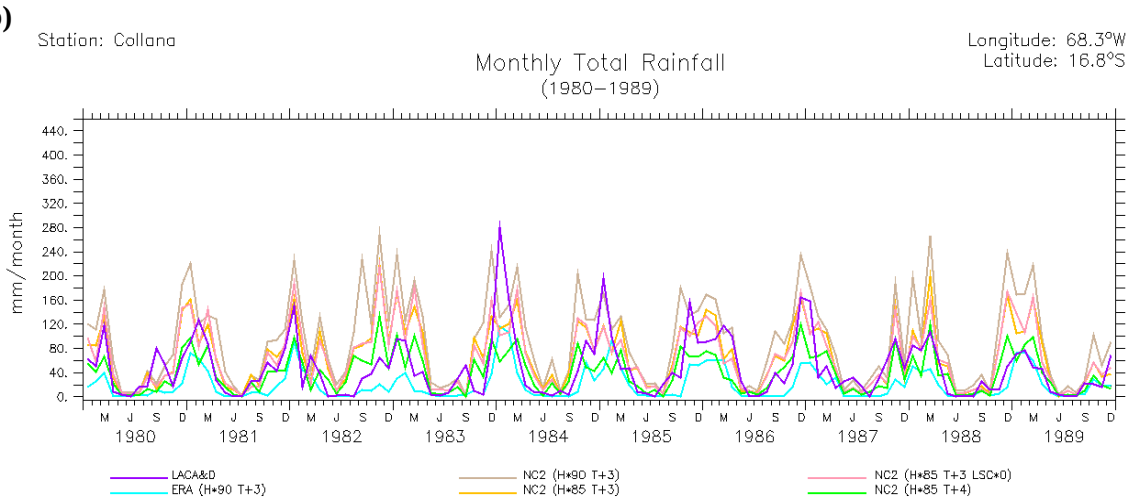
Station: Collana
Longitude: 68.3°W
Latitude: 16.8°S
Monthly Total Rainfall
(1980–1989)
mm/month
440.
400.
360.
320.
280.
240.
200.
160.
120.
80.
40.
0.
M J S D M J S D M J S D M J S D M J S D M J S D M J S D M J S D M J S D
1980 1981 1982 1983 1984 1985 1986 1987 1988 1989
LACA&D
ERA (H*90 T+3)
NC2 (H*90 T+3)
NC2 (H*85 T+3)
NC2 (H*85 T+3 LSC*0)
NC2 (H*85 T+4)

c)

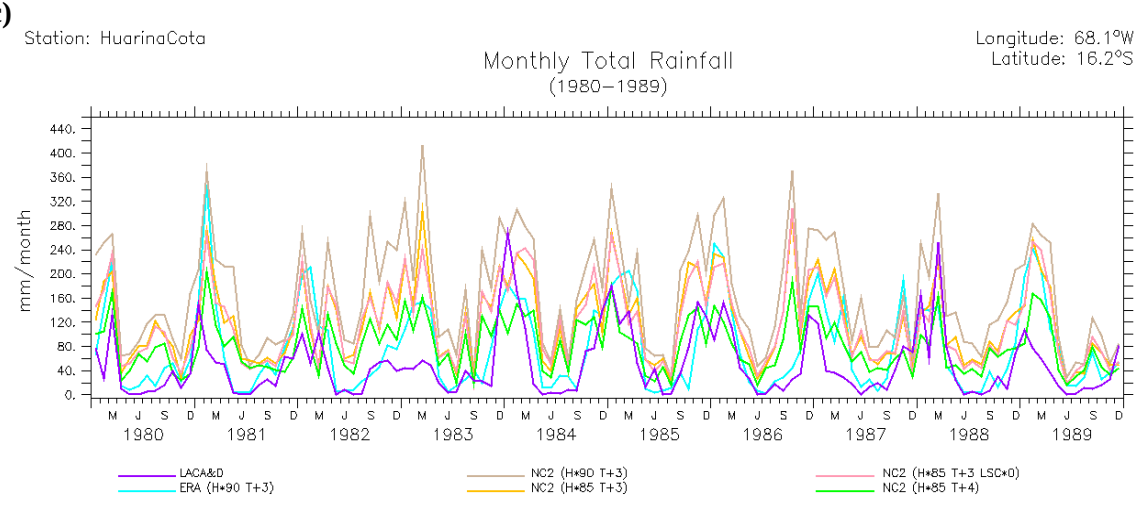
Station: HuarinaCota
Longitude: 68.1°W
Latitude: 16.2°S
Monthly Total Rainfall
(1980–1989)
mm/month
440.
400.
360.
320.
280.
240.
200.
160.
120.
80.
40.
0.
M J S D M J S D M J S D M J S D M J S D M J S D M J S D M J S D M J S D
1980 1981 1982 1983 1984 1985 1986 1987 1988 1989
LACA&D
ERA (H*90 T+3)
NC2 (H*90 T+3)
NC2 (H*85 T+3)
NC2 (H*85 T+3 LSC*0)
NC2 (H*85 T+4)

d)

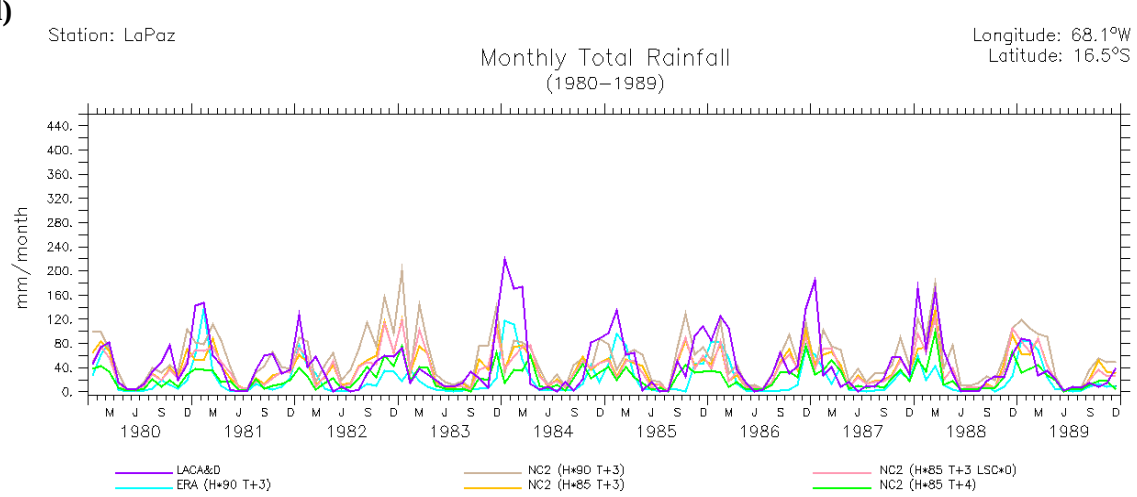

e)

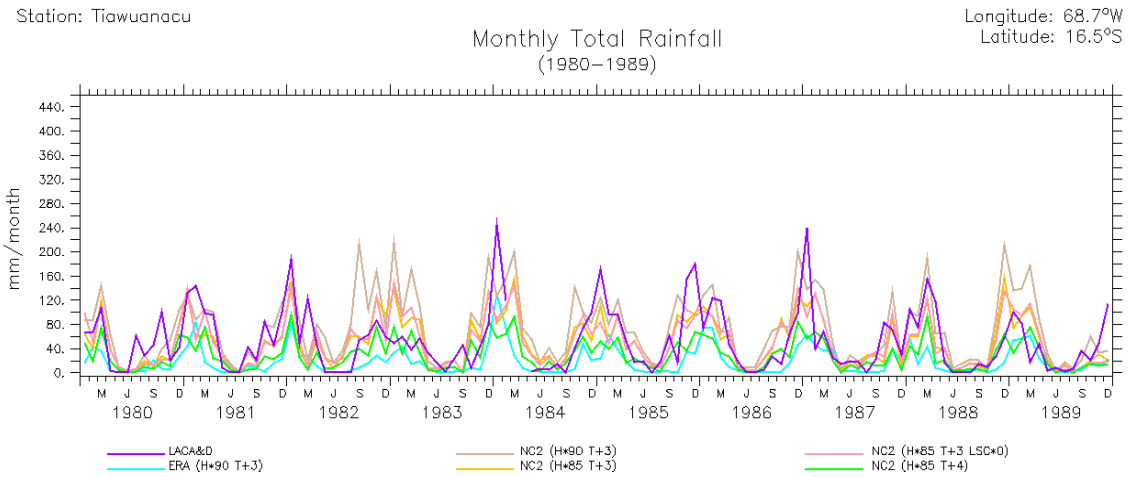

Figure 5.3: Monthly total rainfall (mm) over the 1980-1989 period, computed for each station **(a–e)** and for each test. Observations are in purple.

a)

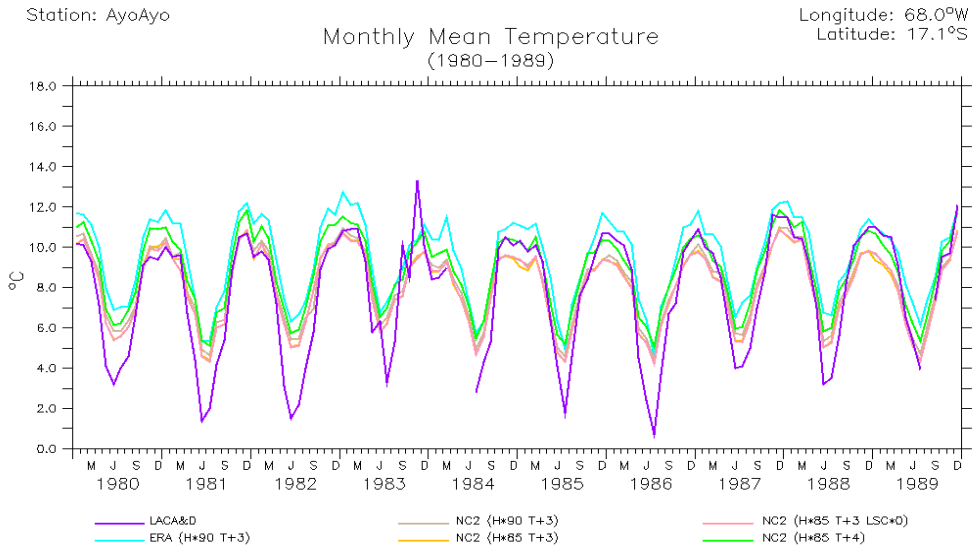
Station: AyoAyo
Longitude: 68.0°W
Latitude: 17.1°S
Monthly Mean Temperature
(1980–1989)
°C
18.0
16.0
14.0
12.0
10.0
8.0
6.0
4.0
2.0
0.0
M J S D M J S D M J S D M J S D M J S D M J S D M J S D M J S D M J S D M J S D
1980 1981 1982 1983 1984 1985 1986 1987 1988 1989
LACA&D
ERA (H*90 T+3)
NC2 (H*90 T+3)
NC2 (H*85 T+3)
NC2 (H*85 T+3 LSC*0)
NC2 (H*85 T+4)

b)

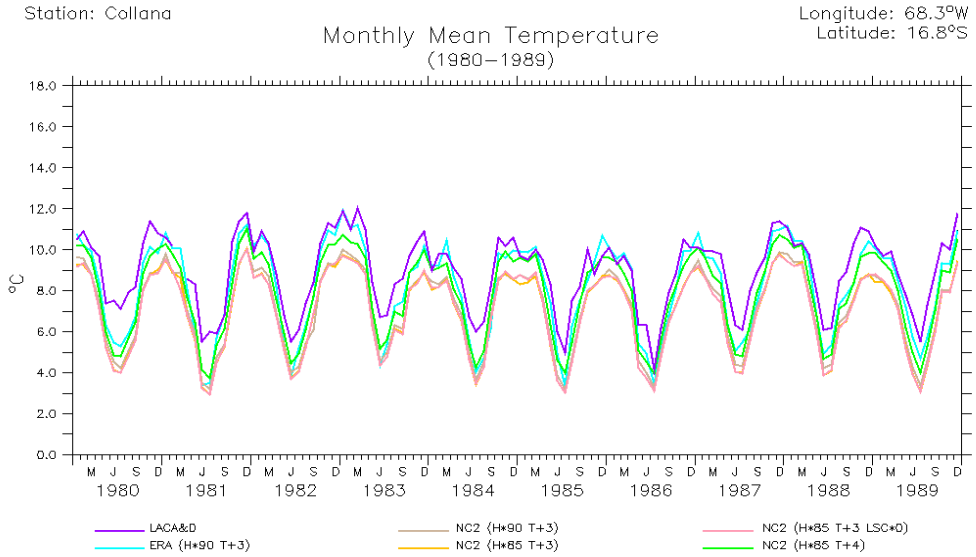
Station: Collana
Longitude: 68.3°W
Latitude: 16.8°S
Monthly Mean Temperature
(1980–1989)
°C
18.0
16.0
14.0
12.0
10.0
8.0
6.0
4.0
2.0
0.0
M J S D M J S D M J S D M J S D M J S D M J S D M J S D M J S D M J S D M J S D
1980 1981 1982 1983 1984 1985 1986 1987 1988 1989
LACA&D
ERA (H*90 T+3)
NC2 (H*90 T+3)
NC2 (H*85 T+3)
NC2 (H*85 T+3 LSC*0)
NC2 (H*85 T+4)

c)

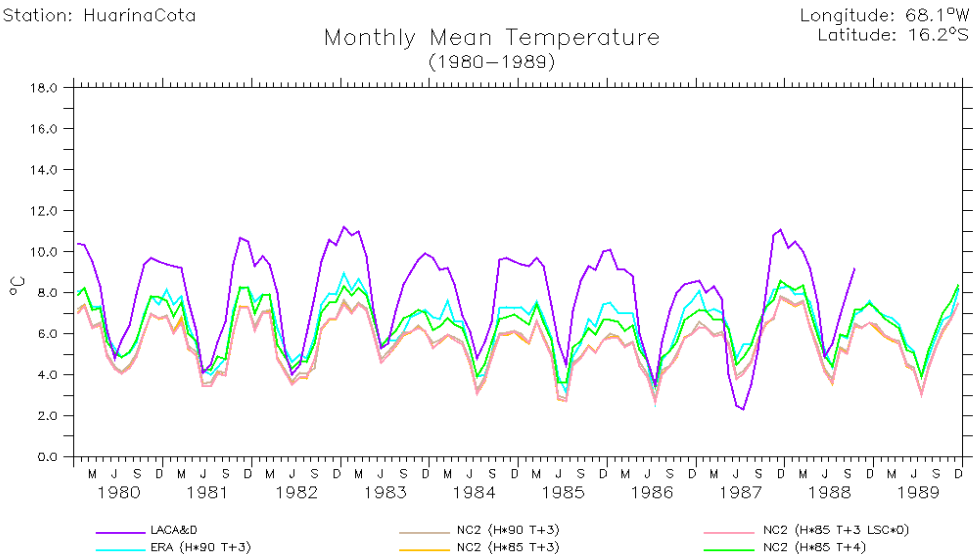
Station: HuarinaCota
Longitude: 68.1°W
Latitude: 16.2°S
Monthly Mean Temperature
(1980–1989)
°C
18.0
16.0
14.0
12.0
10.0
8.0
6.0
4.0
2.0
0.0
M J S D M J S D M J S D M J S D M J S D M J S D M J S D M J S D M J S D
1980 1981 1982 1983 1984 1985 1986 1987 1988 1989
LACA&D
ERA (H*90 T+3)
NC2 (H*90 T+3)
NC2 (H*85 T+3)
NC2 (H*85 T+3 LSC*0)
NC2 (H*85 T+4)

d)

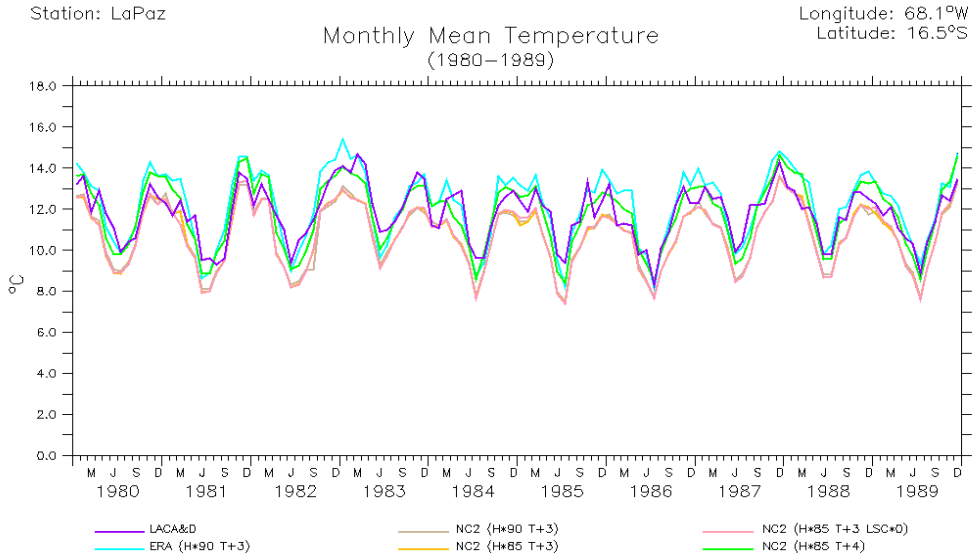
Station: LaPaz
Longitude: 68.1°W
Latitude: 16.5°S
Monthly Mean Temperature
(1980–1989)
°C
18.0
16.0
14.0
12.0
10.0
8.0
6.0
4.0
2.0
0.0
M J S D M J S D M J S D M J S D M J S D M J S D M J S D M J S D M J S D
1980 1981 1982 1983 1984 1985 1986 1987 1988 1989
LACA&D
ERA (H*90 T+3)
NC2 (H*90 T+3)
NC2 (H*85 T+3)
NC2 (H*85 T+3 LSC*0)
NC2 (H*85 T+4)

e)

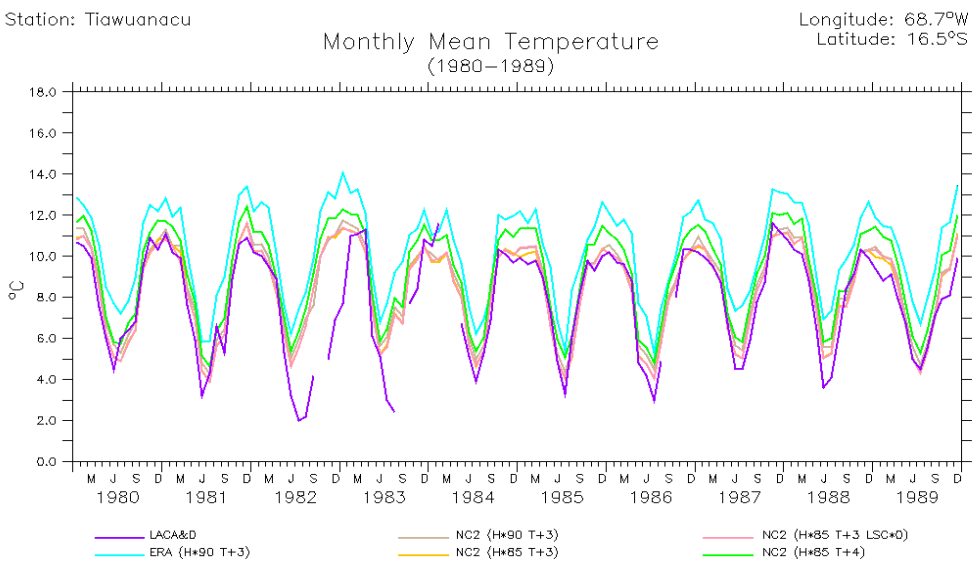

Figure 5.4: Monthly mean near-surface air temperature (°C) over the 1980-1989 period, computed for each station **(a–e)** and for each test. Observations are in purple.

After we demonstrated that despite the corrections we applied on the LBCs, precipitation are not properly modeled by MAR when forced with the NCEP2 reanalysis, we tried to understand why the ERA reanalysis are more reliable than the NCEP2 reanalysis over our study area. Therefore we compared the mean seasonal winds at 200 hPa and 850 hPa simulated with both reanalyses (Figures 5.5 to 5.8).

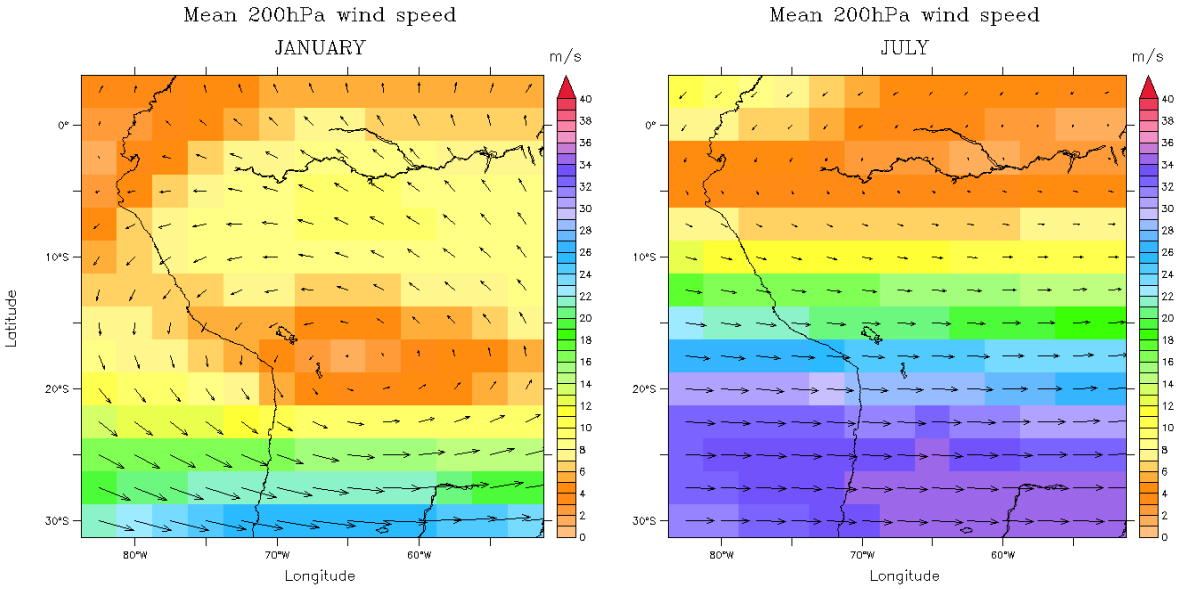

Figure 5.5: Climatological mean (1980-2009) 200 hPa wind speed (m/s) in January and July from NCEP/NCAR-v2. Arrows indicate wind direction.

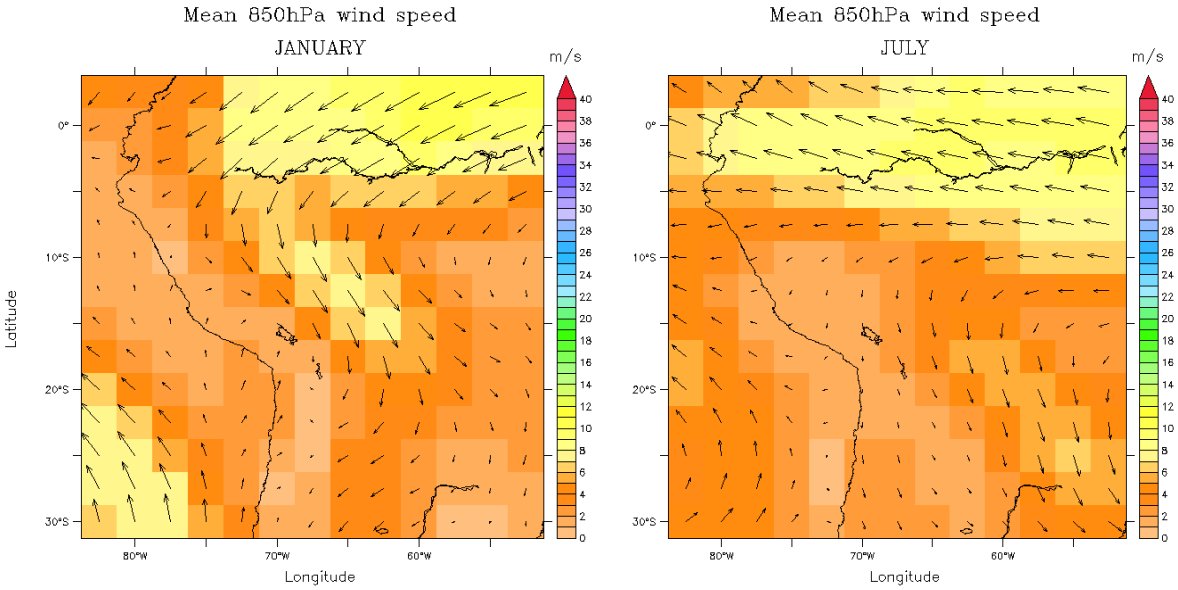

Figure 5.6: Climatological mean (1980-2009) 850 hPa wind speed (m/s) in January and July from NCEP/NCAR-v2. Arrows indicate wind direction.

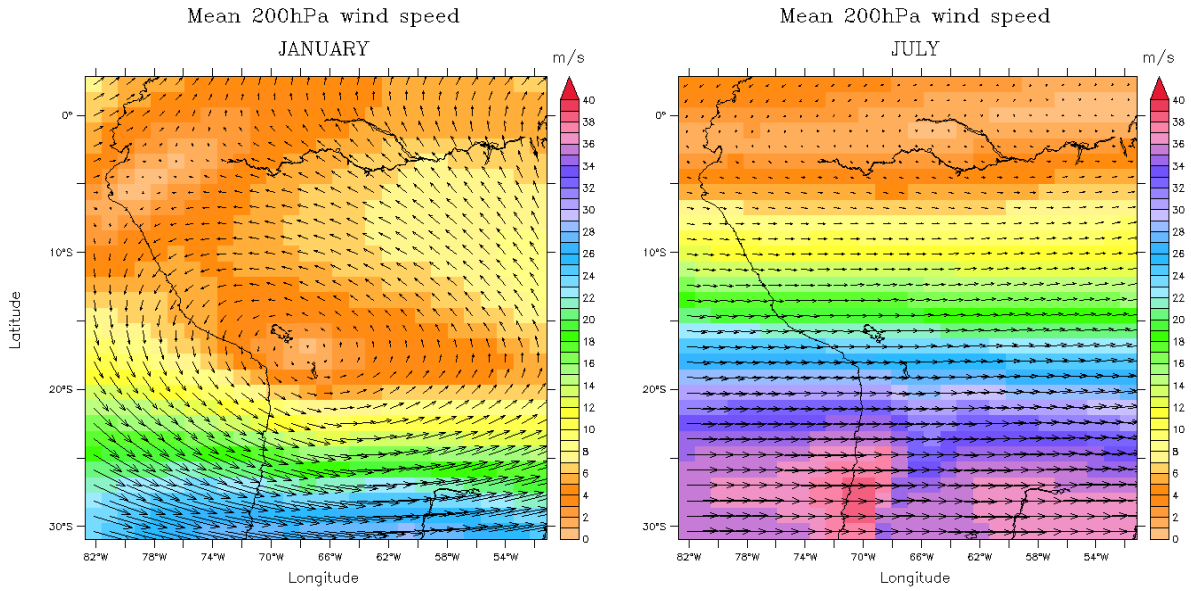

Figure 5.7: Climatological mean (1980-2009) 200 hPa wind speed (m/s) in January and July from ERA-Interim. Arrows indicate wind direction.

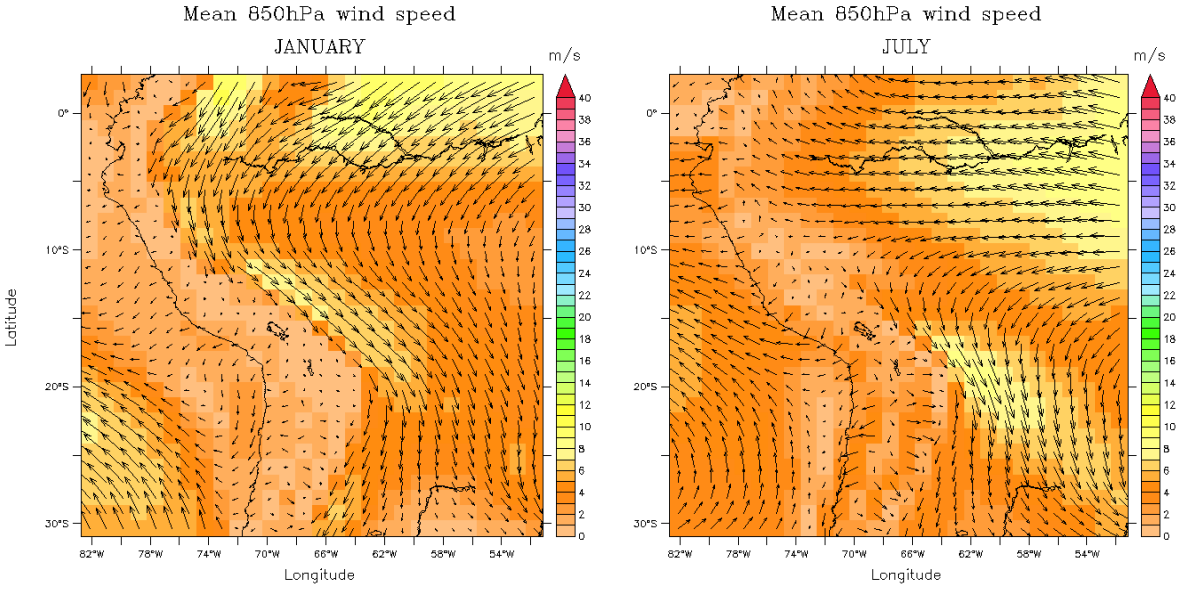

Figure 5.8: Climatological mean (1980-2009) 850 hPa wind speed (m/s) in January and July from ERA-Interim. Arrows indicate wind direction.

The 200 hPa circulation field, displayed in Figures 5.5 and 5.7, suggests that both ERA-Interim and NCEP2 reanalyses are able to reproduce the major climatological features of the upper-level circulation. These zonal patterns include *(i)* the summertime development of an anticyclonic circulation over the Bolivian Altiplano which leads to deep convective activity, and *(ii)* the wintertime northward shift of the subtropical jet stream which reverses the upper-level circulation into a strong westerly flow. However, the main differences between the two reanalyses are related to the position and the intensity of these systems. On the one hand, during the austral summer (January) the Bolivian High is slightly stronger and displaced toward the east in the NCEP2 reanalysis with respect to ERA-Interim. This shift may be explained by the NCEP2 failure to reproduce the location of the Amazonian latent heat source (Nicolini, 2002), which is assumed to play a crucial role in the development of the BH. Several modeling studies demonstrated that a strengthened High leads to significantly higher precipitation amounts over the Bolivian Altiplano (Lenters & Cook, 1999; Vuille, 1999). On the other hand, during the austral winter (July) the subtropical jet is clearly more intense in ERA-Interim than in NCEP2. A stronger westerly flow leads to more frequent and longer dry periods, because enhanced advection of dry air from the Pacific region suppresses any moist air advection from the east (Vuille, 1999).

In Figures 5.6 and 5.8 illustrating the 850 hPa circulation field, it can be observed that, although the northwesterly Low-Level Jet along the eastern Andes is represented in both reanalyses, its intensity and the position of its core are better captured by the higher resolution of ERA-Interim. Indeed, owing to its coarser resolution, the NCEP2 reanalysis fails to accurately reproduce the deflecting effect of the Andes range on the northeasterly trades, and therefore allows the moisture influx to flow further westward than in the ERA simulation. The same typical error was also found in other RCMs and GCMs forced with the NCEP/NCAR reanalysis (e.g. Fernandez *et al.*, 2006; Urrutia & Vuille, 2009; Alves & Marengo, 2010). These studies showed how the misrepresentation of the topography systematically led to an overestimation of precipitation over the Andean regions.

The same previous studies also provided evidence that models forced with reanalyses (NCEP/NCAR as well as ERA) significantly underestimated air temperature over the Andes. Urrutia & Vuille (2009) suggested that this systematic cold bias may be caused by the recurrent error of excessive precipitation over the Andes, which reduces incoming solar radiation and thus lowers near-surface air temperature. Yet it is generally acknowledged that these discrepancies are most probably related to problems in the observed fields that constrain the reanalyses. Indeed, as mentioned in sections 4.2.2.5 and 5.1.1, in tropical South America and especially in the Bolivian Andes the number of stations with temperature data is very small and is even smaller than the number of rainfall data (Alves & Marengo, 2010). As a consequence, interpolation had been relied upon to fill some large gaps in this region, which had inevitably introduced biases in the data series. This issue being the same for all reanalyses, it is thus expected that both ERA and NCEP/NCAR show uniform results as regards temperature, which is indeed consistent with our own results.

In brief, differences in both the upper- and the lower-level circulation between the two reanalyses explain why we had to apply stronger corrections with respect to specific humidity to the NCEP2 reanalysis than to ERA-Interim. In contrast, as cold temperature bias is a common feature to all reanalyses, similar corrections were required.

5.2.2.2. MAR forced with the ERA reanalysis

We further assessed our model performance by analysing the outputs of MAR obtained from the ERA reanalysis. Several statistics were calculated over the 30-year period 1977-2006, for all stations but one. For station Viacha, the period was shortened to 20 years, since there are no observations before 1987.

The statistics included, for precipitation:

(i) the annual and the seasonal total amount, averaged over the whole period (30 values), for both the modeled (MAR) and the observed (Obs) values;

(ii) the mean difference (Δ), averaged over the period, between the modeled annual total precipitation rates and the corresponding observations (30 values);

For near-surface temperature:

(i) the monthly (360 values) and the seasonal (30 values) mean, averaged over the whole period, for both the modeled (MAR) and the observed (Obs) values;

(ii) the mean difference (Δ), averaged over the period, between the modeled monthly temperatures and the corresponding observations (360 values);

For both precipitation and temperature:

(iii) the correlation coefficient (CC) between the modeled monthly values and the corresponding observations (360 values); the CC is also calculated between the seasonal values and the corresponding observations (30 values);

(iv) the standard deviation (STD) for the observed monthly values only (30 values);

(v) the root mean square error (RMSE) between the modeled monthly values and the corresponding observations (360 values); the CC is also calculated between the seasonal values and the corresponding observations (30 values).

(vi) A test was also performed to assess the statistical skill representativeness of the model:

if RMSE < 2*STD(Obs) then representative (R)

if RMSE > 2*STD(Obs) then non-representative (NR)

as commonly accepted in climatology. A model bias is tolerable if its RMSE is lower than two times the 30-year interannual variability of the observed time series.

Precipitation

Station	Annual/ seasonal	Obs (mm)	MAR (mm)	Δ(%)	CC	STD (mm)	RMSE (mm)	Represen-tativeness
Ayo Ayo	Annual	426.9	215.8	-49.5	0.74	37.5	30.9	R
	DJF	230.4	128.3	-44.3	0.52	75.1	120.8	R
	JJA	22.8	7.3	-66.9	0.42	16.7	22.0	R
Collana	Annual	554.6	274.1	-50.6	0.81	48.9	38.4	R
	DJF	295.5	24.5	-44.4	0.60	88.8	150.2	R
	JJA	24.5	6.0	-75.5	0.56	17.5	24.8	R
Huarina Cota	Annual	581.9	943.8	+62.2	0.73	48.9	60.2	R
	DJF	296.5	465.9	+57.1	0.39	97.2	203.4	NR
	JJA	27.5	47.5	+73.0	0.24	21.5	42.2	R
La Paz	Annual	541.3	274.3	-49.3	0.74	45.4	37.9	R
	DJF	285.0	162.2	-43.1	0.49	76.9	140.3	R
	JJA	26.7	7.2	-73.2	0.50	17.9	25.4	R
Tiawuanacu	Annual	552.8	230.3	-58.3	0.72	47.4	43.7	R
	DJF	286.4	137.5	-52.0	0.50	82.8	168.9	NR
	JJA	30.3	7.4	-75.7	0.31	35.7	42.7	R
Viacha	Annual	511.1	228.8	-55.2	0.80	44.8	37.5	R
	DJF	273.1	140.1	-48.7	0.60	85.1	149.4	R
	JJA	22.1	5.8	-73.8	0.61	16.3	21.4	R

Table 5.7: Long-term average (1977-2006) and bias (Δ=MAR-Obs) for the annual and seasonal (DJF and JJA) total precipitation. Correlation coefficient (CC), standard deviation (STD), and root mean square error (RMSE) over 1977-2006 are calculated from the monthly and seasonal values. Values in green are the correlation coefficients that exceed 0.70, the threshold above which we considered a satisfactory correspondence between model and observations. Values in red on the contrary stand for bad representativeness of the observations by the model.

Quantitative estimates of MAR precipitation biases and a more detailed analysis of the mean annual rainfall cycle are also illustrated in Figure 5.9, which shows simulated and observed monthly precipitation averaged over the 30-year period 1977-2006.

MAR simulates well the timing of the peak rainfall season, which occurs during the DJF months, but underestimates the mean seasonal and annual amounts by about 50% on average, when compared to the observations. Although this bias is rather high, it remains quite systematic among all our stations, except one: for Huarina Cota, MAR overestimates the annual amount of precipitation by about 60%.

Generally speaking, biases between model and observations can be explained by three potential sources of error: the quality of the observational data, the quality of the LBCs, and the performance of the model itself. The reliability of the reference data depends on various factors which have already been mentioned in section 5.1.2. Among these factors are the quality of the measurement instruments and the completeness of the time series. For precipitation, as the bias shows a systematic anomaly between almost all stations, these two factors are unlikely to play a major role. Moreover, the precipitation series underwent homogeneity tests that evaluated them as of good quality (see Table 5.1). The reliability of the LBCs has been discussed in the previous section wherein we demonstrated that the ERA reanalysis, despite being fitter than the NCEP/NCAR reanalysis to reproduce the large-scale circulation over our MAR domain, remained yet tainted by errors that even our correctional calibration could not make up for. Finally, the bias in the modeled precipitation fields may partly be related to the parameterization schemes of the model itself. MAR demonstrated a successful implementation under polar and temperate latitudes because its physics are adapted to those climates, but in the Tropics, the atmosphere is less stable then under higher latitudes, and the atmospheric processes governing the tropical climate are slightly different.

Concerning the excessive precipitation simulated in Huarina Cota, the distinctive behavior of MAR over this location is linked to the particular situation of the station, which lies at the bottom of a very narrow valley in the middle of the Cordillera Real. As the dimension of this valley is smaller than the resolution of MAR, it is not represented in our model. This explains why the closest pixel to the station is modeled at an altitude more than 500 meters higher than the actual elevation of the weather station, and why the precipitation amounts are largely overestimated. This bias merits particular attention, insofar as it may suggest that precipitation is strongly dependent upon altitude in our model. However, as no altitude-related precipitation gradient is observed for the other stations, which are all located in the Altiplano, we deduce that MAR overestimates precipitation exclusively over the mountains of the Cordillera Real.

a)

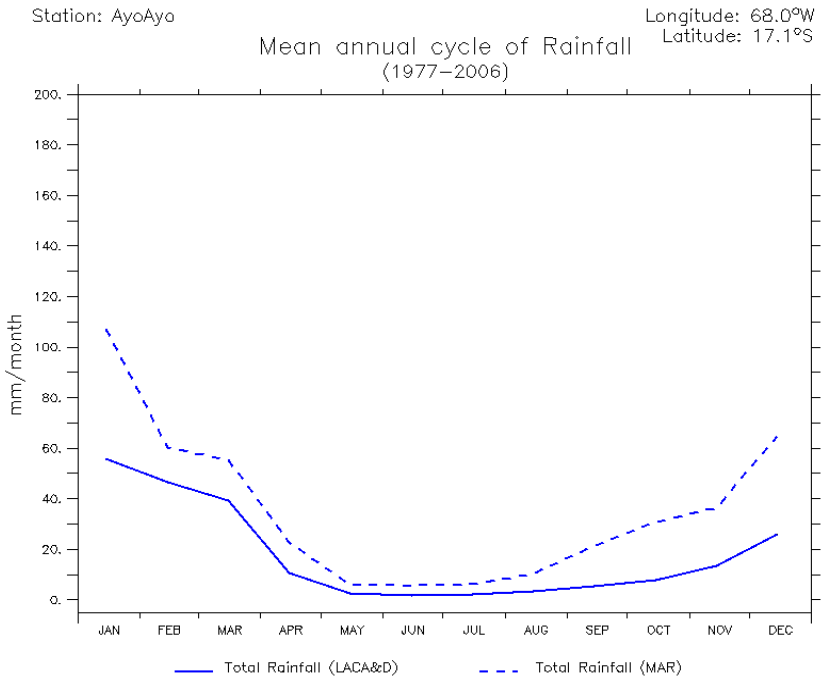
Station: AyoAyo
Longitude: 68.0°W
Latitude: 17.1°S
Mean annual cycle of Rainfall
(1977–2006)
mm/month
200.
180.
160.
140.
120.
100.
80.
60.
40.
20.
0.
JAN
FEB
MAR
APR
MAY
JUN
JUL
AUG
SEP
OCT
NOV
DEC
Total Rainfall (LACA&D)
Total Rainfall (MAR)

b)

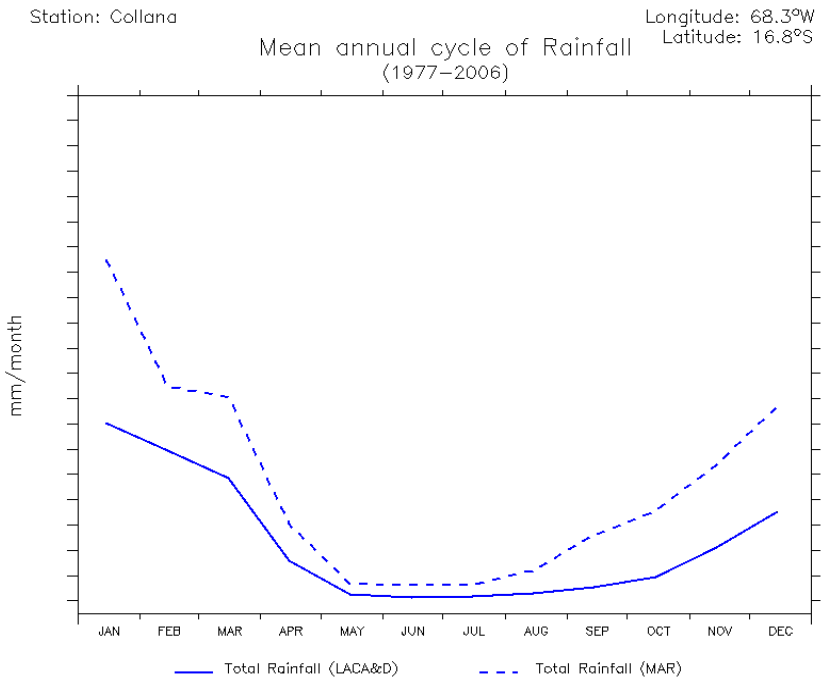
Station: Collana
Longitude: 68.3°W
Latitude: 16.8°S
Mean annual cycle of Rainfall
(1977–2006)
mm/month
JAN
FEB
MAR
APR
MAY
JUN
JUL
AUG
SEP
OCT
NOV
DEC
Total Rainfall (LACA&D)
Total Rainfall (MAR)

c)

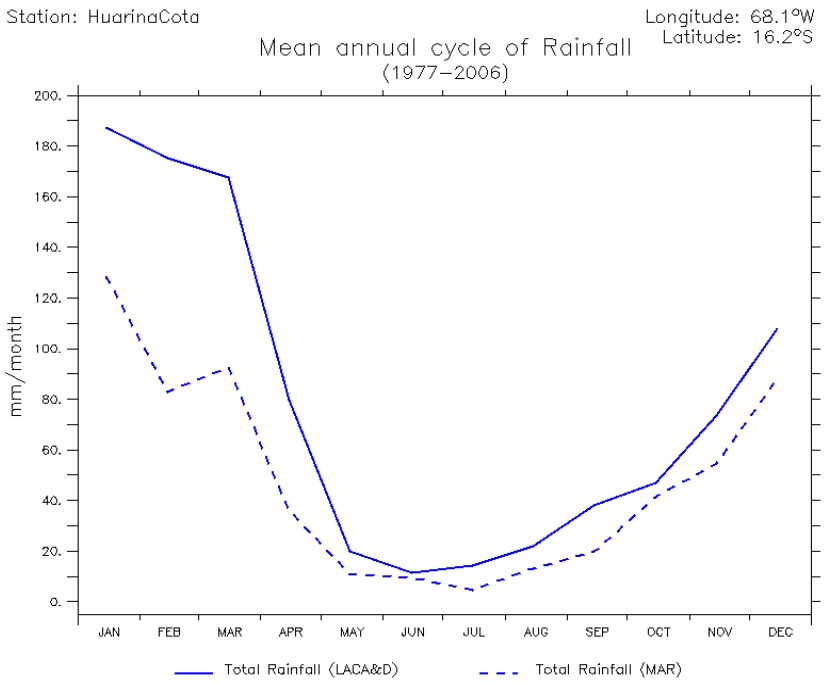
Station: HuarinaCota
Longitude: 68.1°W
Latitude: 16.2°S
Mean annual cycle of Rainfall
(1977–2006)
mm/month
200.
180.
160.
140.
120.
100.
80.
60.
40.
20.
0.
JAN
FEB
MAR
APR
MAY
JUN
JUL
AUG
SEP
OCT
NOV
DEC
Total Rainfall (LACA&D)
Total Rainfall (MAR)

d)

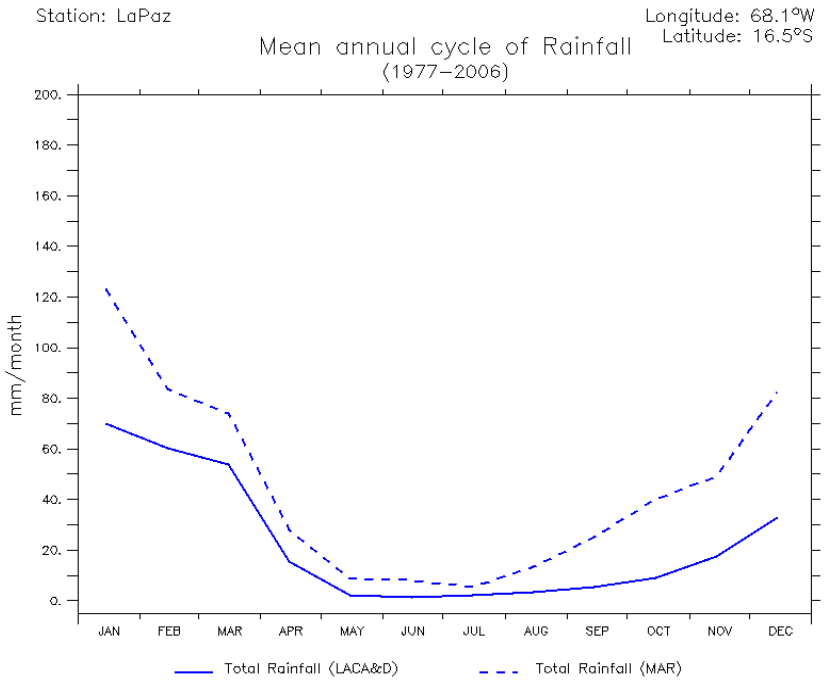
Station: LaPaz
Longitude: 68.1°W
Latitude: 16.5°S
Mean annual cycle of Rainfall
(1977–2006)
mm/month
200.
180.
160.
140.
120.
100.
80.
60.
40.
20.
0.
JAN
FEB
MAR
APR
MAY
JUN
JUL
AUG
SEP
OCT
NOV
DEC
Total Rainfall (LACA&D)
Total Rainfall (MAR)

e)

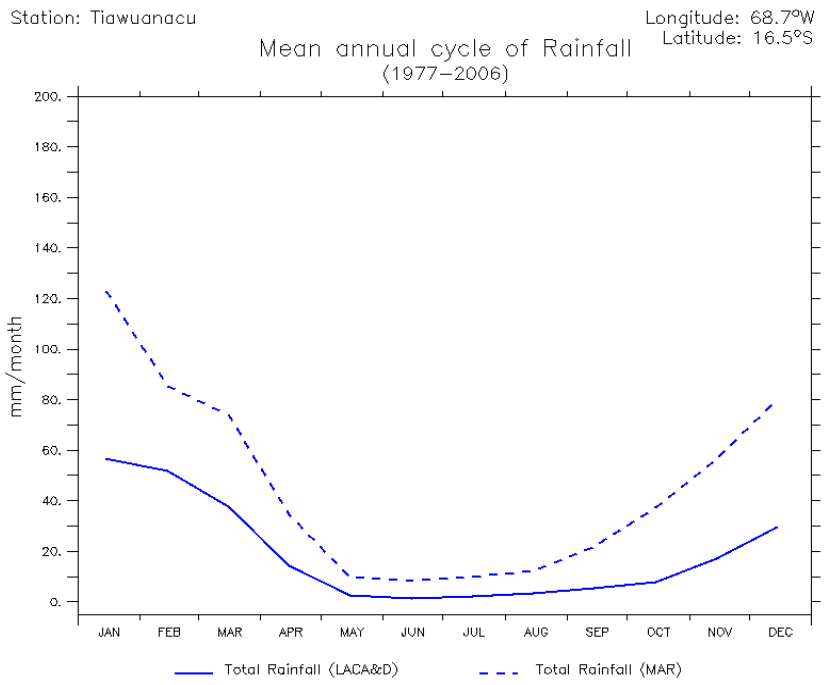

f)

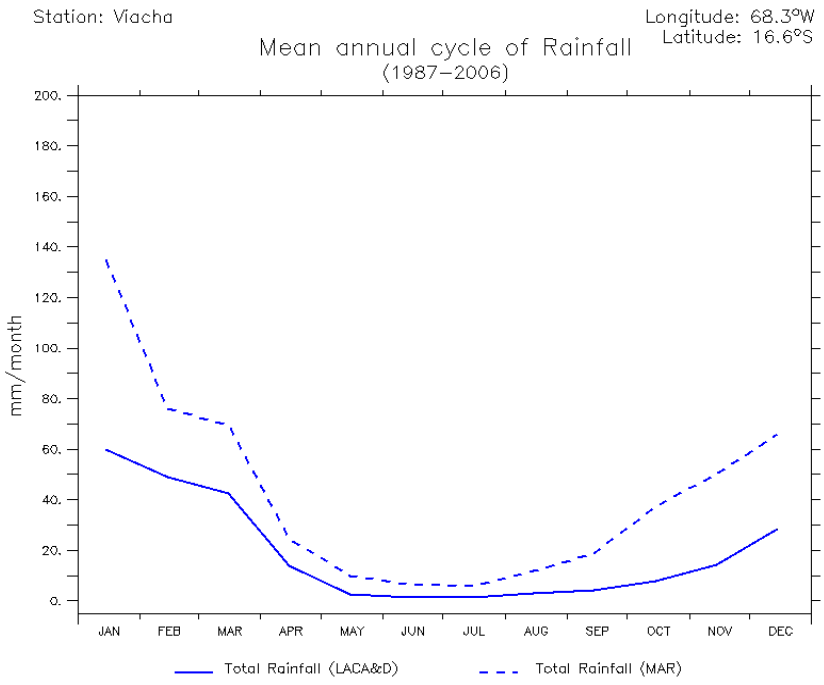

Figure 5.9: Long-term mean (1977-2006) for annual cycle of rainfall (mm), computed for each station **(a–f)**. The continuous line is for the modeled values; the dashed line is for the observations.

Near-surface air temperature

Station	Monthly/ seasonal	Obs (°C)	MAR (°C)	Δ(°C)	CC	STD (°C)	RMSE (°C)	Represen-tativeness
Ayo Ayo	Monthly	7.5	9.5	+2.0	0.96	3.0	2.4	R
	DJF	10.3	11.5	+1.2	0.66	0.9	1.3	R
	JJA	3.4	6.7	+3.3	0.66	1.3	3.4	NR
Collana	Monthly	9.1	8.2	-0.9	0.95	1.8	1.2	R
	DJF	10.6	10.4	-0.2	0.73	0.8	0.6	R
	JJA	6.7	5.2	-1.5	0.82	0.8	1.5	R
Huarina Cota	Monthly	8.0	6.5	-1.5	0.85	2.0	1.9	R
	DJF	9.6	7.7	-1.9	0.60	0.9	2.0	NR
	JJA	5.5	4.8	-0.7	0.26	1.5	1.6	R
La Paz	Monthly	12.1	12.2	+0.1	0.88	1.4	0.8	R
	DJF	13.0	13.7	+0.7	0.74	1.0	1.0	R
	JJA	10.4	10.0	-0.4	0.72	0.8	0.7	R
Tiawuanacu	Monthly	7.8	10.3	+2.5	0.90	2.4	2.7	R
	DJF	10.0	12.5	+2.5	0.27	0.9	2.6	NR
	JJA	4.7	7.4	+2.7	0.48	1.4	3.0	NR
Viacha	Monthly	8.3	9.5	+1.2	0.95	2.2	1.4	R
	DJF	10.3	11.8	+1.5	0.54	0.9	1.7	R
	JJA	5.3	6.3	+1.0	0.61	1.1	1.3	R

Table 5.8: Long-term average (1977-2006), bias (Δ=MAR-Obs), correlation coefficient (CC), standard deviation (STD), and root mean square error (RMSE) for the monthly and seasonal (DJF and JJA) near-surface air temperature. The color code is the same as in Table 5.7.

Figure 5.10 displaying the annual cycle of near-surface air temperature shows a better agreement between MAR and the observations than for precipitation. However, unlike the annual cycle of precipitation, those figures exhibit a significant degree of dispersion among the stations. Although we are aware that temperature observations are dubious in our study area and should thus be used with much caution, we tried nonetheless to explore some other reasons explaining these non-systematic biases.

a)

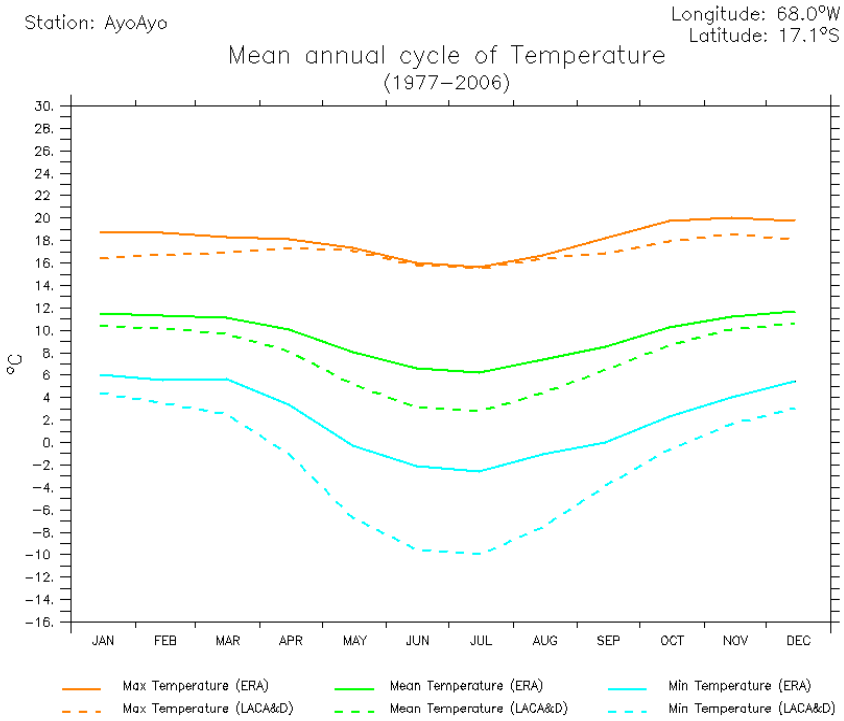
Station: AyoAyo
Longitude: 68.0°W
Latitude: 17.1°S
Mean annual cycle of Temperature
(1977–2006)
°C
JAN FEB MAR APR MAY JUN JUL AUG SEP OCT NOV DEC
Max Temperature (ERA)
Max Temperature (LACA&D)
Mean Temperature (ERA)
Mean Temperature (LACA&D)
Min Temperature (ERA)
Min Temperature (LACA&D)

b)

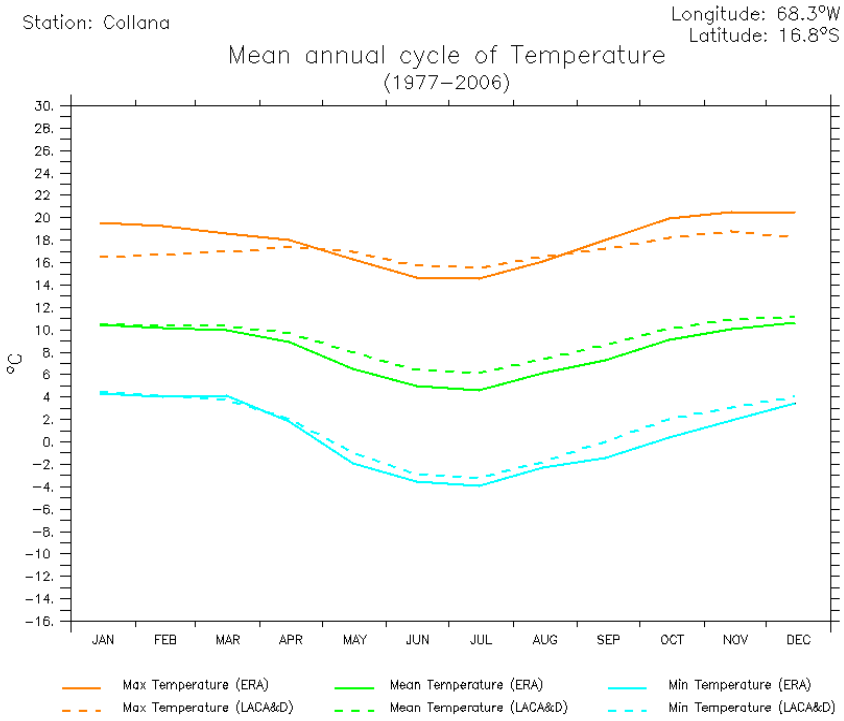
Station: Collana
Longitude: 68.3°W
Latitude: 16.8°S
Mean annual cycle of Temperature
(1977–2006)
°C
JAN FEB MAR APR MAY JUN JUL AUG SEP OCT NOV DEC
Max Temperature (ERA)
Max Temperature (LACA&D)
Mean Temperature (ERA)
Mean Temperature (LACA&D)
Min Temperature (ERA)
Min Temperature (LACA&D)

c)

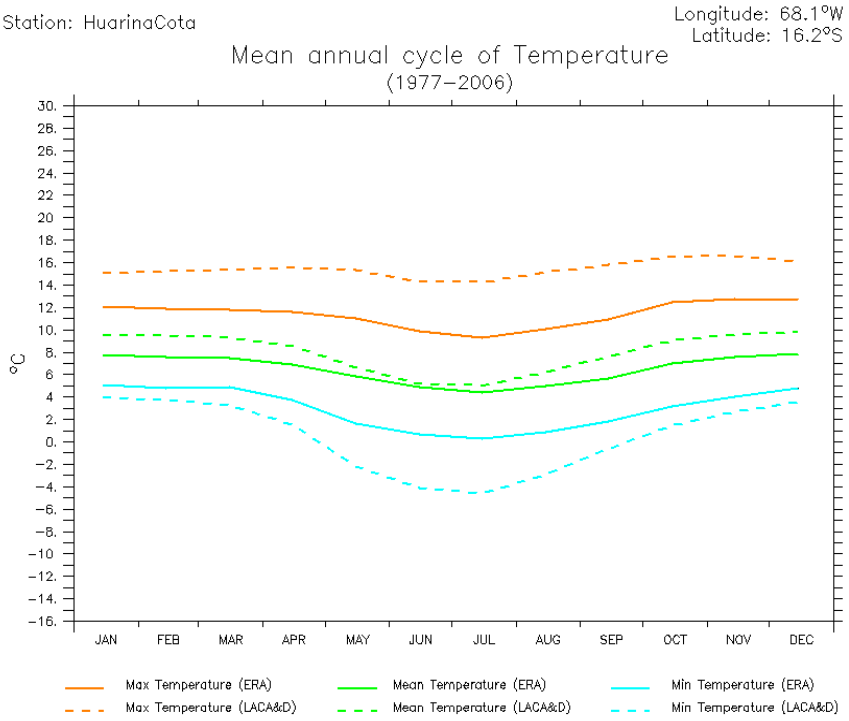
Station: HuarinaCota
Longitude: 68.1°W
Latitude: 16.2°S
Mean annual cycle of Temperature
(1977–2006)
°C
JAN FEB MAR APR MAY JUN JUL AUG SEP OCT NOV DEC
Max Temperature (ERA)
Max Temperature (LACA&D)
Mean Temperature (ERA)
Mean Temperature (LACA&D)
Min Temperature (ERA)
Min Temperature (LACA&D)

d)

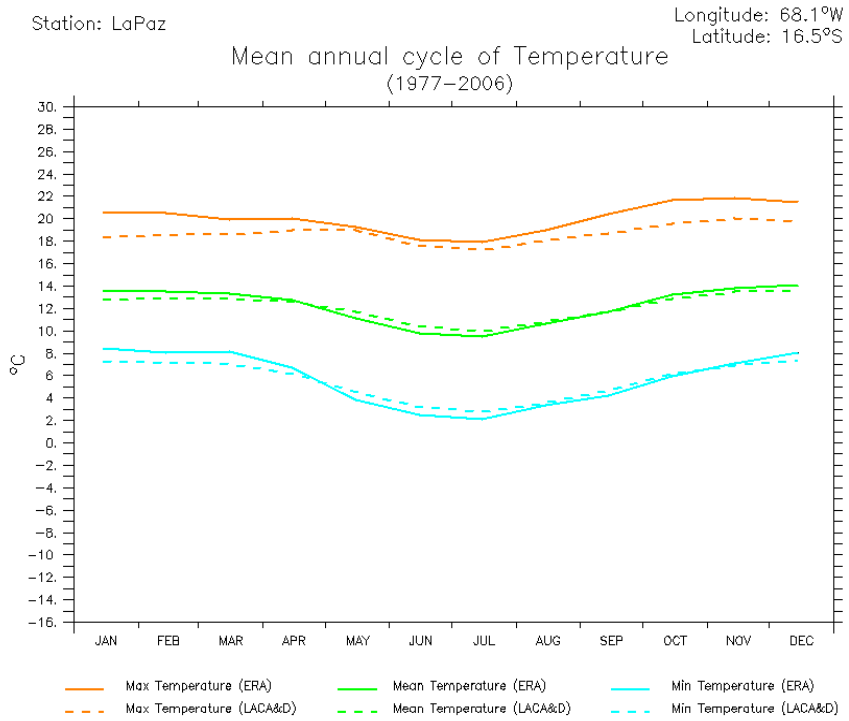
Station: LaPaz
Longitude: 68.1°W
Latitude: 16.5°S
Mean annual cycle of Temperature
(1977–2006)
°C
JAN FEB MAR APR MAY JUN JUL AUG SEP OCT NOV DEC
Max Temperature (ERA)
Max Temperature (LACA&D)
Mean Temperature (ERA)
Mean Temperature (LACA&D)
Min Temperature (ERA)
Min Temperature (LACA&D)

e)

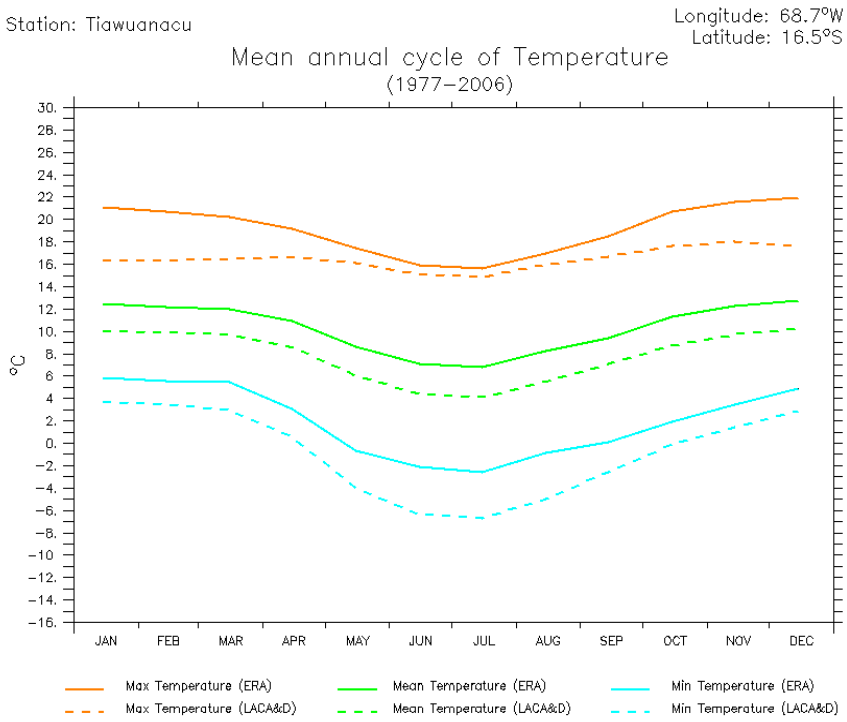

f)

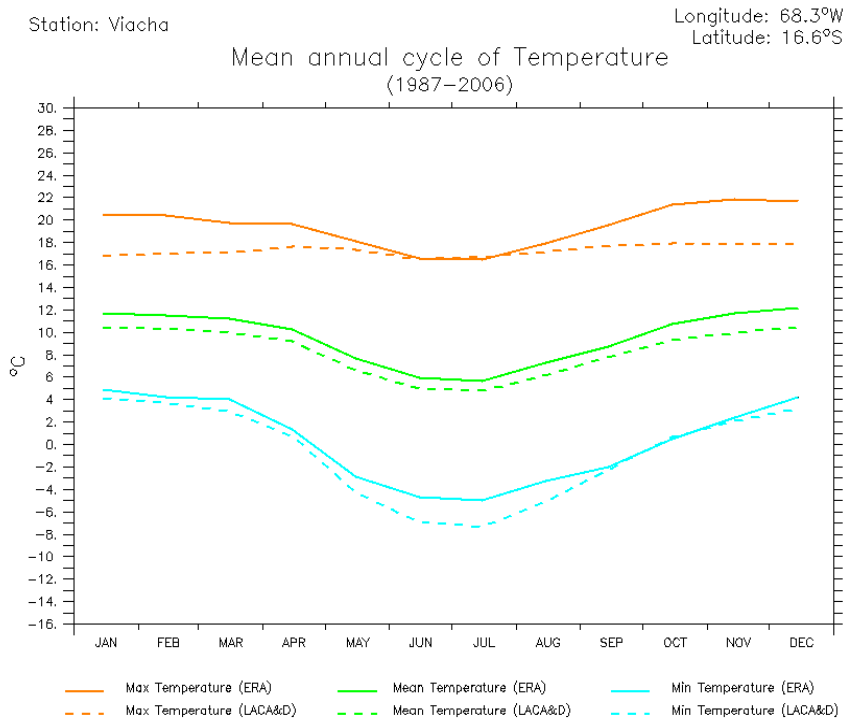

Figure 5.10: Long-term mean (1977-2006) for annual cycle of maximum, average and minimum near-surface air temperature (°C), computed for each station **(a–f)**. The continuous line is for the modeled values; the dashed line is for the observations.

Most often, the first cause of bias in temperature fields is the model's bad representativeness of its domain topography. In our case however, confronting the temperature bias with the surface height bias revealed no coherent link between these two variables (see Table 5.9).

Station	Elevation (m)			Annual temperature (°C)		
	Station	Model	Bias	Station	Model	Bias
Ayo Ayo	3880	3915	+35	7.5	9.5	+2.0
Collana	3940	4115	+175	9.1	8.2	-0.9
Huarina Cota	3825	4343	+518	8.0	6.5	-1.5
La Paz	3632	3628	-4	12.1	12.2	+0.1
Tiawuanacu	3629	3871	+242	7.8	10.3	+2.5
Viacha	3850	3875	+25	8.3	9.5	+1.2

Table 5.9: Elevation and mean (1977-2006) annual near-surface air temperature for each station, with biases between the model (forced with the ERA reanalysis) and the observations.

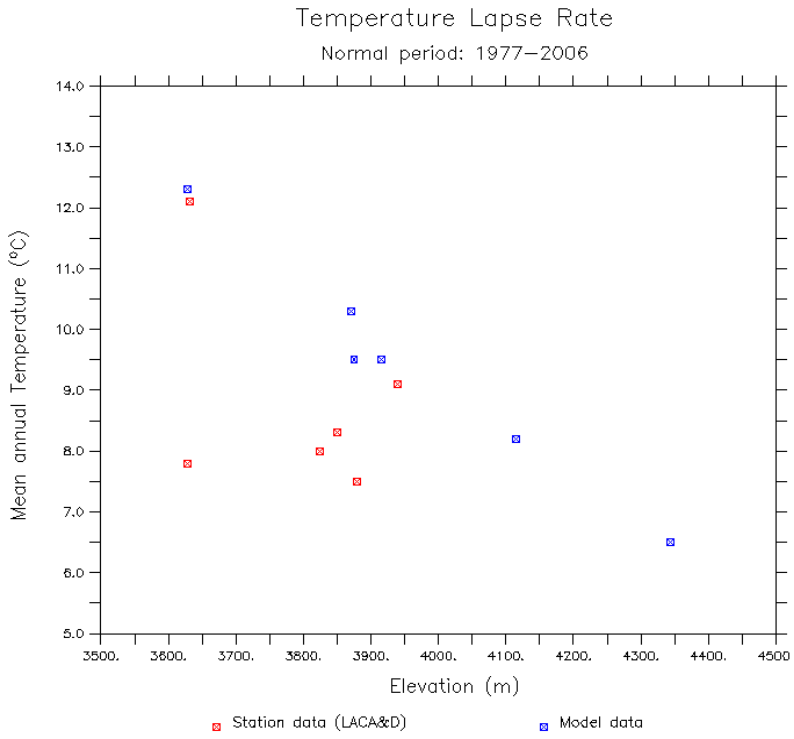

Figure 5.11: Scatterplot of long-term mean (1977-2006) annual near-surface air temperature (°C) versus elevation. Each station is represented by a point. The red points are the observed values; the blue points are the modeled values.

When plotting temperature as a function of altitude (Figure 5.11), MAR produces a lapse rate of approximately -0.7°C/100m, which is quite consistent with what we know about temperature variability in mountainous regions. By contrast, it seems that in the observed field temperature does not decrease linearly with elevation as expected.

Here it is important to note that the regression calculation has no real statistical relevance, since it was computed from only six stations, which is largely insufficient. Therefore, we relied on Fernandez *et al.* (2006), whose regression calculation included climatological mean (1961-1990) annual surface air temperature observations from 279 station records covering the Andes between the 1°N and the 23°S. They excluded the low-elevation stations to the west of the Andes (open circles in Figure 5.12), which are influenced by the cold oceanic Humboldt Current and are therefore much colder than the other stations of the Andes. They found a lapse rate of -0.52°C/100m, proving thereby that altitude is indeed the principal factor governing the spatial distribution of temperature over complex terrains, and this even though temperature lapse rates undergo seasonal and diurnal variations.

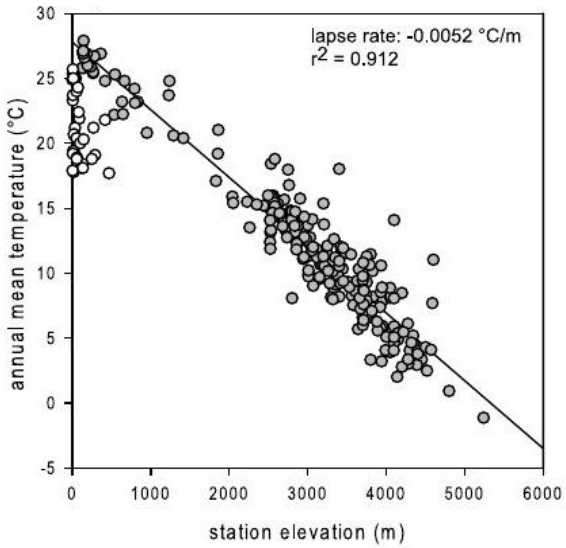

Figure 5.12: Scatterplot of long-term mean (1961-1990) annual surface air temperature (°C) versus elevation based on station data. Open circles (low-elevation stations on the western slope of the Andes) were excluded from the lapse rate calculation. Source: Fernandez *et al.* (2006)

Conclusion

We finally conclude that MAR forced with the ERA reanalysis works rather well over our domain, since the correlations between the model and the observations are all superior to 0.70 for both the annual totals of precipitation and the annual means of near-surface temperature. At the seasonal timescale however, the performance of our model is less satisfactory, especially for precipitation. Although the timing in the seasonality of precipitation is adequately reproduced, a systematic negative bias taints the total annual and seasonal amounts of precipitation, which is linked to the

strong corrections we had to apply to the LBCs. However, without those corrections, our model would have overestimated tremendously the precipitating amounts, and the regional heterogeinities would probably have been less distinct in that case.

Regarding near-surface temperature, our model matches very well with the observations, but unlike precipitation, the bias is not systematic. Since MAR succeeds in accounting for the temperature gradient with respect to altitude, we deduce that the error principally stems from the bad quality of the observations. As a result, the evaluation of the simulated temperature remains uncertain. Fortunately, precipitation is a more crucial parameter than temperature in the climatic context of our study area.

6. Results

In this chapter we first continue the evaluation of MAR by comparing the modeled climatological maps to qualitative information we found in the scientific literature. We analyse annual and seasonal mean values of surface pressure, total and convective precipitation, total cloud cover and cloud optical depth, near-surface temperature, specific humidity, as well as the 850 hPa, 500 hPa and 300 hPa wind fields. The climatologies are calculated over the 30-year period 1980-2009 because the ERA reanalysis we used to force our model is more reliable after 1979; indeed, the ERA-Interim reanalysis (1979–onwards) is corrected by satellite-based observations and has a finer resolution than the ERA-40 reanalysis (1958–1978) (see section 4.2.2.1 in Chapter 4).

Second, our study focuses on the Chacaltaya region with interannual and decadal trends of the aforementioned parameters. In this stage we also include surface heat and solar/infrared radiation parameters. We then evaluate the impact of the most severe El Niño events of the last decades over our study area and finally conclude with a synthesis of the major outcomes of our research.

6.1. Spatial distribution: climatology

Surface pressure Surface pressure, depicted in Figure 6.1, is quasi-invariant throughout the year and gives a synthetic idea of the topography of the study area. Over the highest summits reaching above 5,000 meters a.s.l., surface pressure drops to less than 550 hPa.

Precipitation Mean precipitation during the austral summer (DJF) and winter (JJA) is illustrated in Figure 6.2. Precipitation accounts for all kind of precipitating events, which include rainfall, snowfall and convective precipitation. The total annual amount of precipitation is displayed in Figure 6.3, and the annual convective precipitation in Figure 6.4.

As expected, the summer months concentrate the most of the total annual amount of precipitation. The spatial distribution is dynamically influenced by orography: precipitation is focused along the steep eastern slopes of the Cordillera Real, while on the leeside of the range precipitation amounts are strongly reduced. Nevertheless, although the main features are quite consistent with the literature, at a smaller scale the model differs significantly from the observations. MAR simulates an annual optimum of rainfall exceeding 800 mm between 2,500 and 4,500 meters a.s.l. to the east of the Cordillera Real. According to Roche *et al.* (1990) and Wagnon (1999) however, the maximum rainfall amount is more likely situated around 1,500–2,000 meters a.s.l. This comes from a too strong dependence of precipitation to altitude in the model, leading to unrealistically large amounts of precipitation over the highest elevations.

Besides, convective precipitation (Figure 6.4) exhibits a scattered pattern suggesting that MAR is numerically unstable when representing convection.

Another inconsistency concerns Lake Titicaca, which is described in the literature as a powerful regional precipitation generator. Compared to the annual amounts given by Roche *et al.* (1990), in the model simulation the lake produces less than the half of what is expected. Moreover,

precipitation is shifted westward over the lake; this displacement can probably be explained by the direction of the prevailing winds during the wet season (DJF).

Total cloud cover and cloud optical depth (COD) The total amount of cloudiness simulated by MAR includes upper, middle and lower cloud cover. The upper-level class of cloud cover as defined in MAR includes clouds at a pressure level inferior to 440 hPa (i.e. 6,000–7,000 meters a.s.l.). The lower-level class includes clouds at a pressure level superior to 680 hPa (i.e. 3,000–3,500 meters a.s.l.). Since the topography of the study area mostly exceeds 4,000 meters a.s.l. in elevation, the simulated cloud cover belongs almost entirely to the upper-level class of cloud cover. Figure 6.5 shows the mean cloudiness during the austral summer (DJF) and winter (JJA). Cloud optical depth (COD) values are displayed in Figure 6.6.

Cloud cover exhibits the same pattern as precipitation, with values increasing as a direct function of altitude. Nevertheless, unlike precipitation, cloudiness seems to spread equally along the eastern and the western flanks of the Cordillera Real, at least during the wet season (DJF). As the low COD values along the western slopes suggest, these clouds are thin and sufficiently elevated in the troposphere to pass above the highest peaks of the mountain range. By contrast, during the dry season cloudiness is more important to the east as compared to the west. This difference in cloud cover distribution between summer and winter is probably related to the seasonality of the prevailing winds: during the winter months, the strong westerlies impede and obstruct the moist advection flux from the east, so that upper-level clouds can not progress further westward.

In MAR, cloud cover is absent all year-round in the northeastern part of the study area, which corresponds to the moist yungas ecoregion. The yungas are actually characterized by high humidity rates, since they form the continuity of the Amazonian forest (Fund, 2014). The failing of MAR to produce any clouds in the area which should normally be the cloudiest of the integration domain is probably related to the strong corrections (humidity -15%, temperature +3°C) we applied to the LBCs to fit the model to the observations in the Altiplano.

Near-surface temperature Near-surface temperature is simulated by the model at 3 meters above the surface. The mean seasonal distribution is illustrated in Figure 6.7. As directly dependent on altitude, here temperature exhibits a very strong spatial gradient, with mean temperatures averaging about 10°C over the high Altiplano in the southwestern half of the domain, whereas in the yungas and the lowlands in the northeastern half, temperatures locally exceed 30°C.

On the contrary, seasonal variability is not very marked. In most regions, the seasonal amplitude in temperature remains below 10°C. The thermal contrast is even lesser for Lake Titicaca; as water has a higher heat capacity than soil, the lake keeps its surface warmer than the surrounding lands during the winter months.

Specific humidity Unlike relative humidity, specific humidity is not sensitive to changes in pressure or temperature. This property makes it a very useful parameter to identify moving air masses, as can be seen in Figure 6.8.

The model successfully reproduces the separating effect of the Cordillera Real between the dry Pacific influx to the west and the moist Amazonian advection to the east. The seasonality of these two antagonist air masses is also well captured by MAR, with a clear prevailing influence of the dry conditions over the entire Altiplano and both western and eastern slopes of the Cordillera

during the dry season (JJA), while during the wet season (DJF) humid conditions dominate the eastern flank of the range and mitigate somewhat the dryness of the Altiplano. Owing to its high resolution, the model can also account for the moisture influx through the large, northeastward oriented valleys, which spill moist air into the dry Altiplano. Finally, the influence of Lake Titicaca is visible too, as it keeps slightly higher values of specific humidity over its surface.

Low-level circulation (850 hPa) The summertime lower-tropospheric wind field, displayed for January in Figure 6.9, concerns only the northeastern corner of our domain, where topography is below the 850 hPa pressure field. This field shows the southeastward deviation of the Low-Level Jet (LLJ) by the Andes. The LLJ is the vector of the warm, moist air which generates the heavy precipitation when it ascends along the eastern slopes of the Andes.

A few isolated erratic pixels show values exceeding 30 m/s (displayed in red in Figure 6.9) because part of the time they belong to higher levels than 850 hPa.

Mid-level circulation (500 hPa) The 500 hPa wind field (Figure 6.10) reflects the near-surface atmospheric circulation over the Cordillera Real. The summertime pattern (January) reveals how the Andean Oriental Cordillera utterly disintegrates the mid-level easterly flow, while along its western flank the mountain barrier reinforces the anticyclonic curvature of the Pacific influx. These southeasterly winds are accelerated over Lake Titicaca, which offers a broad, smooth surface over which air can easily flow; this explains the asymmetric distribution of precipitation above and around the lake, the western shores being more watered than the eastern ones.

The wintertime situation (July) shows that the westerly flow is only slightly affected by the Andean mountain range at this time of the year. By contrast to the easterly flow which prevails during the austral summer, the westerlies are strong winds driven by the subtropical jet, which is located further south beyond our study area.

High-level circulation (300 hPa) In the upper-tropospheric wind field (Figure 6.11), we can see that the Andes still alter the atmospheric circulation during the summer season (January), although at a lower rate than in the mid-level circulation field since the easterly flow strengthens with increasing altitude. Another major feature of the regional summertime circulation is the Bolivian High (BH). The climatological position of its core is not clear in Figure 6.11, probably because the anticyclone undergoes interannual fluctuations both in position and intensity, in response to the lateral displacements of the South Atlantic Convergence Zone (SACZ), located in the southeast out of our domain.

During the austral winter (July), the westerlies thoroughly dominate the upper-level circulation. The flow is too strong to be deflected (even slightly) by the Andes, but a gradient is nonetheless visible for windspeed, as the westerlies lose some of their strength when they cross the mountain crests.

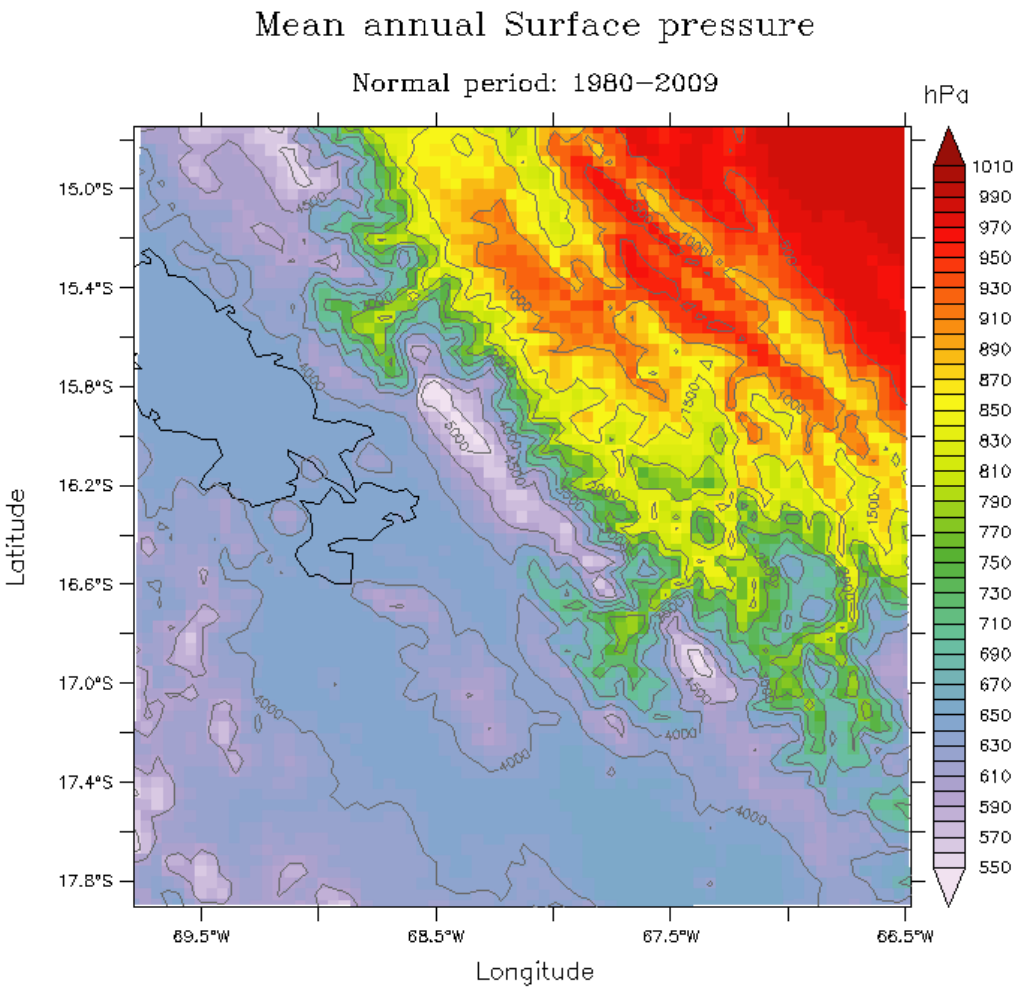

Figure 6.1: Annual surface pressure (hPa) averaged over 1980-2009. Isolines are the lines of equal surface height.

a)

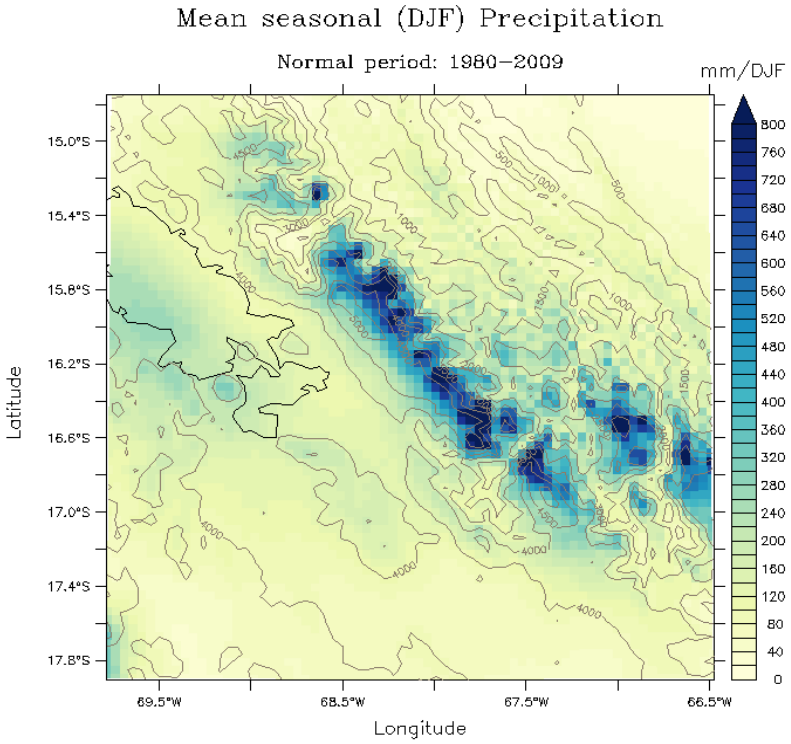

b)

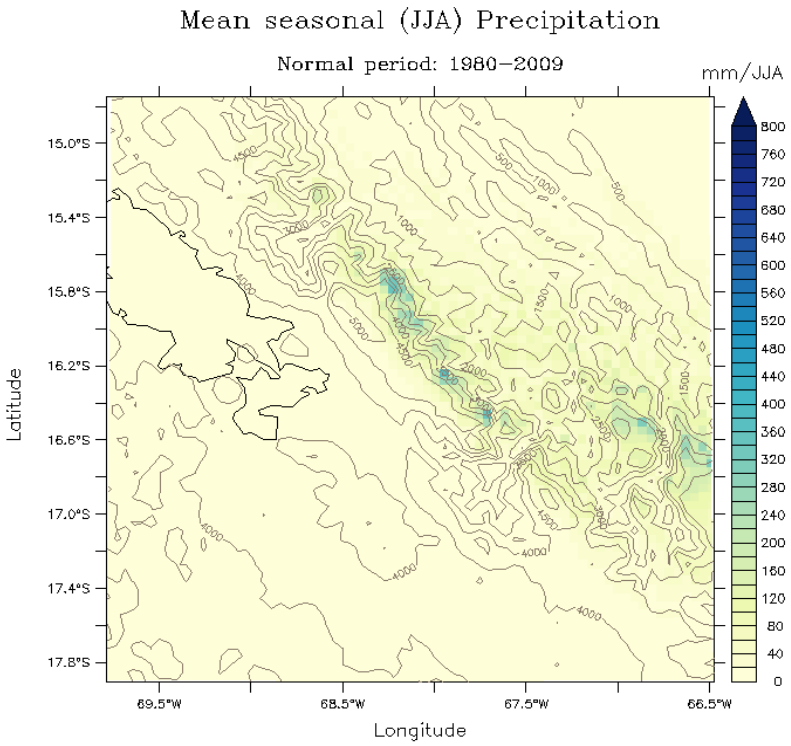

Figure 6.2: Summer (DJF) **(a)** and winter (JJA) **(b)** total precipitation (mm) averaged over 1980-2009. Total precipitation includes rainfall, snowfall and convective precipitation.

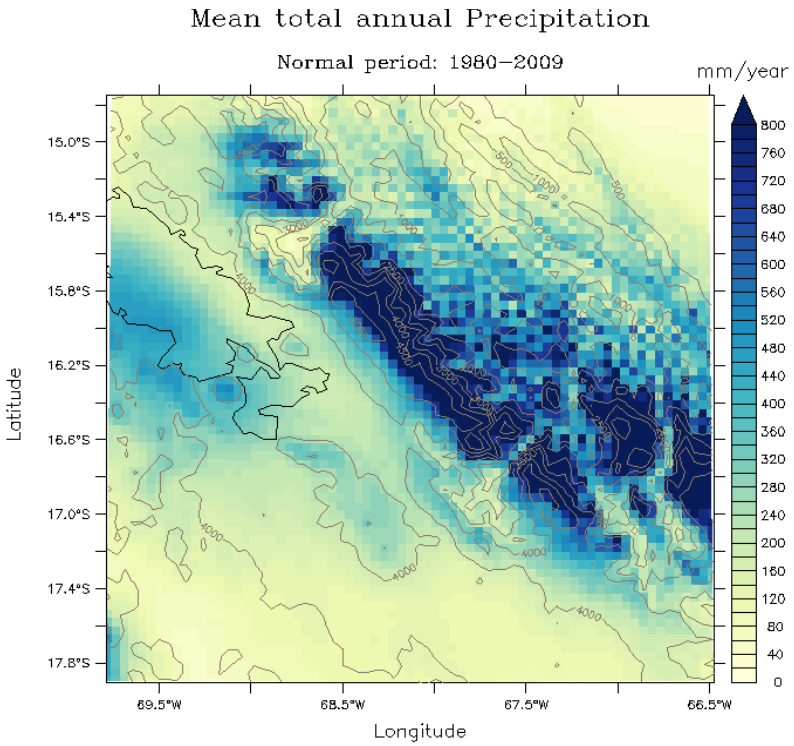

Figure 6.3: Annual total precipitation (mm) averaged over 1980-2009.

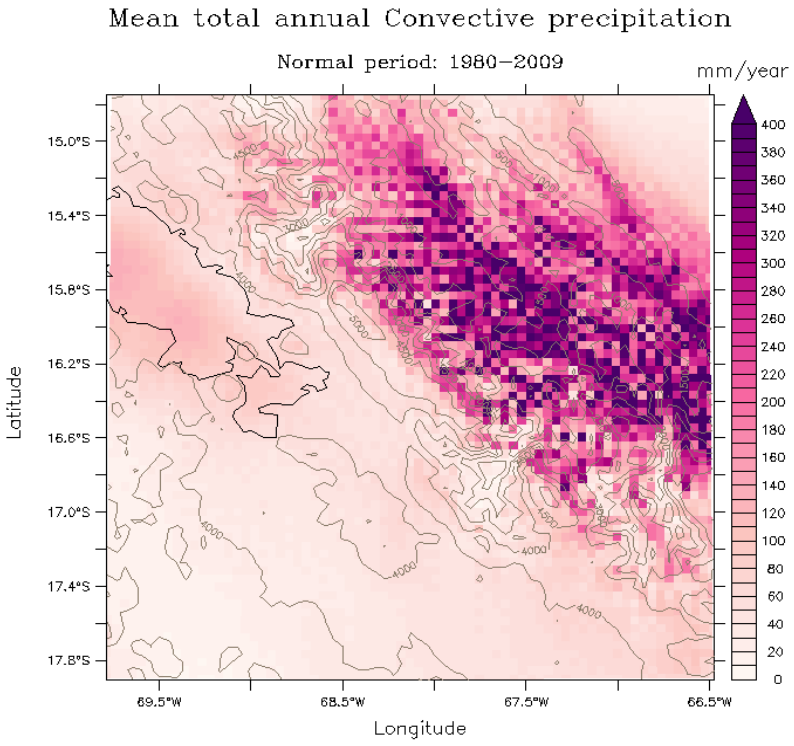

Figure 6.4: Annual convective precipitation (mm) averaged over 1980-2009.

a)

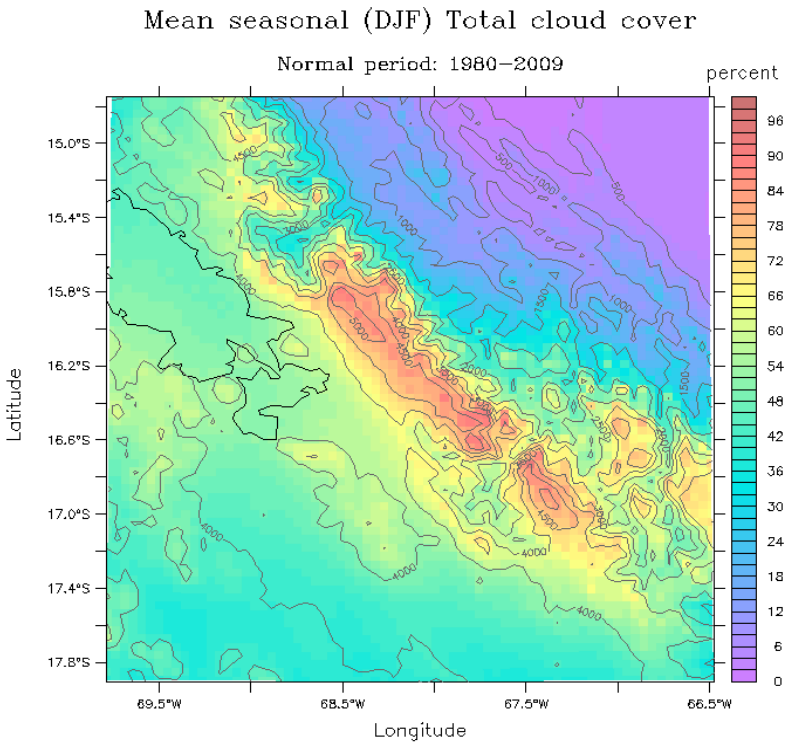

b)

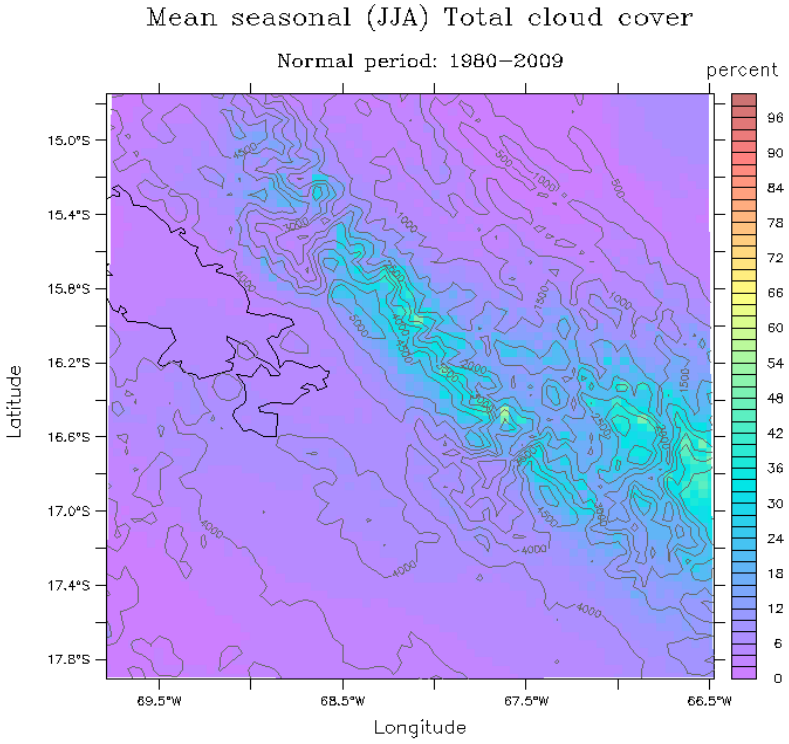

Figure 6.5: Summer (DJF) **(a)** and winter (JJA) **(b)** total cloud cover (%) averaged over 1980-2009.

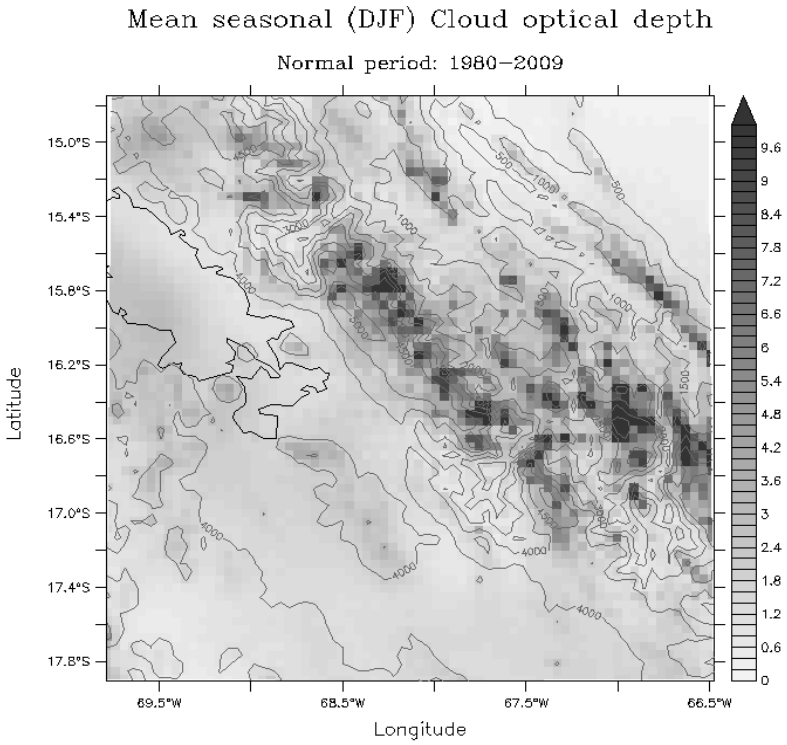

Figure 6.6: Summer (DJF) cloud optical depth averaged over 1980-2009.

a)

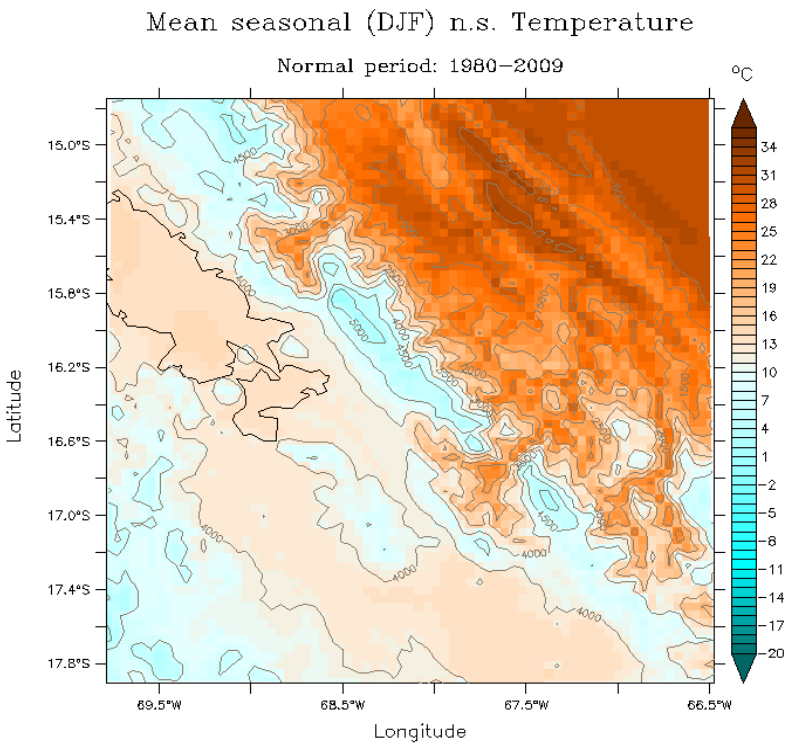

b)

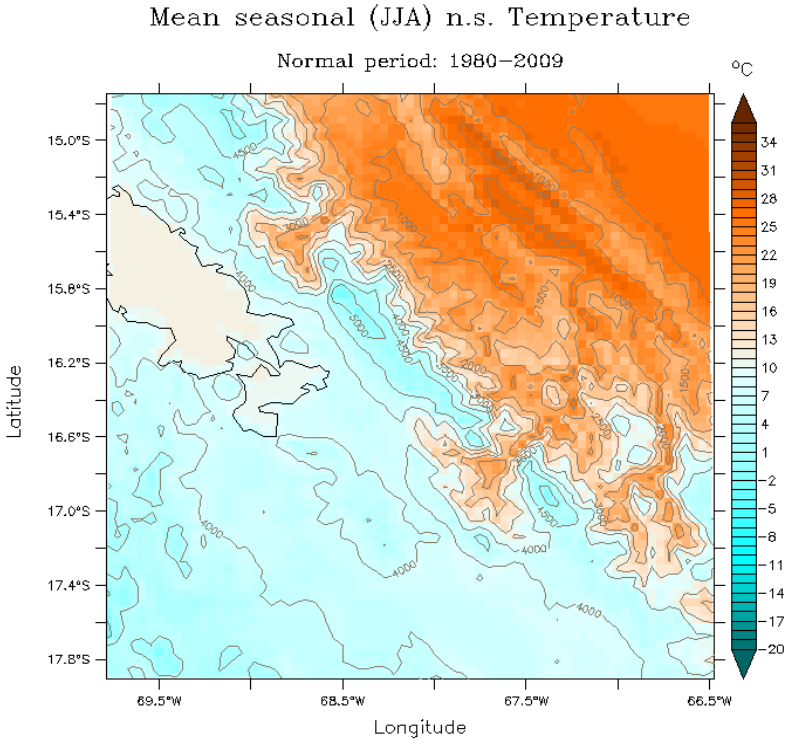

Figure 6.7: Summer (DJF) **(a)** and winter (JJA) **(b)** near-surface (n.s.) air temperature (°C) averaged over 1980-2009.

a)

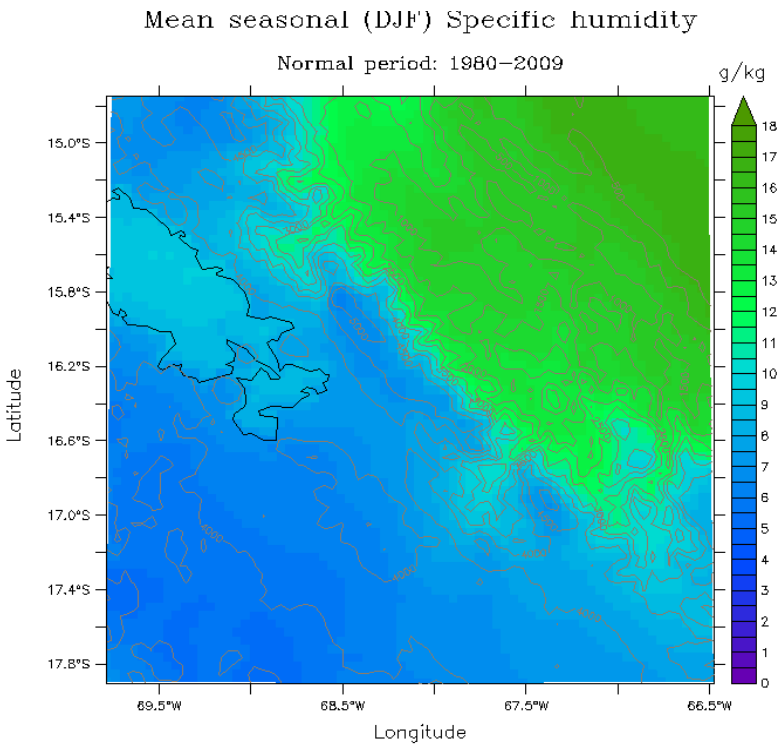

b)

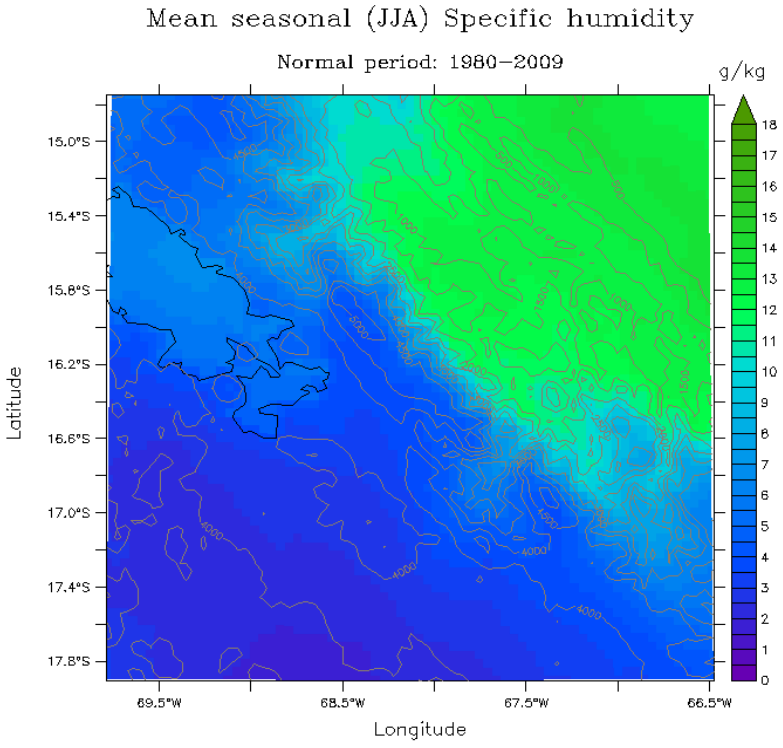

Figure 6.8: Summer (DJF) **(a)** and winter (JJA) **(b)** specific humidity (g/kg) averaged over 1980-2009.

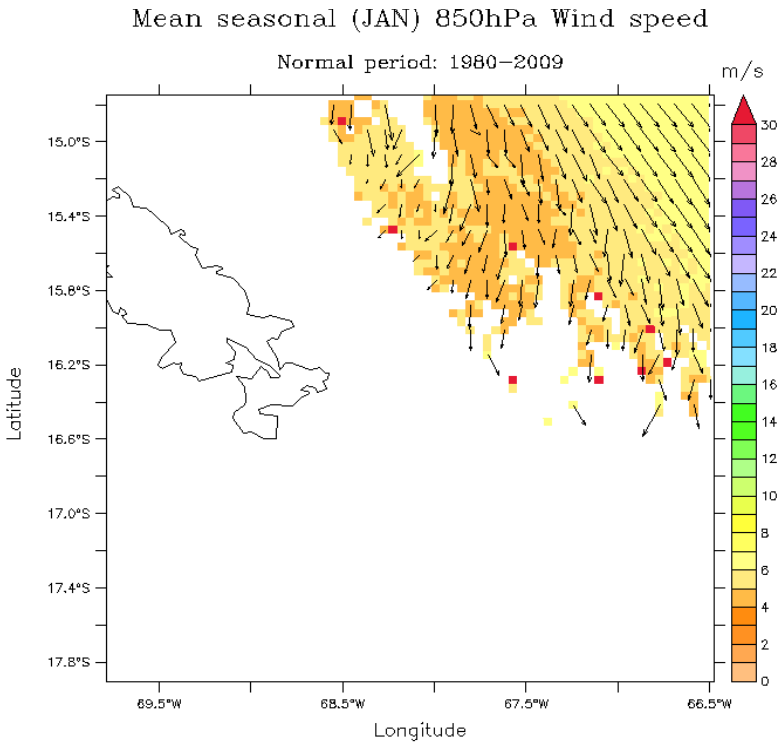

Figure 6.9: Summer (January) 850 hPa horizontal wind speed (m/s) averaged over 1980-2009. Arrows indicate wind direction.

a)

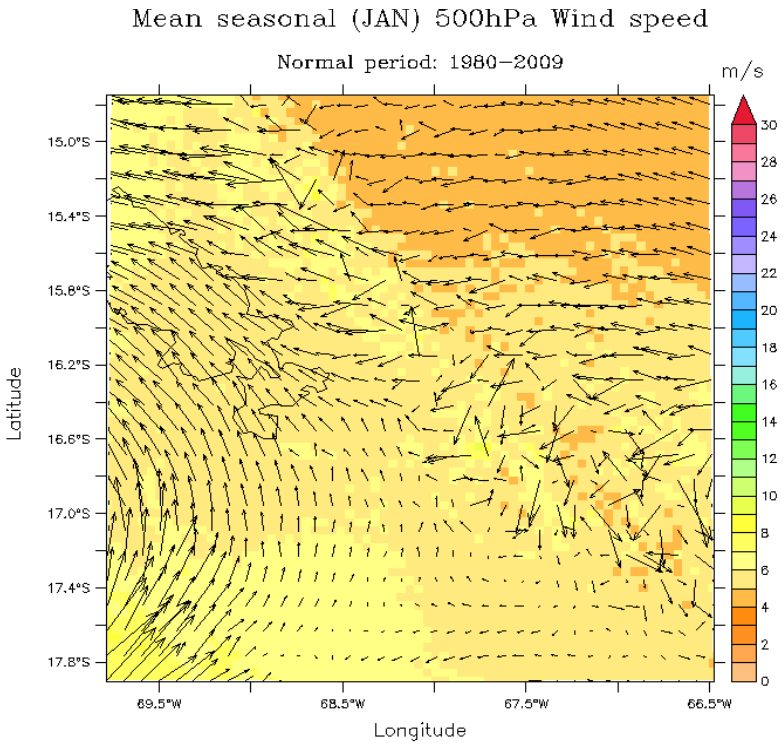

b)

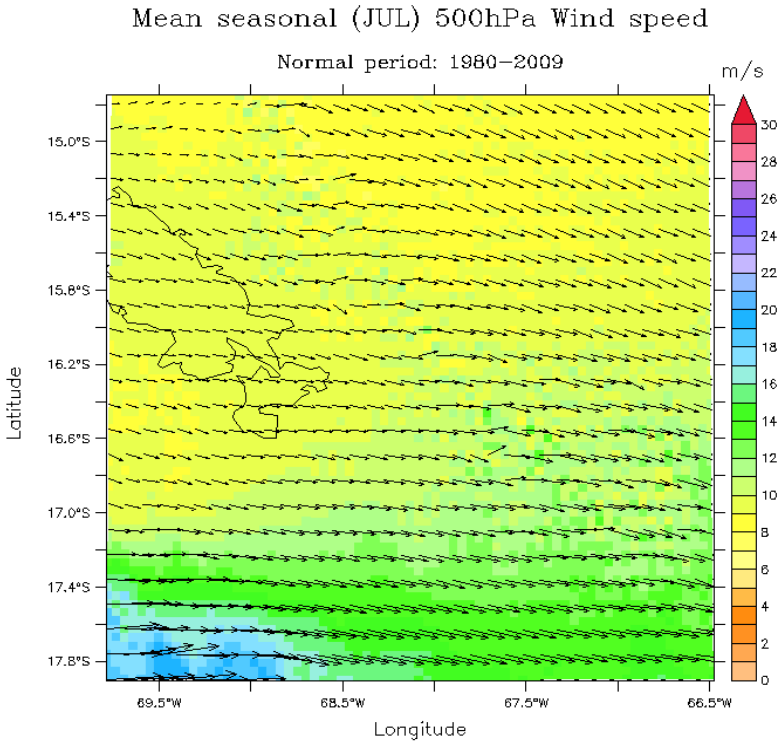

Figure 6.10: Summer (January) **(a)** and winter (July) **(b)** 500 hPa horizontal wind speed (m/s) averaged over 1980-2009. Arrows indicate wind direction.

a)

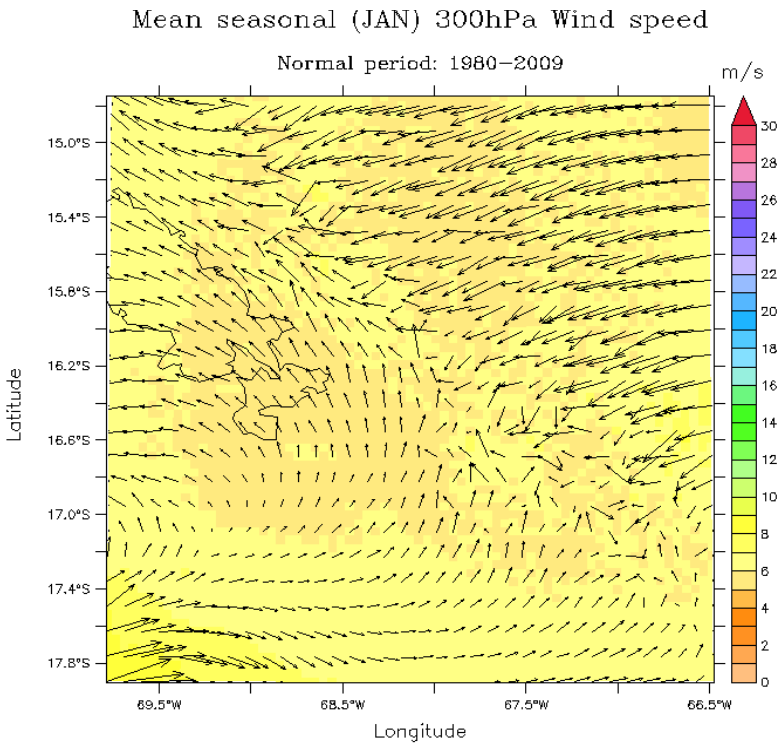

b)

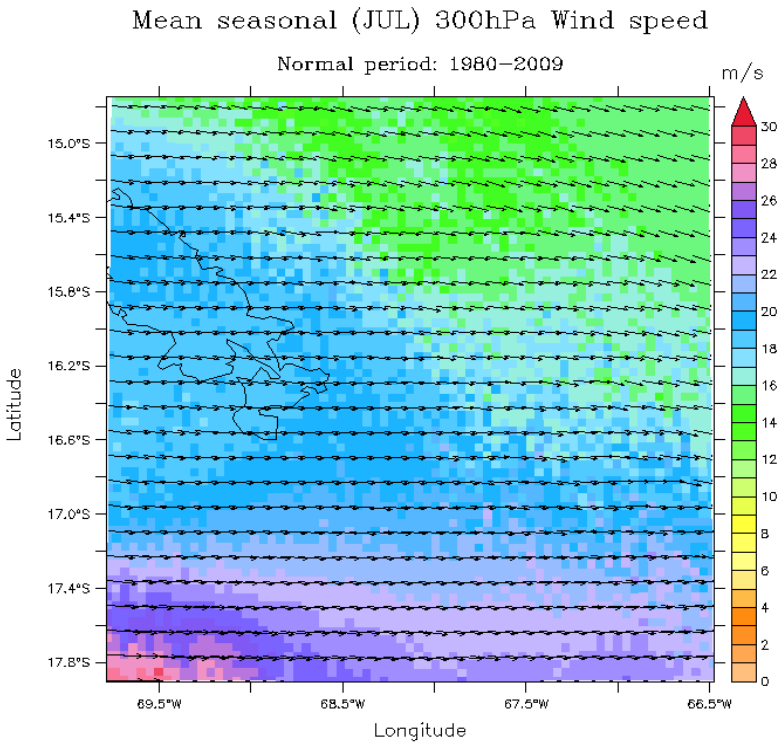

Figure 6.11: Summer (January) **(a)** and winter (July) **(b)** 300 hPa horizontal wind speed (m/s) averaged over 1980-2009. Arrows indicate wind direction.

6.2. Temporal evolution and trends

We extracted a number of modeled parameters from the central pixel of our domain, which is centered over the Chacaltaya Mountain, and performed linear regression analysis to assess the trend of those parameters from 1960 onwards. We adjusted an equation of the type $A=a+b*t$ to each time series (A_i, t_i), where A_i represents the value of the parameter for the year t_i. We also evaluated the significance of the trends by computing the uncertainty range defined for the 95% confidence interval:

$$\begin{cases} e_1 = \sum(\text{trend}(a_i) - a_i)^2 \\ e_2 = \sum(t_i - \text{mean}(t_i))^2 \\ \text{range} = \sqrt{e_1/((2010 - 1958 - 1) \times e_2)} \times k \end{cases}$$

where t_i is the i^{th} year of the time series, a_i the value of the parameter for the year t_i, trend(a_i) the value of the trend for the year t_i, and k=1.96 for the 95% level of confidence. The trend is significant if its value is higher than the uncertainty range.

Table 6.1 provides, for each parameter, the annual and long-term (1960-2014) trends, expressed both in absolute and relative (%) values with respect to their average. Figures 6.13 to 6.19 show the annual evolution between 1960 and 2014 of the same parameters, as well as their linear trend.

Modeled parameter	Unit	Trend yr^{-1}		Trend over 55 years (1960-2014)	
		Absolute values	Relative values (%)	Absolute values	Relative values (%)
n.s. Minimum temperature	°C	+0.020	-	+1.1	-
n.s. Maximum temperature	°C	+0.032	-	+1.8	-
n.s. Average temperature	°C	+0.028	-	+1.5	-
300 hPa Average temperature	°C	+0.033	-	+1.8	-
Total precipitation	mm yr^{-1}	-3.949	-0.648	-217.2	-35.6
n.s. Specific humidity	g/kg	-0.0002	-0.003	-0.01	-0.2
300 hPa Specific humidity	g/kg	-0.0008	-0.143	-0.04	-7.9
Total cloud cover	%	-0.354	-0.650	-19.46	-35.7
Latent heat flux	W/m^2	+0.023	+0.516	+1.2	+28.4
Sensible heat flux	W/m^2	+0.117	+0.138	+6.4	+7.6
Net all-wave radiation	W/m^2	-0.272	-0.386	-14.9	-21.2
Downward short-wave radiation	W/m^2	+0.587	+0.253	+32.3	+13.9
Downward long-wave radiation	W/m^2	-0.271	-0.112	-14.9	-6.2

Table 6.1: Trends expressed in absolute and relative values for mean annual near-surface (n.s.) minimum, maximum and average temperature, 300 hPa average temperature, total annual precipitation, mean annual near-surface (n.s.) and 300 hPa specific humidity, cloud cover, latent and sensible heat fluxes, net all-wave radiation, downward short-wave and long-wave radiation.

All trends are significant, which means that the region of the Chacaltaya Mountain has effectively experienced a climate change since 1960. The most significant changes concern precipitation and cloud cover, which both decreased by more than one third (35%) of their initial amount between 1960 and 2014. Specific humidity also dropped, especially in the upper troposphere, suggesting an increased entrainment of dry air from the free troposphere into the boundary layer. Additional evidence for the drying of the lower troposphere is provided by the less negative latent heat flux.

Sensible heat flux increased as a consequence of the atmospheric warming. Average daily near-surface temperature rose of 1.1°C in 55 years, or 0.2°C per decade, which is more than the 0.15°C per decade trend computed for the entire tropical zone (1°N–23°S) over 1950-1994 by Vuille *et al.* (2003). This corroborates some previous observational studies declaring that the warming is more intense along the western slopes of the Andes than the eastern. Besides, the temperature increase is clearly more pronounced for maxima than for minima, which means that the warming took place rather during daytime than during nighttime. Enhanced daytime warming results from an increase in the downward short-wave radiation, which can only be related to a

decrease in low clouds, since those clouds have a stronger reflecting (albedo) effect on sunlight than high clouds have. High clouds by contrast, are more transparent to solar radiation, but they efficiently absorb infrared energy emitted by the earth's surface, and thereby increase the greenhouse effect. Deep convective clouds, due to their large vertical extension, strongly affect both short- and long-wave radiation equally, so that they have a neutral impact on surface temperature.

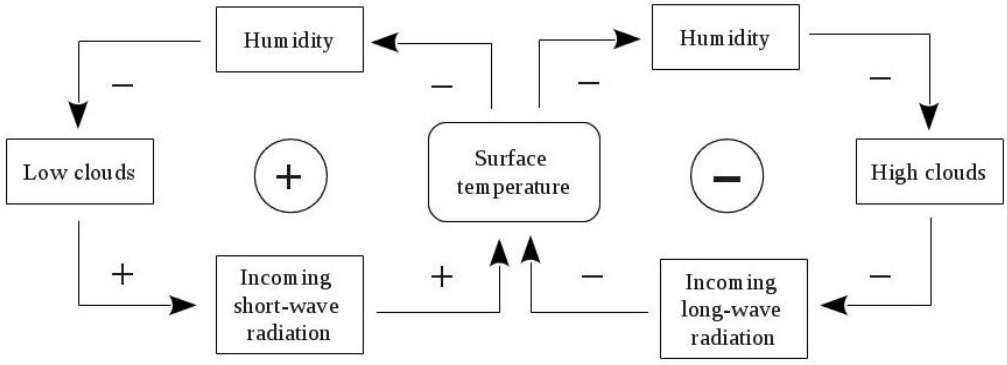

Figure 6.12: Cloud feedback loops. Low clouds affect short-wave radiation via albedo as opposed to high clouds affecting long-wave radiation via greenhouse effect.

As the increasing trend in the downward short-wave flux is more pronounced than the decreasing trend in the long-wave flux, we deduce that MAR produces a more positive low cloud feedback as compared to the negative high cloud feedback. Conversely, if the high cloud feedback had prevailed over the low cloud feedback, a reduced amount in high cloudiness would have been characterized by *(i)* a more negative trend in the incoming long-wave radiation, *(ii)* a warming occurring predominately during nighttime, and *(iii)* probably a less significant warming in the lower troposphere due to the negative sign of the high cloud feedback.

Furthermore, the vertical temperature profile changed as a result of a decrease in the lapse rate. Indeed, average temperature in the upper troposphere (300 hPa) increased at a more pronounced rate than in the lower troposphere (near-surface).

Throughout the entire analysed period (1960-2014), the net all-wave radiation budget was in negative imbalance, and became further negative. Figure 6.17 shows how closely the interannual variability in the radiation budget reflects the evolution of the total cloud cover (Figure 6.15).

Tables 6.2 and 6.3 provide a detailed account of the decadal evolution between 1960 and 2014 of the main climatic variables. For each period, we calculated the anomaly of the decadal mean value from the mean value of the previous decade. The decadal averages were calculated from the annual and seasonal values. We considered only the austral summer season (DJF), because the summer months are the most important ones for the seasonality of glacier ablation, as precipitation and high temperatures both occur exclusively during summer.

Modeled parameter	Unit	1970-79	1980-89	1990-99	2000-09	2010-14
n.s. Average temperature	°C	+0.4	+0.5	+0.1	+0.2	+0.3
n.s. Minimum temperature	°C	+0.4	+0.2	+0.1	+0.2	+0.2
n.s. Maximum temperature	°C	+0.4	+0.7	+0.1	+0.0	+0.3
Total precipitation	mm yr^{-1}	+149.7	-250.8	-17.2	+28.3	-3.8
n.s. Specific humidity	g/kg	-1.2	-3.2	+1.1	-0.2	+2.5
Total cloud cover	%	0.0	-16.1	-5.8	-2.0	0.0

Table 6.2: Decadal anomaly with respect to the previous decade, calculated for mean annual near-surface average, minimum and maximum temperature, total annual precipitation, mean annual specific humidity, and cloud cover.

Modeled parameter	Unit	1970-79	1980-89	1990-99	2000-09	2010-14
n.s. Average temperature	°C	+0.3	+0.5	+0.2	0.0	-0.2
n.s. Minimum temperature	°C	+0.4	+0.4	+0.1	+0.2	-0.1
n.s. Maximum temperature	°C	0.0	+0.8	+0.3	-0.3	-0.3
Total precipitation	mm/DJF	+70.6	-88.8	-11.6	+39.6	+14.6
n.s. Specific humidity	g/kg	+0.1	+0.1	+0.1	+0.1	+0.1
Total cloud cover	%	+1.0	-6.0	-3.0	+2.0	0.0

Table 6.3: Decadal anomaly with respect to the previous decade, calculated for mean seasonal (DJF) near-surface average, minimum and maximum temperature, total DJF precipitation, mean DJF specific humidity, and cloud cover.

These tables reveal that the 1980s decade constitutes a break point for almost all climatic parameters. Figures 6.13 to 6.19 reveal that the rupture in the trends started during the second half of the 1970s, and more precisely after 1976-77, which is the year of the great Pacific Shift. Throughout the 1980s until the late 1990s, the region of the Chacaltaya underwent overall drier and warmer climatic conditions. The next Pacific shift occurred in 1999 and started the current cold PDO phase. This event is also visible in the plotted time series, as it generated a short reversal in the long-term evolution of the various parameters. The decreasing trends in precipitation and cloud cover both seem to have slowed down since 1999, while temperatures have experienced fewer sharp variations compared to the previous decades (with one exception in 2009).

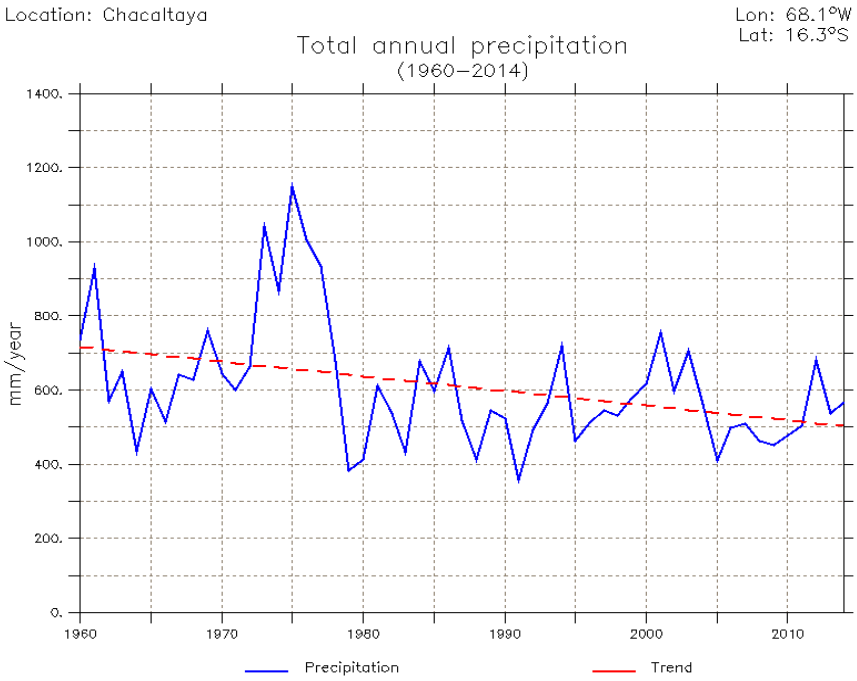

Figure 6.13: Evolution of the annual total precipitation amount (mm) over 1960-2014 in the Chacaltaya region. The red dashed curve represents the long-term trend over the same period.

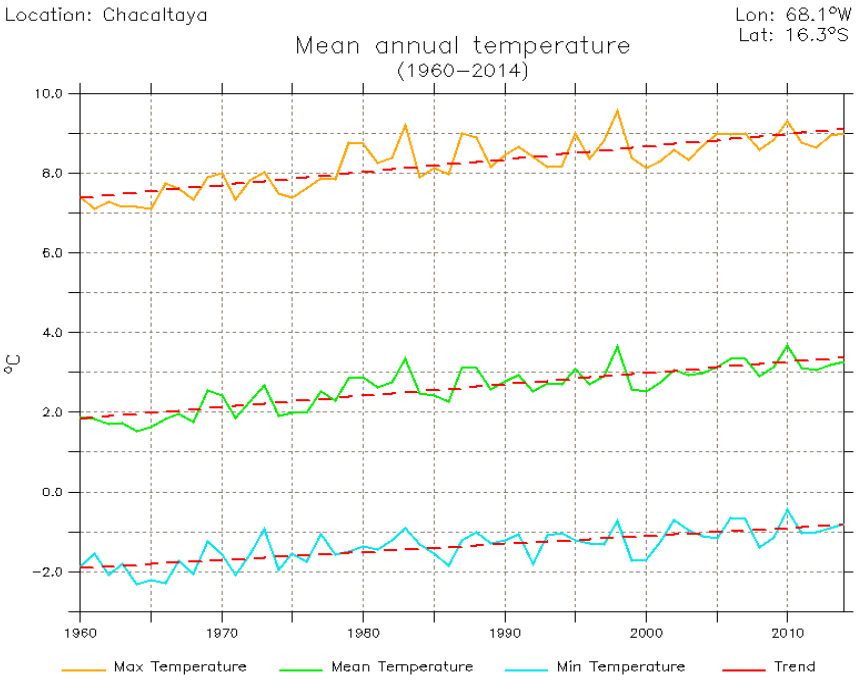

Figure 6.14: Evolution of the annual average, minimum and maximum near-surface temperature (°C) over 1960-2014 in the Chacaltaya region.

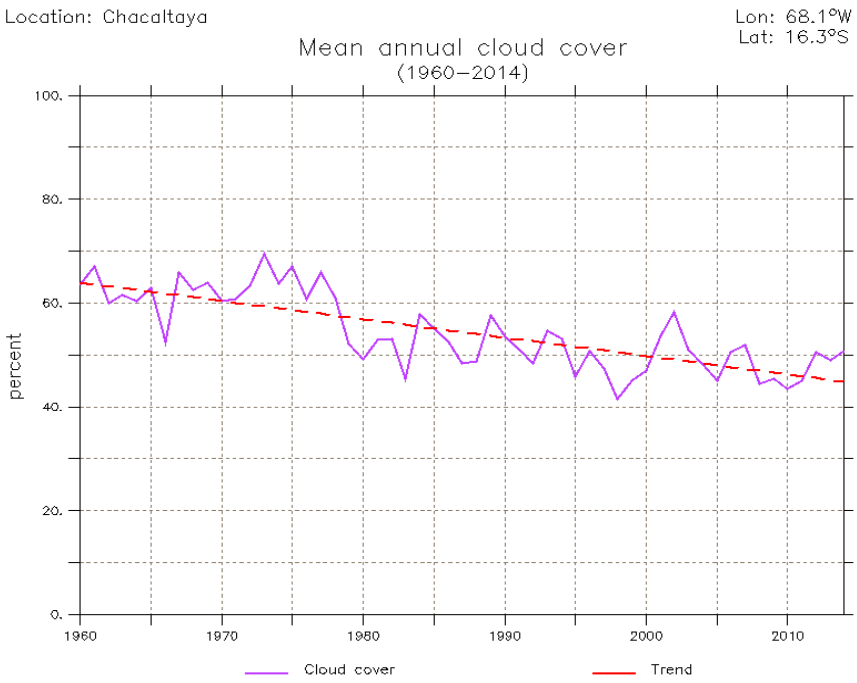

Figure 6.15: Evolution of the annual cloud cover (%) over 1960-2014 in the Chacaltaya region.

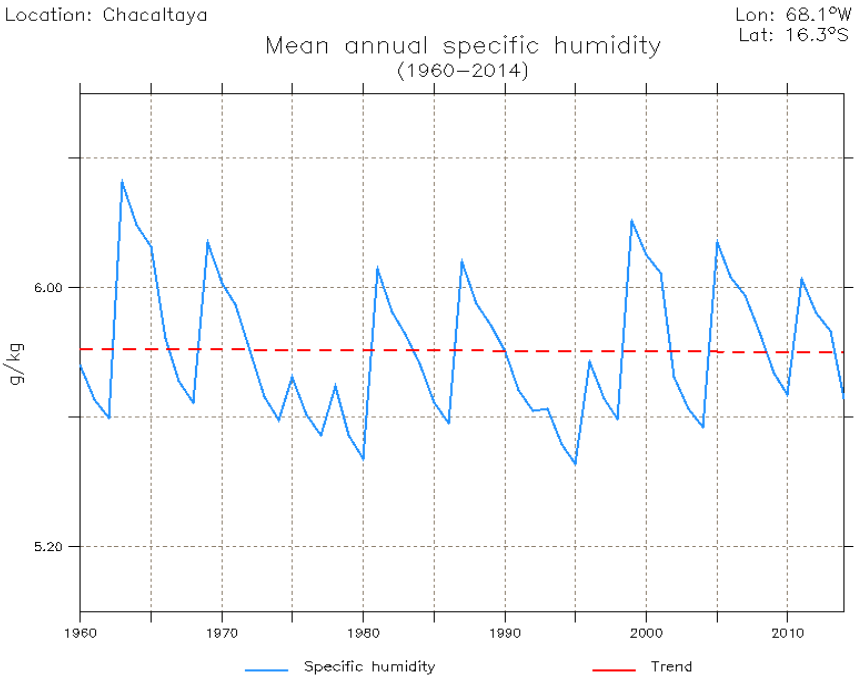

Figure 6.16: Evolution of the annual near-surface specific humidity (g/kg) over 1960-2014 in the Chacaltaya region.

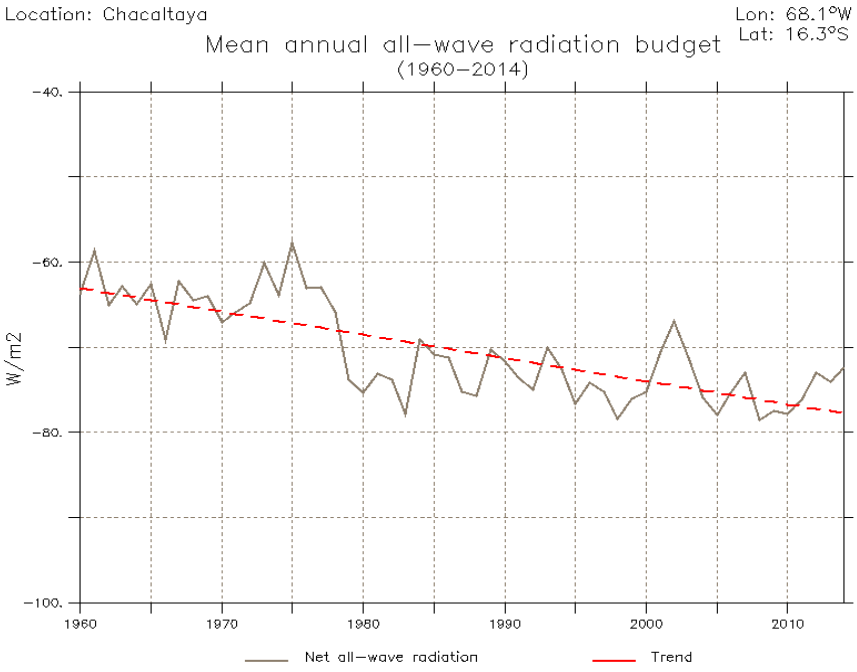

Figure 6.17: Evolution of the annual net all-wave radiaton budget (W/m²) over 1960-2014 in the Chacaltaya region.

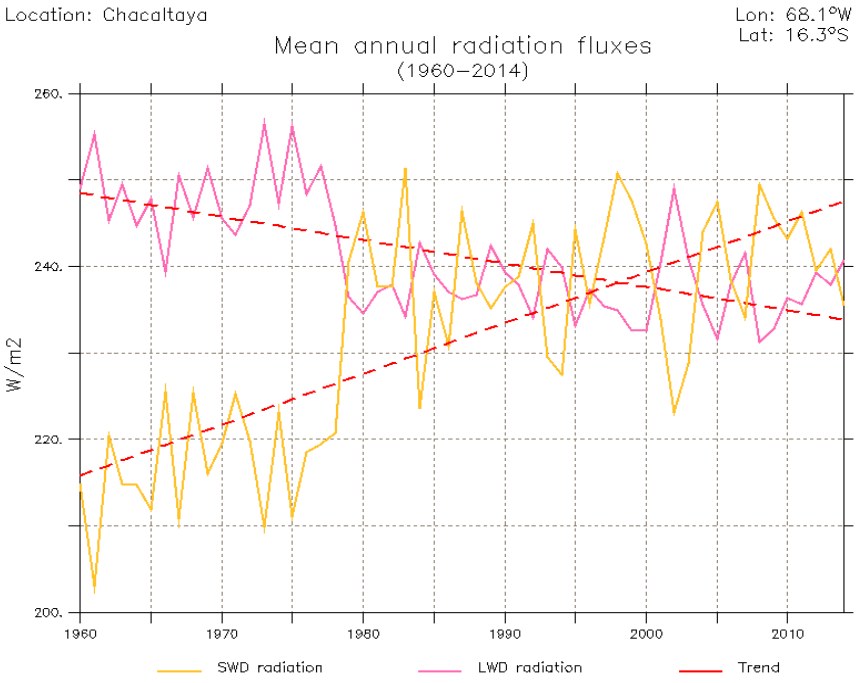

Figure 6.18: Evolution of the annual downward short-wave (SWD) and the downward long-wave (LWD) radiation fluxes (W/m²) over 1960-2014 in the Chacaltaya region.

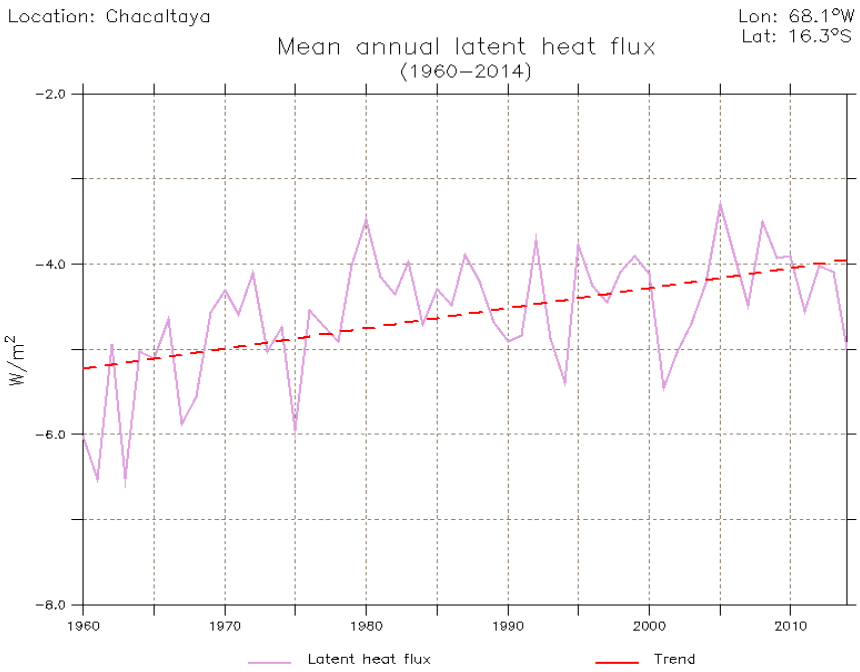

Figure 6.19: Evolution of the annual latent heat flux (W/m²) over 1960-2014 in the Chacaltaya region.

6.3. El Niño / La Niña events

We start with an identification of the ENSO phases in the region of the Chacaltaya Mountain, by plotting the annual anomalies for precipitation, temperature, cloud cover and specific humidity, displayed in Figures 6.20 to 6.23. Then we extend our analysis to our entire domain, in order to study the spatial variability of the ENSO signal.

6.3.1. ENSO signals in the Chacaltaya region

Table 6.4 resumes the most important ENSO phases identified between 1960 and 2014 at the Chacaltaya Mountain. Each phase is characterized in terms of precipitation, temperature, cloudiness and specific humidity anomalies, with respect to our reference period 1980-2009. The combination of these climatic parameters is responsible for the more or less pronounced ablation experienced by the Chacaltaya Glacier.

		Precipitation	Temperature	Cloudiness	Humidity
1982-83	El Niño	Drier	Warmer	Less cloudy	More humid
1984	La Niña	Wetter	Colder	Cloudier	0
1985-86	La Niña	Wetter	**The coldest**	Cloudier	Less humid
1987-88	El Niño	Drier	Warmer	0	More humid
1991	El Niño	**The driest**	0	0	0
1994	La Niña	Wetter	0	0	Less humid
1998 (1997-99)	El Niño	0	**Almost the warmest**	**The least cloudy**	**The most humid**
2000-01	La Niña	**The wettest**	Colder	Cloudier	More humid
2002-03	La Niña	Wetter	0	**The cloudiest**	0
2005	El Niño	Drier	0	Less cloudy	More humid
2009-10	El Niño	Drier	**The warmest**	Less cloudy	0

Table 6.4: List of the most important ENSO events identified between 1980 and 2014 in the Chacaltaya region. Each event is characterized by anomalies in precipitation, temperature, cloud cover and specific humidity. The strongest anomalies of the period are shown in bold. Non-significant anomalies are represented by a zero. El Niño events are shaded in light orange, and La Niña events in light blue.

From the continuous mass balance monitoring since 1991, we know that the Chacaltaya Glacier underwent three major ablation peaks during the 1990s decade: a very strong one in September 1997–February 1999, and two others in September 1994–December 1995 and September 1991–April 1992 (for more information, see section 2.4.2 in Chapter 2). From the mass balance reconstruction studies, it is believed that during the 1980s, both the 1982-1983 and 1987-1988 El Niño events also induced strongly negative mass balance on the glacier. Of the five mentioned El Niño phases, four can be identified by the modeled annual anomalies.

El Niño 1982-1983 The first strong El Niño phase (1982-83) combined the ideal climatic conditions to cause intense ablation to the glacier. A deficit in precipitation prevented the glacier from gaining mass through snowfall and decreased the albedo of its surface, inducing thereby enhanced heat absorption by the glacier. More humidity in the air limited the sublimation process and increased the melting, which led to considerable higher ablation rates. Moreover, melting was supported by the anomalous warm temperatures. Finally, the reduced cloudiness allowed incoming solar short-wave radiation to reach the surface without much attenuation, which provided further energy available for the melting.

El Niño 1987-1988 The second warm ENSO phase that occurred in the 1980s was almost a replication of the strong 1982-1983 event, but its effect was less intense because the climatic conditions were slightly less extreme.

El Niño 1991-1992 The 1991-1992 El Niño contrasts with the two previous events, since it was characterized by no anomaly with the exception of the extreme dryness of year 1991. The precipitation deficit of 1991 is the most severe one of the whole 1980-2014 simulation period.

El Niño 1997-1998 The mega El Niño of 1997-1998 exhibited the exact opposite characteristics compared to the 1991-1992 phase. Precipitation showed no significant behavior, but humidity, cloudiness and temperature endured the most extreme anomalies of the period. The combination of enhanced humidity, very reduced cloudiness and high temperatures offered the perfect mix for very high melting rates.

El Niño 2004-2005 & 2009-2010 Of the two warm phases which occurred during the 21st century, the second is the most remarkable one. According to our simulation, 2010 experienced the highest temperatures of the 55 years long period of our analysis. Unfortunately, this outcome can not be confirmed by observations since the LACA&D measurements end in 2006. This warm ENSO event is probably responsible for the complete and definite disappearance of the Chacaltaya Glacier.

El Niño 1994-95 Finally, the 1994-1995 El Niño is the only important ENSO phase which is not clearly reflected in the modeled anomalies. Monitoring measurements reveal that the mass balance of the Chacaltaya became strongly negative during two very short periods of time, situated respectively around December–January 1994 and October–November 1995. Our model however provides no hint of any climatic cause explaining this sharp mass loss. Actually, 1994 exhibits rather La Niña-like conditions, since anomalies indicate that precipitation was higher that year. In 1995, our model even simulates the lowest values of specific humidity of the 1980-2014 period.

The literature tells us that while 1995 was neither entirely part of a warm or a cold ENSO phase, 1994 was certainly not part of a La Niña phase. Nevertheless, comparing the modeled amounts of precipitation to the observations attests that MAR accurately simulates precipitation during those years. Consequently, we deduced two major conclusions. First, these results support those of Vuille *et al.* (2000), who found that in some parts of Bolivia, and more specifically in the eastern Altiplano, the ENSO signal is modified by local climatic processes. In the Cordillera Real, precipitation is mainly generated by convection, which is partly related to the seasonal presence of the Bolivian High during the austral summer. Both in 1994 and 1995, the Bolivian High formed over the Altiplano as it usually does during the non-El Niño phases. The irregular behavior of this high pressure system during the ENSO events is still poorly understood. Second, there may have been other factors than the ENSO inducing strong negative mass balance on the Chacaltaya Glacier, and those causes might be non-climatic. These perspectives will be discussed in Chapter 7.

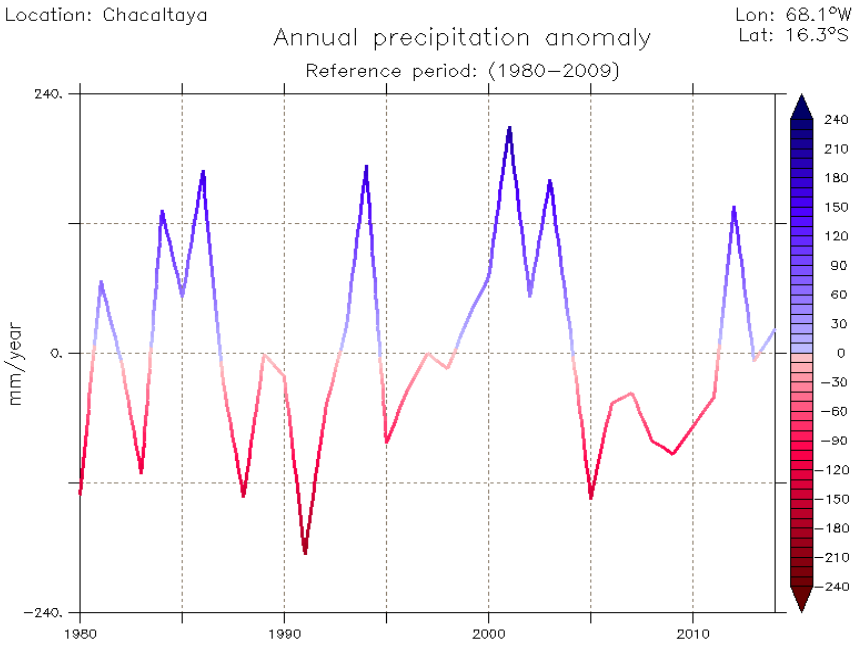

Figure 6.20: Evolution of the annual precipitation anomaly (mm) over 1980-2014 in the Chacaltaya region. The reference period is 1980-2009.

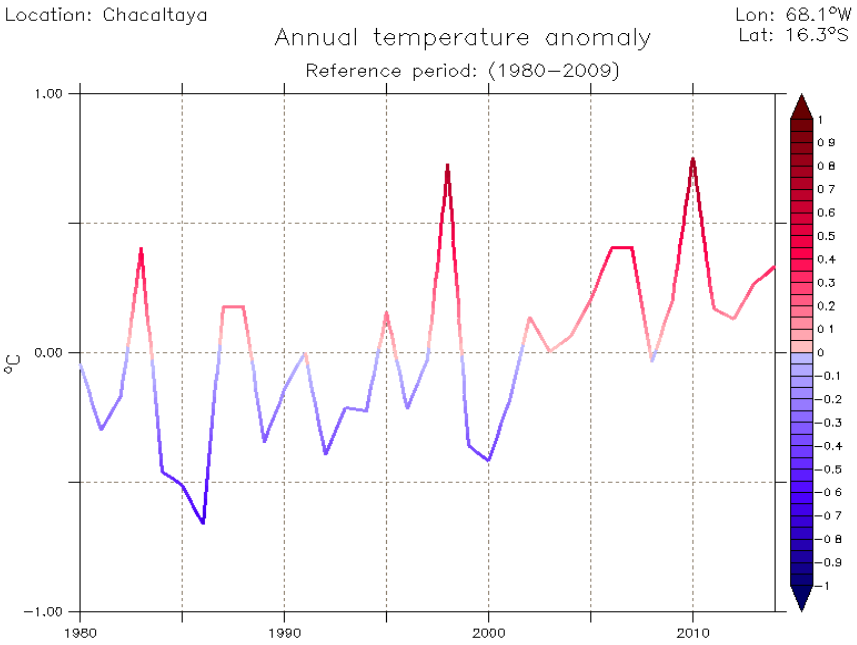

Figure 6.21: Evolution of the annual near-surface temperature anomaly (°C) over 1980-2014 in the Chacaltaya region. The reference period is 1980-2009.

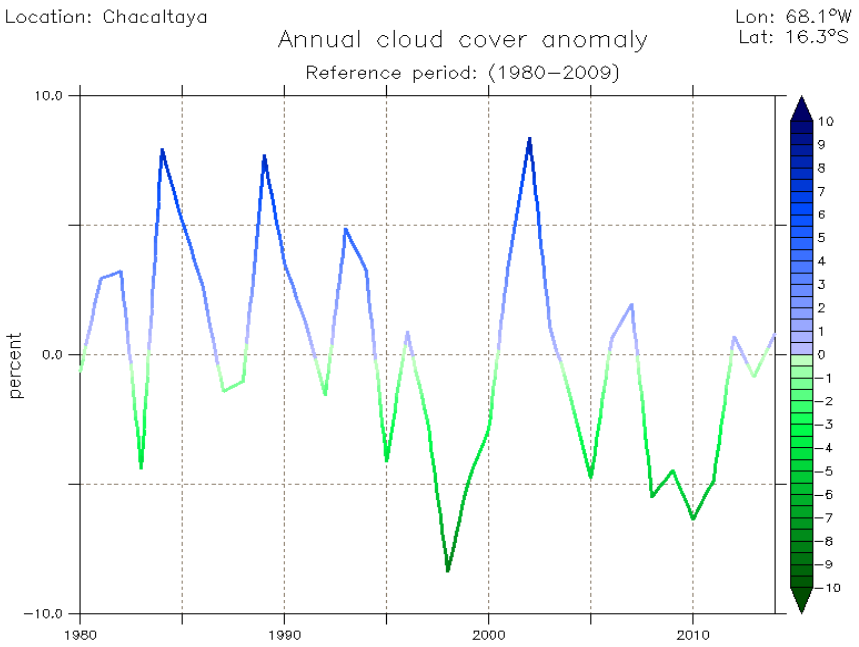

Figure 6.22: Evolution of the annual cloud cover anomaly (%) over 1980-2014 in the Chacaltaya region. The reference period is 1980-2009.

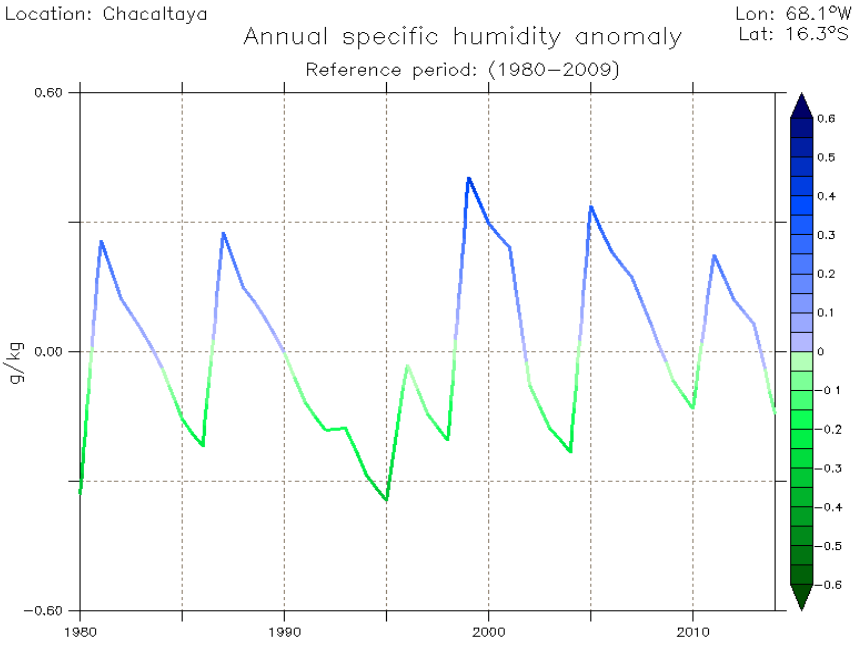

Figure 6.23: Evolution of the annual specific humidity anomaly (g/kg) over 1980-2014 in the Chacaltaya region. The reference period is 1980-2009.

6.3.2. Spatial variability of ENSO signals at the regional scale

We concentrate here on the most notable ENSO phases of these past decades in order to analyse the spatial distribution of the anomalies in precipitation and near-surface temperature and cloudiness over the eastern Bolivian Andes during these particular events. We also study the regional circulation near the surface by looking at the 500 hPa wind speed.

El Niño 1982-1983 In the Chacaltaya region, this ENSO phase is characterized by warmer and drier conditions than usual. Figure 6.24 shows that temperature anomaly is almost uniform throughout the study area, with a slightly more intense warming over Lake Titicaca and along the western slopes of the Andes. In contrast, the precipitation deficit is very localized and concerns a very limited area. The cloud cover anomaly is also highly contrasted, but follows a regular distribution, consistent with the prevailing antagonist air masses. The enhanced westerlies can account for the reduced cloudiness, as dry Pacific air is advected further inside the continent, and even overflows the Cordillera Real to prevail over the western Amazon Basin. The Bolivian High is absent of our study area, which suggests that it has weakened and shifted northward, as it is thought to happen during El Niño phases.

La Niña 1983-1984 This La Niña event, illustrated in Figure 6.25, is the utter opposite situation with respect to the 1982-83 El Niño. The Bolivian High is strengthened and displaced southward, so that the mid-tropospheric circulation is dominated by the moist easterly influx, which provides large amounts of water vapor to the west of the Cordillera Real. Accordingly, cloud cover and precipitation are enhanced throughout the Altiplano.

El Niño 1991-1992 Our model simulated the year 1991 as the driest of the 1960-2014 period in the Chacaltaya region. As can be observed in Figure 6.26, the precipitation deficit touched a large area, by contrast to the 1982-83 El Niño. This area coincides with the climatological zone which concentrates the major part of the precipitation, and corresponds to the situation of the majority of the dry events that befell the eastern Bolivian Andes. As the 500 hPa wind field suggests, such droughts can be related to the enhanced westerlies.

El Niño 1997-1998 The peculiarity of this event is the spatial homogeneity of the anomalies, which mainly concern temperature and cloudiness (Figure 6.27). The impact of this El Niño phase was exceptionally strong for all regions in the Tropics. However, in our study area, the winds show no anomalous behavior, which would explain why no significant anomalies are observed in the precipitation.

La Niña 2002-2003 The 2002-2003 La Niña phase is to the 1991-1992 El Niño what the 1983-1984 La Niña is to the 1982-1983 El Niño. This cold ENSO phase is predominately driven by precipitation anomalies, which concentrate over the climatological area where precipitation generally occur (Figure 6.28).

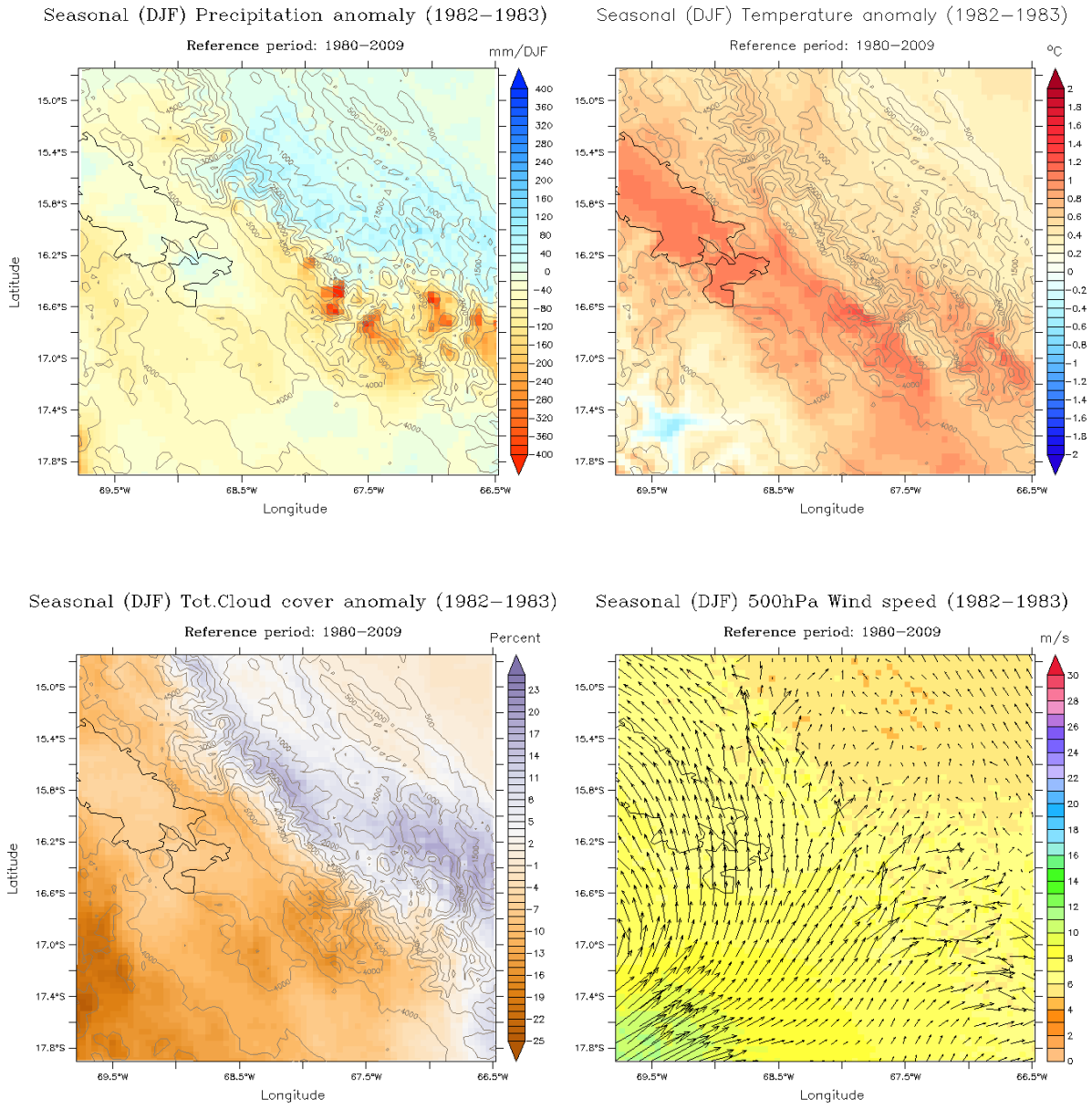

Figure 6.24: Summertime (DJF) precipitation **(upper left)**, near-surface temperature **(upper right)**, and total cloud cover **(lower left)** anomalies, as well as the 500 hPa wind speed during December 1982 – February 1983 **(lower right)**.

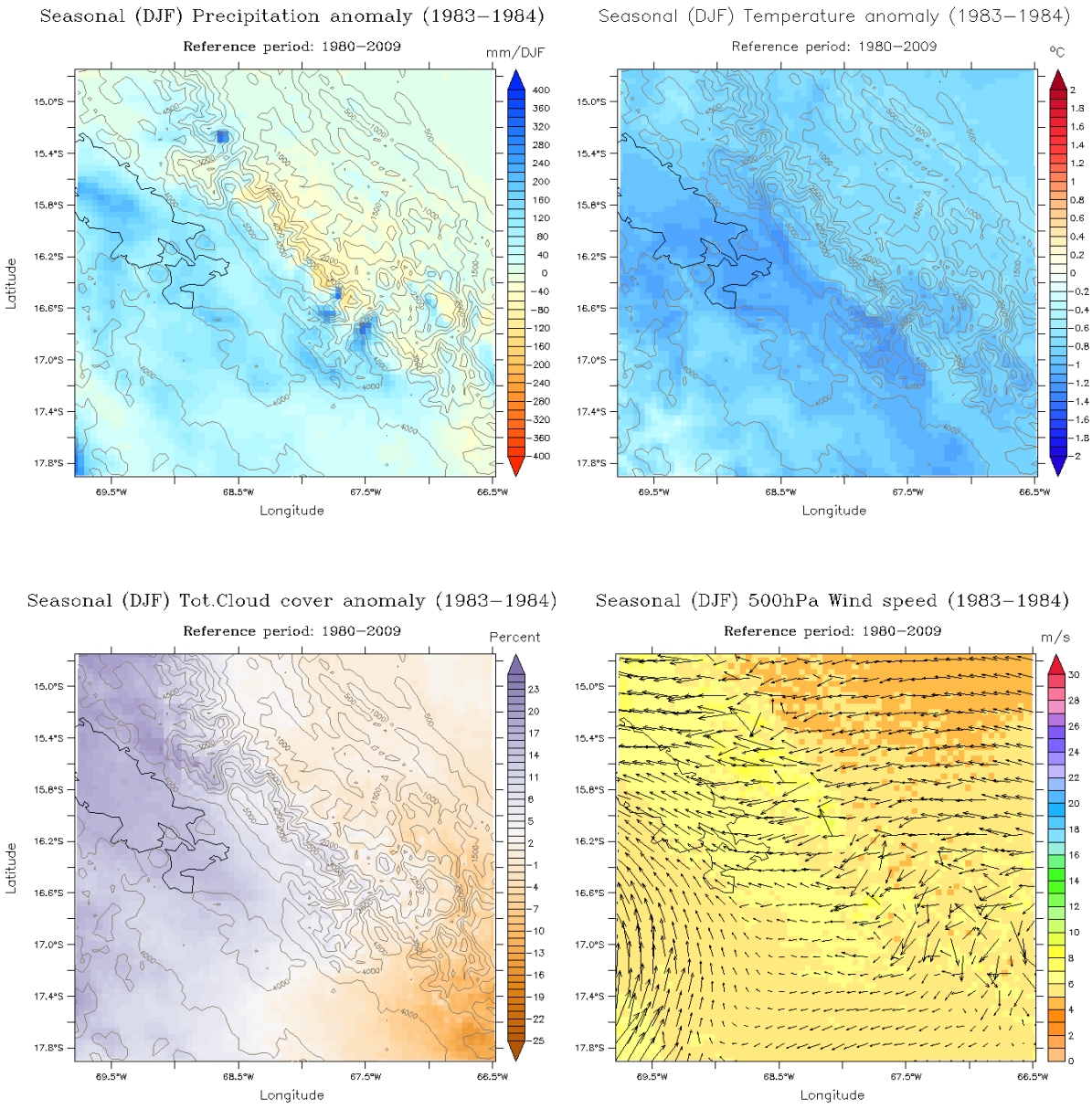

Figure 6.25: Summertime (DJF) precipitation **(upper left)**, near-surface temperature **(upper right)**, and total cloud cover **(lower left)** anomalies, as well as the 500 hPa wind speed during December 1983 – February 1984 **(lower right)**.

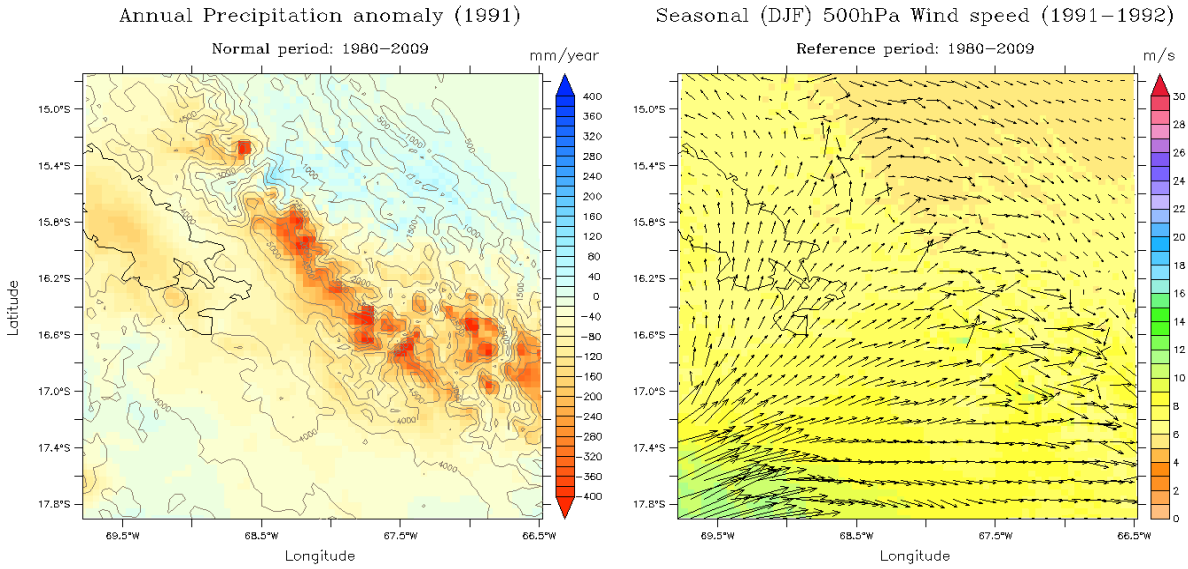

Figure 6.26: Annual total precipitation anomaly in 1991 **(left)**, and 500 hPa wind speed during December 1982 – February 1983 **(right)**.

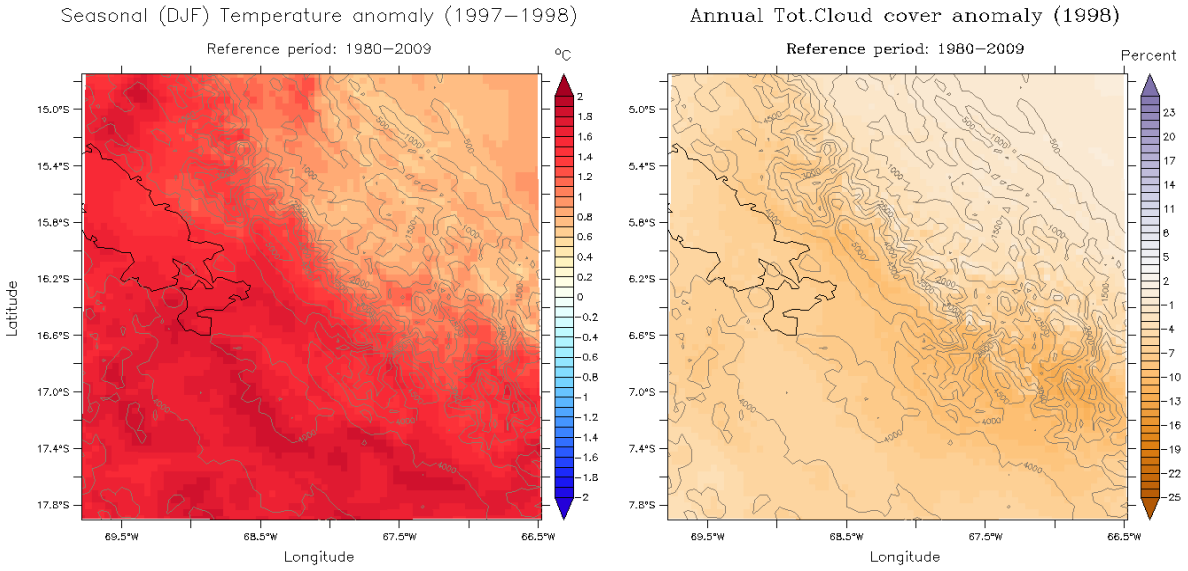

Figure 6.27: Summertime (DJF) precipitation anomaly **(left)** during December 1997– February 1998, and annual cloud cover anomaly in 1998 **(right)**.

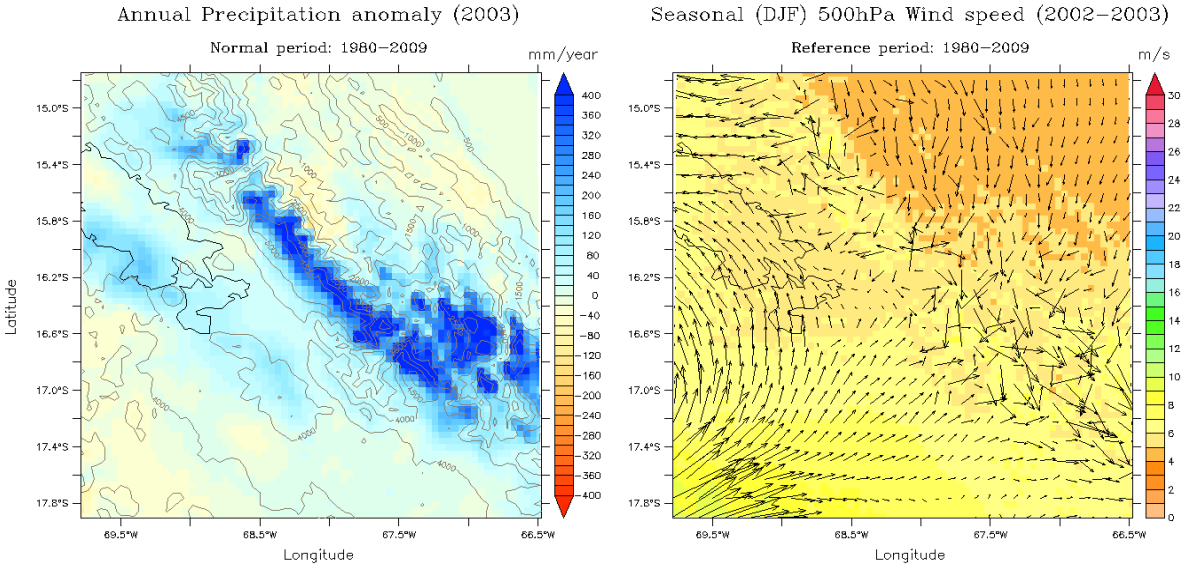

Figure 6.28: Annual total precipitation anomaly in 2003 **(left)**, and 500 hPa wind speed during December 2002 – February 2003 **(right)**.

6.4. Discussion and summary

In the previous Chapter, we found that MAR forced with the ERA-Interim reanalysis successfully simulates the seasonality of precipitation over the Altiplano and also properly accounts for the large-scale anomalies during important ENSO phases. Despite a quite systematic underestimation by approximately 50% of the annual total amounts of precipitation, the correlations between modeled monthly rates and the corresponding in situ observations are overall satisfactory. Therefore, we reasonably consider the MAR results as representative of the climate over the area covered by the ground observations. However, this area (i.e. the Altiplano) concerns only a limited portion of our MAR domain.

The modeled precipitation maps reveal a too strong dependence of precipitation and cloudiness to altitude, which leads to an overestimation of both parameters over the high summits of the Cordillera Real, whereas in the lower elevations of our study area the amounts of precipitation and cloudiness are by far underestimated. As we lack in situ observations to confirm this assertation, we rely on the scientific literature to infer that this dry bias is more severe to the east of the Cordillera Real than to the west. Indeed, since the eastern lowlands (i.e. the yungas) actually receive huge amounts of water vapor from the Amazon Basin, they should therefore be much more covered by clouds than the Altiplano, which experiences a drier climate due to the leeside effect of the Cordillera.

Near-surface temperature and specific humidity are overall well simulated by MAR, which faithfully reproduces the poor thermal seasonality, as well as the antagonism between the western dry Pacific and the eastern moist Amazonian air masses. The high resolution of MAR allows a detailed account of the regional mean atmospheric circulation over the Bolivian highlands.

The Chacaltaya Mountain is centrally located with respect to the two prevailing air masses, and thus benefits from both atmospheric conditions. Moreover, since the Chacaltaya lies just at the western rim of the simulated band of excessive precipitation, the modeled amounts of precipitation should thus be considered cautiously.

The trends between 1960 and 2014 show a significant decrease in precipitation and cloud cover. MAR has a largely positive short-wave cloud feedback, where low clouds dominate the cloud feedback. This means that the warming of the surface is rather enhanced by the reduced amount of low cloudiness, than it is mitigated by the reduced amount of high cloudiness. We suspect MAR to produce more low clouds than in reality, and we relate this discrepancy to the parameterization of the convection scheme, since MAR shows numerical instability for convective precipitation. However, there are no reliable observations to support this hypothesis.

The enhanced drying and warming trend of the upper troposphere with respect to the lower troposphere supports the theory of the intensification of the meridional overturning Hadley circulation, which might be responsible for the moistening of the inner tropics and the drying of the outer tropics.

For almost all those parameters, the changes were the most significant during the 1980s decade. More precisely, the Pacific Shift of 1977 started a 22 years long PDO warm phase during which several very strong El Niño events took place and brought unfavorable climatic conditions for tropical glaciers.

There is no general rule defining the behavior of the atmosphere during El Niño events. While the 1991-1992 El Niño was exclusively driven by a strong deficit in precipitation, the mega El Niño phase of 1997-1999 was characterized by excessive rates in both humidity and temperature.

Furthermore, the spatial distribution of the anomalies during ENSO events differs drastically between precipitation and temperature. While temperature anomalies are uniform throughout the study area, precipitation anomalies are highly contrasted at local and regional scales, and more particularly over the most rugged terrains.

The 1994-1995 El Niño constitutes an exception since the event is not reflected in the anomalies simulated by MAR. This can partly be explained by the strength of the local processes which control the climate in the Bolivian Andes, and which thus interfere with the ENSO signal. In addition, we suggest that other causes, possibly of non-climatic nature, could also be responsible for sudden strong ablation periods undergone by the Chacaltaya Glacier.

7. Conclusion and perspectives

7.1. Sources of uncertainty

This study firstly aimed to evaluate the accuracy and skill of the MAR model in reproducing the spatial climate variability over the Bolivian tropical Andes. Nevertheless, when discussing the performance of a model for a specific climatic context, it should always be remembered that climate models can only be partially validated, and that model results are thus inevitably tainted by a certain degree (sometimes high) of uncertainty. In this section, we summarize the main modeling issues we encountered through our study, and we provide several insights for improving the use of MAR over tropical latitudes.

7.1.1. In situ meteorological observations

Availability The available climatic observational network in South America is very poor compared to other continents, and is hence by far insufficient to accurately monitor and document the rapid and local climatic changes taking place in the tropical Andes. More particularly, there is a crucial need for in situ observations at the highest elevation sites, where tropical glaciers are found and where changes are thus likely to be more dramatic than at lower elevations.

Quality The LACA&D authors emphasized the unreliability of the temperature observations stemming from ground weather stations in Bolivia. Working with observations of dubious quality makes it hard to draw reliable conclusions from comparisons between model and data. In contrast, most of the precipitation time series successfully passed the homogeneity tests applied to the data collected by LACA&D. However, the little meta-information (if there is any) provided by the data providers allows no assessment of the environmental context in which the weather instruments are installed. In mountainous terrains such as the Andes, the microclimatic conditions may alter the observations significantly. A very common issue is the undercatch of precipitation (especially snowfall) by the rain gauges, mainly due to wind turbulences, and which leads to underestimated rates of precipitation.

Both low availability and poor quality of observational data had major implications on our study.

(i) Impact on the reanalyses Since they are outputs from GCMs in which observations are assimilated, reanalysis data sets are less reliable in the parts of the world where in situ observations are scarce. In our case, the NCEP/NCAR-v2 reanalysis turned out to be totally inefficient to represent the regional mean atmospheric circulation over our study area. Even with the ERA-Interim reanalysis, which we used in our final simulations, we had to apply strong corrections with respect to temperature and humidity to obtain satisfactory results with MAR.

(ii) Consequences for the MAR evaluation Since the only ground stations available in our study area are almost all located in the Altiplano, within a range of altitude barely exceeding 4,000 meters a.s.l., they provide a very limited representativeness of the Bolivian contrasted climates. In addition, the weather station located in the Cordillera Real lies at the bottom of a narrow valley, and fails thus to be representative of its surrounding mountain peaks. It is important to remember that although MAR matches the observations at the locations of the stations, it does not necessarily validate its performance for locations situated in a different topographic context. When comparing simulations to the scientific literature, we see indeed that MAR provides less realistic results to the east of the Cordillera Real, and that the biases increase with decreasing altitude (and also decreasing distance from the lateral boundaries).

7.1.2. Model performance and insufficiencies

7.1.2.1. Model resolution

Although the high resolution of MAR allows to accurately represent the mean regional atmospheric circulation over our area of interest, a 5 km model grid turns out to be still too coarse to adequately resolve the extremely uneven topography of the Andes. Climatic conditions in mountainous terrains exhibit considerable spatial variability due to strong local effects. The geometry of the site, which includes altitude, exposure and slope steepness, has a crucial role in the distribution of temperature, humidity, precipitation and is also responsible for local wind regimes. Narrow valleys and peaks of inferior dimension of the model spatial resolution are smoothed away by the model grid, and only the main features of the relief are explicitely represented. Therefore, precipitation biases resulting from the elevation biases between model and data could not be avoided without enhancing the spatial resolution of MAR.

Besides, in the specific case of the Chacaltaya Glacier, the corresponding surface variables simulated by MAR belong to the 5 km grid pixel centered on the Chacaltaya Mountain summit. As the size of the glacier was largely inferior to 5 km² (in 1940 its extent was only of 0.22 km²), these variables can not reflect the exact conditions (in particular slope and solar exposure) experienced by the glacier surface; they provide rather a mean state of the glacier and its non-glaciated surroundings. To study (for instance) the evolution of albedo at the glacier surface in relation with precipitation and aerosols, a finer spatial resolution is required.

7.1.2.2. Model parameterization

It seems relevant to mention that of all the RCMs that have been implemented over South America so far, none was initially developed to study this continent. MAR makes no exception to the rule, since it was originally designed for process studies in the polar regions. A consequence of this is that the parameterizations and approximations of the model may no longer be valid once applied to tropical climates.

Convective adjustement Since the nature of precipitation is mainly convective in our study area, as it is typically the case under tropical latitudes, our MAR simulations are highly sensitive to the

parameterization of convection and subgrid-scale clouds. The parameterization of convective clouds belongs to one of the greatest challenges in climate modeling and is usually a source of considerable uncertainty.

The deficiencies in the representation of convective clouds may lead to significant biases in precipitation and radiative fluxes, which in our case are key parameters for climate and glacier variability. We indeed detected a numerical instability in our model when analysing the spatial distribution of convective precipitation. Moreover, we also suspect that MAR fails to produce enough clouds over the northeastern part of the integration domain. Two direct consequences of a negative bias in cloudiness would be an underestimation of downward long-wave radiation, and an overestimation of incoming short-wave radiation. However, we lack local observations to support this hypothesis. Satellite-based observations are available at too coarse resolutions to be used to this end. For a strongly contrasted climatic context like the Bolivian Andes, there is a crucial need for high resolution observations.

Finally, it would be interesting to further investigate the sensitivity of our model to several convective schemes applied at very high resolutions over the tropical Andes. The convective scheme used here was initially developed by Bechtold (Bechtold *et al.*, 2001) for spatial resolutions of 10–200 km over temperate climates.

7.2. Further investigation topics

The final purpose of this work was to assess, with the help of MAR, the long-term evolution of the key parameters which allegedly drive the mass and energy balance of outer tropical glaciers. We found that precipitation and cloud cover underwent the most significant changes, as they both decreased by about 35% between 1960 and 2014. The reduced cloudiness also directly affected the radiation budget. Meanwhile, temperature increased at a rate consistent with the outcomes of previous studies (Vuille *et al.*, 2008). Anomalies in those parameters occurred more frequently and intensely during the warm PDO phase between 1977 and 1999, which attests the relevance of accounting for the large-scale variability of the atmosphere-ocean system when studying the climate change in the tropical Andes. Nevertheless, the spatial heterogeneity of the ENSO signal across the Bolivian Andes, combined with the absence of El Niño anomalies during short periods of strong negative mass balance in the Chacaltaya Glacier, both imply that additional processes might also have played a role in the rapid recession of the glacier.

Therefore, we complete the last chapter of this study with several suggestions for further investigations that might be interesting to carry out in the light of the ongoing climate changes altering the tropical cryosphere.

7.2.1. Changes in the tropical large-scale atmospheric circulation

Our results partly corroborate the assumption made by recent works (e.g. Chen *et al.*, 2002) that a strengthening of the meridional overturning circulation (i.e. the Hadley cell) is currently causing a moistening of the inner tropics and a drying of the outer tropics. According to other studies

(Vecchi *et al.*, 2006; Vecchi & Soden, 2007), changes in the large-scale atmospheric circulation also concern the zonal asymmetric overturning circulation (i.e. the Walker cell), which by contrast is rather weakening and thereby altering the tropical circulation toward more El Niño-like conditions.

To further examine these assumed changes, long-term (50 years) simulations should be run over South America between the latitudes of 1°S and 30°S. RCMs should be preferred over GCMs in order to properly account for the deflecting effect of the Andes mountains on the regional winds. A model such as MAR could be very useful for this purpose, since it allows various spatial resolutions and also contains enough vertical levels to study in detail the vertical profile of the upper, middle and lower troposphere.

7.2.2. The impact of aerosols

Aerosols have been mentioned in section 2.2.3 (Chapter 2) as agents intervening in the energy balance of tropical glaciers. On the one hand, atmospheric aerosols enhance the greenhouse effect by intercepting the infrared radiation released by the earth's surface and by re-emitting it toward the ground. On the other hand, aerosols particles decrease the albedo of the glaciers surface when they are deposited on them, which in turn increases the capacity of glaciers to absorb solar radiation and causes them to melt faster than usual. Furthermore, aerosols also affect the atmospheric hydrological cycle by modulating the development of convective clouds and precipitation (Tao *et al.*, 2012).

Airborne aerosols are mostly produced by natural processes, such as volcanic eruptions and biomass burning. In South America however, anthropogenic activities are probably more contributing to aerosol production than in many other parts of the world. More particularly, the deforestation of the Amazonian forest is thought to release massive amounts of biogenic aerosols in the atmosphere (Andrade *et al.*, 2012). The Bolivian Altiplano is even more concerned by high aerosols loads, because of the smog produced by the two important cities La Paz and El Alto.

Owing to their lifetime of several weeks, and due to the deep convective activity which introduces them into the free troposphere, atmospheric aerosols over the Altiplano can be transported over very long distances, and thus impact climate at a nearly global scale. Nevertheless, glaciers located in the neighborhood of the aerosols sources, like the Chacaltaya, are inevitably the most impacted.

In December 2011, the Astrophysical Observatory (*Instituto de Investigaciones Físicas*) station, established since 1942 at the Chacaltaya Mountain (5,240 meters a.s.l.), was equipped with new instruments under the initiative of the Global Atmosphere Watch (GAW). Since 2012, the Chacaltaya GAW Station provides detailed information about the composition of the middle and upper troposphere, including measurements of GHG concentration, as well as aerosol microphysical, optical, hygroscopic and chemical properties. Also in 2012, an Automatic Weather Station (AWS) was installed at 5,380 meters a.s.l. in the northwestern ridge of Mount Chacaltaya. In the future, these observations will deliver precious information about the evolution of the climate at a high elevation site (> 5,000 meters a.s.l.), which will be very useful to constrain both climate and chemistry-transport models (Andrade *et al.*, 2012).

7.2.3. Model projections for future water resource management

Andean glaciers constitute the main source of freshwater for the countries along the western coast of South America. In the semi-desertic regions such as the Altiplano, local indigenous populations rely almost entirely upon those high-altitude water resources to complement rainfall during the dry season (Bradley *et al.*, 2006). These communities need freshwater for self consumption, but also for agriculture, which is well developed around Lake Titicaca. Moreover, many large cities like La Paz and El Alto use hydropower as a major energy source for electricity production.

The increasing stress on glacier-fed water resources is furthermore exacerbated by the global trend of demographic growth and associated urbanization, to which Bolivia makes no exception. As a consequence, there is an urgent need to secure sufficient water supplies for those growing urban centers (Buytaert & De Bièvre, 2012).

With the help of high resolution RCMs using the IPCC scenarios as forcings, future projections of climate change could be performed to anticipate the changes in tropical Andean glaciers and associated runoff.

References

Alves L. M., & Marengo J. (2010). Assessment of regional seasonal predictability using the PRECIS regional climate modeling system over South America. *Theoretical and Applied Climatology*, *100*(3-4), pp. 337-350.

Andrade M., Laj P., Wiedensohler A., Bonasoni P., Ramonet M., Krejci R., Sellegri K., Weingartner E., Whiteman D., Ginot P., Zaratti, F. (2012). First atmospheric observations from the high altitude Chacaltaya GAW station (Bolivia - 5200 m). *EGU General Assembly Conference Abstracts*, *14*, p. 10350.

Bechtold P., Bazile E., Guichard F., Mascart P., Richard E. (2001). A mass-flux convection scheme for regional and global models. *Quarterly Journal of the Royal Meteorological Society*, *127*(573), pp. 869-886.

Bellprat O., Kotlarski S., Lüthi D., Schär C. (2012). Objective calibration of regional climate models. *Journal of Geophysical Research: Atmospheres (1984–2012)*, *117*(D23).

Bradley R. S., Keimig F. T., Diaz H. F., Hardy D. R. (2009). Recent changes in freezing level heights in the Tropics with implications for the deglacierization of high mountain regions. *Geophysical Research Letters*, *36*(17).

Brun E., David, P., Sudul, M., & Brunot, G. (1992). A numerical model to simulate snow-cover stratigraphy for operational avalanche forecasting. *Journal of Glaciology*, *38*, pp. 13-22.

Casassa G., Haeberli W., Jones G., Kaser G., Ribstein P., Rivera A., Schneider, C. (2007). Current status of Andean glaciers. *Global and Planetary Change*, *59*(1), pp. 1-9.

Chen J., Carlson B. E., Del Genio A. D. (2002). Evidence for strengthening of the tropical general circulation in the 1990s. *Science*, *295*(5556), pp. 838-841.

Chevallier P., Pouyaud B., Suarez W., Condom T. (2011). Climate change threats to environment in the tropical Andes: glaciers and water ressources. *Regional Environmental Change*, *11*(1), pp.179-187.

Coudrain A., Francou B., Kundzewicz Z. W. (2005). Glacier shrinkage in the Andes and consequences for water ressources – Editorial. *Hydrological Sciences Journal*, *50*(6), pp. 925-932.

Curtis S., & Hastenrath S. (1999). Long-term trends and forcing mechanisms of circulation and climate in the equatorial Pacific. *Journal of Climate*, *12*(4), pp. 1134-1144.

De Ridder K., & Gallée H. (1998). Land surface-induced regional climate change in southern Israel. *Journal of Applied Meteorology*, *37*(11), pp. 1470-1485.

Dee D. P., Uppala S. M., Simmons A. J., Berrisford P., Poli P., Kobayashi S., ... ,Vitart F. (2011). The ERA-Interim reanalysis: Configuration and performance of the data assimilation system. *Quarterly Journal of the Royal Meteorological Society*, *137*(656), pp. 553-597.

Duynkerke P. G. (1988). Application of the E-ε turbulence closure model to the neutral and stable atmospheric boundary layer. *Journal of the Atmospheric Sciences*, *45*(5), pp. 865-880.

Favier V., Wagnon P., Ribstein P. (2004). Glaciers of the outer and the inner tropics: A different behaviour but a common response to climatic forcing. *Geophysical Research Letters*, *31*(16), pp. 1-5.

Fernandez J. P. R., Franchito S. H., Rao V. B. (2006). Simulation of the summer circulation over South America by two regional climate models. Part I: Mean climatology. *Theoretical and Applied Climatology*, *86*(1-4), pp. 247-260.

Fettweis X. (2006). *Reconstruction of the 1979-2005 Greenland ice sheet surface mass balance using satellite data and the regional climate model MAR* (Doctoral dissertation, Université Catholique de Louvain). Retrieved from *http://hdl.handle.net/2268/36720*

Fettweis X. (2007). Reconstruction of the 1979-2006 Greenland ice sheet surface mass balance using the regional climate model MAR. *The Cryosphere Discussions*, *1*(1), pp. 123-168.

Francou B., Ramirez E., Cáceres B., Mendoza J. (2000). Glacier evolution in the tropical Andes during the last decades of the 20th century: Chacaltaya, Bolivia, and Antizana, Ecuador. *AMBIO: A Journal of the Human Environment*, *29*(7), pp. 416-422.

Francou B., Vuille M., Wagnon P., Mendoza J., Sicart J. E. (2003). Tropical climate change recorded by a glacier in the central Andes during the last decades of the twentieth century: Chacaltaya, Bolivia, 16°S. *Journal of Geophysical Research: Atmospheres (1984–2012)*, 108(D5), p. 4154.

Francou B., Ribstein P., Wagnon P., Ramirez E., Pouyaud B. (2005). Glaciers of the tropical Andes: indicators of global climate variability. *Global change and mountain regions*, pp. 197-204.

Fund W. (2014). Bolivian Yungas. Retrieved from *http://www.eoEarth.org/view/article/150721*

Gallée H. (1995). Simulation of the mesocyclonic activity in the Ross Sea, Antarctica. *Monthly Weather Review*, *123*(7), pp. 2051-2069.

Gallée H., & Schayes G. (1994). Development of a three-dimensional meso-γ primitive equation model: katabatic winds simulation in the area of Terra Nova Bay, Antarctica. *Monthly Weather Review*, *122*(4), pp. 671-685.

Garreaud R. (2000). Cold air incursions over subtropical South America: Mean structure and dynamics. *Monthly Weather Review*, *128*(7), pp. 2544-2559.

Garreaud R., & Aceituno P. (2001). Interannual rainfall variability over the South American Altiplano. *Journal of Climate*, *14*(12), pp. 2779-2789.

Garreaud R., Vuille M., Clement A. C. (2003). The climate of the Altiplano: observed current conditions and mechanisms of past changes. *Palaeogeography, palaeoclimatology, palaeoecology*, *194*(1), pp. 5-22.

Garreaud R. D., Vuille M., Compagnucci R., Marengo J. (2009). Present-day south american climate. *Palaeogeography, Palaeoclimatology, Palaeoecology*, *281*(3), pp. 180-195.

Gioda A., & Prieto M. D. R. (1999). Histoire des sécheresses Andines; Potosi, El Niño et le petit âge glaciaire.

Giorgi F. (2011). *Regional Climate Modeling: Lecture I* [Powerpoint slides].
Retrieved from *http://www.to.isac.cnr.it/aosta_old/aosta2011/LecturesSeminars/giorgi1-2.pdf*

Hardy D. R., Vuille M., Braun C. R., Keimig F. R., Bradley R. S. (1998). Annual and daily meteorological cycles at high altitude on a tropical mountain. *Bulletin of the American Meteorological Society*, *79*(9), pp. 1899-1913.

Hastenrath S. (1991). Climate Dynamics of the Tropics. Atmospheric Sciences Library, 8.

Insel N., Poulsen C. J., Ehlers T. A. (2010). Influence of the Andes Mountains on South American moisture transport, convection, and precipitation. *Climate Dynamics*, *35*(7-8), pp. 1477-1492.

Jeschke M. L. (2009). Glacier Retreat in the Bolivian Andes as a Consequence of Global Climate Change. *Impacts on regional water supply according to the simulation of future runoff from Zongo Glacier*, pp. 1-55.

Jomelli V., Favier V., Rabatel A., Brunstein D., Hoffmann G., Francou B. (2009). Fluctuations of glaciers in the tropical Andes over the last millennium and palaeoclimatic implications: A review. *Palaeogeography, Palaeoclimatology, Palaeoecology*, *281*(3), pp. 269-282.

Kaser G. (1999). A review of the modern fluctuations of tropical glaciers. *Global and Planetary Change*, *22*(1), pp. 93-103.

Kaser G. (2001). Glacier-climate interaction at low latitudes. *Journal of Glaciology*, *47*(157), pp. 195-204.

Kotlarski S. (2014). *Validation of Regional Climate Models* [Powerpoint slides]. Retrieved from *http://www.iac.ethz.ch/people/svenk/kotlarski_VALUEtrainingschool_trieste_nov2014_topdf.pdf*

Lang C. (2011). Modeling of the surface mass balance in Svalbard with the regional climate model MAR over 1958-2010 (Master's Thesis, Université de Liège). Retrieved from *http://hdl.handle.net/2268/158867*

Lange S., Rockel B., Volkholz J., Bookhagen B. (2014). Regional climate model sensitivities to parametrizations of convection and non-precipitating subgrid-scale clouds over South America. *Climate Dynamics*, *44*(9-10), pp. 2839-2857.

Lefebre F., Gallée H., Van Ypersele J. P., Greuell W. (2003). Modeling of snow and ice melt at ETH Camp (West Greenland): A study of surface albedo. *Journal of Geophysical Research: Atmospheres (1984–2012)*, *108*(D8).

Lefebre F., Fettweis X., Gallée H., Van Ypersele J. P., Marbaix P., Greuell W., Calanca P. (2005). Evaluation of a high-resolution regional climate simulation over Greenland. *Climate dynamics*, *25*(1), pp. 99-116.

Lejeune Y., L'Hôte Y., Chevallier P. (2003). Instrumentation et constitution d'une base de données météorologiques et nivologiques dans les Andes; Station Charquini, 4795 m, Bolivie. *Météo-France/CNRM, Note de Centre*, *21*, 63 p.

Lejeune Y., Bouilloud L., Etchevers P., Wagnon P., Chevallier P., Sicart J. E., … , Habets F. (2007). Melting of snow cover in a tropical mountain environment in Bolivia: Processes and modeling. *Journal of Hydrometeorology*, *8*(4), pp. 922-937.

Lenters J. D., & Cook K. H. (1997). On the origin of the Bolivian high and related circulation features of the South American climate. *Journal of the Atmospheric Sciences*, *54*(5), pp. 656-678.

Lenters J. D., & Cook K. H. (1999). Summertime precipitation variability over South America: Role of the large-scale circulation. *Monthly Weather Review*, *127*(3), pp. 409-431.

Liebmann B., Kiladis G. N., Marengo J., Ambrizzi T., Glick J. D. (1999). Submonthly convective variability over South America and the South Atlantic convergence zone. *Journal of Climate*, *12*(7), pp. 1877-1891.

Marbaix P., Gallée H., Brasseur O., Van Ypersele J. P. (2003). Lateral boundary conditions in regional climate models: a detailed study of the relaxation procedure. *Monthly weather review*, *131*(3), pp. 461-479.

Mark B. G. (2008). Tracing tropical Andean glaciers over space and time: Some lessons and transdisciplinary implications. *Global and Planetary change*, *60*(1), pp. 101-114.

Martínez R., Ruiz D., Andrade M., Blacutt L., Pabón D., Jaimes E., Pabón, Ena Jaimes, Gloria León, Villacís M., Quintana J., Montealegre E., Euscátegui C. (2011). Synthesis of the Climate of the Tropical Andes. *Climate Change and Biodiversity in the Tropical Andes*, pp. 97-109.

Ménégoz M., Gallée H., Krinner G., Delaygue G. (2014). *LMDz avec la physique du modèle MAR* [Powerpoint slides]. Retrieved from *http://lmdz.lmd.jussieu.fr/le-projet-lmdz/reunion-utilisateurs/2014/presentations/Delaygue.pdf*

Mölg T. (2009). *Tropical glaciers: Atmospheric Forcings (mass and energy balance) and Large-Scale Linkages* [Lecture notes]. University of Innsbruck. Retrieved from: *https://www.projects.science.uu.nl/iceclimate/karthaus/2009/more/lecturenotes/ThomasMoelg.pdf*

Morcrette J. J. (2002). The surface downward longwave radiation in the ECMWF forecast system. *Journal of climate*, *15*(14), pp. 1875-1892.

Nicolini M., Salio P., Katzfey J. J., McGregor J. L., Saulo A. C. (2002). January and July regional climate simulation over South America. *Journal of Geophysical Research: Atmospheres (1984–2012)*, *107*(D22), ACL-12.

Oerlemans J. (2001). Glaciers and climate change: a meteorologist's view. *Journal of Glaciology*, *48*, 173 p.

Pesquero J. F., Chou S. C., Nobre C. A., Marengo J. A. (2010). Climate downscaling over South America for 1961–1970 using the Eta Model. *Theoretical and applied climatology*, *99*(1-2), pp. 75-93.

Rabatel A. (2005). *Chronologie et interprétation paléoclimatique des fluctuations des glaciers dans les Andes de Bolivie (16 S) depuis le maximum du Petit Age Glaciaire (17ème siècle)* (Doctoral dissertation, Université Joseph Fourier – Grenoble I).

Rabatel A., Machaca A., Francou B., Jomelli V. (2006). Glacier recession on Cerro Charquini (16 S), Bolivia, since the maximum of the Little Ice Age (17th century). *Journal of Glaciology*, *52*(176), pp. 110-118.

Rabatel A., Francou B., Jomelli V., Naveau P., Grancher D. (2008). A chronology of the Little Ice Age in the tropical Andes of Bolivia (16 S) and its implications for climate reconstruction. *Quaternary Research*, *70*(2), pp. 198-212.

Rabatel A., Francou B., Soruco A., Gomez J., Cáceres B., Ceballos J. L., Basantes R., Vuille M., Huggel C., Scheel M., Lejeune Y., Arnaud Y., Condom T., Consoli G., Favier V., Jomelli V., Galarraga R., Ginot P., Maisincho L., Mendoza J., Ménégoz M., Ramirez E., Ribstein P., Suarez W., Villacis M., Wagnon P. (2013). Current state of glaciers in the tropical Andes: a multi-century perspective on glacier evolution and climate change. *The Cryosphere*, 7(1), pp. 81-102.

Ramirez E., Francou B., Ribstein P., Descloitres M., Guerin R., Mendoza J., Gallaire R., Pouyaud B., Jordan, E. (2001). Small glaciers disappearing in the tropical Andes: a case-study in Bolivia: Glaciar Chacaltaya (16 S). *Journal of Glaciology*, *47*(157), pp. 187-194.

Rangecroft S., Harrison S., Anderson K., Magrath J., Castel A. P., Pacheco P. (2013). Climate change and water resources in arid mountains: an example from the Bolivian Andes. *Ambio*, *42*(7), pp. 852-863.

Rangecroft S., Harrison S., Anderson K. (2015). Rock glaciers as water stores in the Bolivian Andes: an assessment of their hydrological importance. *Arctic, Antarctic, and Alpine Research*, *47*(1), pp. 89-98.

Remedio A., Grassl H., Jacob D. (2013). *Connections of low level jets and mesoscale convective systems in South America* (Doctoral dissertation, Universität Hamburg, Hamburg).

Ribstein P., Tiriau E., Francou B., Saravia R. (1995). Tropical climate and glacier hydrology: a case study in Bolivia. *Journal of Hydrology*, *165*(1), pp. 221-234.

Ribstein P., Pouyaud B., Sicart J. E., Wagnon P., Ramirez E., Francou B. (1999). Variabilité climatique et fonctionnement hydrologique d'un glacier tropical. Comité National Français de Géodésie et Géophysique, Rapport Quadriennal, 1995–1998, Section 6, pp. 279-287.

Ribstein P. (2002). *Climat et glaciers des Andes tropicales: impacts hydrologiques* ("Habilitation à Diriger des Recherches: Géosciences et Ressources Naturelles", Université Pierre et Marie Curie: Paris). Retrieved from: *http://www.documentation.ird.fr/hor/fdi:010053258*

Roche M. A., Aliaga A., Campos J., Pena J., Cortes J., Rocha N. (1990). Hétérogénéité des précipitations sur la cordillère des Andes boliviennes. *Hydrology in Mountainous Regions. Hydrological Measurements; the Water Cycle. IAHS*, *193*, pp. 381-388.

Seiler C., Hutjes R. W., Kabat P. (2013). Climate variability and trends in Bolivia. *Journal of Applied Meteorology and Climatology*, *52*(1), pp. 130-146.

Sicart J. E., Hock R., Six D. (2008). Glacier melt, air temperature, and energy balance in different climates: The Bolivian Tropics, the French Alps, and northern Sweden. *Journal of Geophysical Research: Atmospheres (1984–2012)*, *113*(D24).

Soriano C., Jorba O., Baldasano J. M. (2002). One-way nesting versus two-way nesting: does it really make a difference?. *Air Pollution Modeling and its Application XV,* pp. 177-185. Springer US.

Soruco A. (2008). *Etude du retrait des glaciers depuis cinquante ans dans les bassins hydrologiques alimentant en eau la ville de La Paz – Bolivie (16°S)* (Doctoral dissertation, Université Joseph Fourier – Grenoble I).

Soruco A., Vincent C., Francou B., Gonzalez J. F. (2009a). Glacier decline between 1963 and 2006 in the Cordillera Real, Bolivia. *Geophysical Research Letters*, *36*(3).

Soruco A., Vincent C., Francou B., Ribstein P., Berger T., Sicart J. E., Wagnon P., Arnaud Y., Favier V., Lejeune, Y. (2009b). Mass balance of Glaciar Zongo, Bolivia, between 1956 and 2006, using glaciological, hydrological and geodetic methods. *Annals of Glaciology*, *50*(50), pp. 1-8.

Soruco A., Vincent C., Rabatel A., Francou B., Thibert E., Sicart J. E., Condom T. (2015). Contribution of glacier runoff to water resources of La Paz city, Bolivia (16 S). *Annals of Glaciology*, *56*(70), pp. 147-154.

Tao W. K., Chen J. P., Li Z., Wang C., Zhang C. (2012). Impact of aerosols on convective clouds and precipitation. *Reviews of Geophysics*, *50*(2).

Todd M. C., Washington R., James T. (2003). Characteristics of summertime daily rainfall variability over South America and the South Atlantic Convergence Zone. *Meteorology and Atmospheric Physics*, *83*(1-2), pp. 89-108.

UNEP (United Nations Environment Programme). (2013). Where will the water go? Impacts of accelerated glacier melt in the Tropical Andes. Retrieved from: *http://na.unep.net/geas/getUNEPPageWithArticleIDScript.php?article_id=104*

Vecchi G. A., Soden B. J., Wittenberg A. T., Held I. M., Leetmaa A., Harrison M. J. (2006). Weakening of tropical Pacific atmospheric circulation due to anthropogenic forcing. *Nature*, *441*(7089), pp. 73-76.

Vecchi G. A., & Soden B. J. (2007). Global warming and the weakening of the tropical circulation. *Journal of Climate*, *20*(17), pp. 4316-4340.

Vera C., Baez J., Douglas M., Emmanuel C. B., Marengo J., Meitin J., Nogues-Paegle J., Paegle J., Penalba O., Salio P., Saulo C., Silva Dias M. A., Silva Dias P., Zipser, E. (2006). The South American low-level jet experiment. *Bulletin of the American Meteorological Society*, *87*(1), pp. 63-77.

Vincent C., Ribstein P., Favier V., Wagnon P., Francou B., Le Meur E., Six D. (2005). Glacier fluctuations in the Alps and in the tropical Andes. *Comptes Rendus Geoscience*, *337*(1), pp. 97-106.

Vuille M. (1999). Atmospheric circulation over the Bolivian Altiplano during dry and wet periods and extreme phases of the Southern Oscillation. *International Journal of Climatology*, *19*(14), pp. 1579-1600.

Vuille M., & Bradley R. S. (2000). Mean annual temperature trends and their vertical structure in the tropical Andes. *Geophysical Research Letters*, *27*(23), pp. 3885-3888.

Vuille M., Bradley R. S., Keimig F. T. (2000). Interannual climate variability in the Central Andes and its relation to tropical Pacific and Atlantic forcing. *Journal of Geophysical Research-Atmostpheres*, *105*(D10), pp. 12447-12460.

Vuille M., Hardy D.R., Braun C., Keimig F.T., Bradley R. S. (2001). Climate variability on intraseasonal to interannual timescales on the Bolivian Altiplano with special emphasis on the Nevado Sajama region. *Ecologia en Bolivia - Revista del Instituto de Ecologia*, *35*, pp. 17-40.

Vuille M., Bradley R. S., Werner M., Keimig F. (2003). 20th century climate change in the tropical Andes: observations and model results. *Climate Variability and Change in High Elevation Regions: Past, Present & Future*, *59*, pp. 75-99.

Vuille M., Francou B., Wagnon P., Juen I., Kaser G., Mark B. G., Bradley R. S. (2008). Climate change and tropical Andean glaciers: Past, present and future. *Earth-Science Reviews*, *89*(3), pp. 79-96.

Wagnon, P. (1999). *Analyse du bilan d'energie d'un glacier tropical application a la relation glacier-climat* (Doctoral dissertation, Université Joseph Fourier – Grenoble I).

Wagnon P., Ribstein P., Kaser G., Berton P. (1999a). Energy balance and runoff seasonality of a Bolivian glacier. *Global and planetary change*, *22*(1), pp. 49-58.

Wagnon P., Ribstein P., Francou B., Pouyaud B. (1999b). Annual cycle of energy balance of Zongo glacier, Cordillera Real, Bolivia. *Journal of Geophysical Research: Atmospheres (1984–2012)*, *104*(D4), pp. 3907-3923.

Wagnon P., Ribstein P., Francou B., Sicart J. E. (2001). Anomalous heat and mass budget of Glaciar Zongo, Bolivia, during the 1997/98 El Nino year. *Journal of Glaciology*, *47*(156), pp. 21-28.

WGMS (World Glacier Monitoring Service). (2011). Glacier Mass Balance Bulletin No. 11 (2008–2009). Zemp M., Nussbaumer S. U., Gärtner-Roer I., Hoelzle M., Paul F., Haeberli W. (eds.), ICSU(WDS)/IUGG(IACS)/UNEP/UNESCO/WMO, World Glacier Monitoring Service, Zurich, Switzerland, 102 p.

Yu L., Zhang Z., Zhou M., Zhong S., Lenschow D.H., Hsu H.-M., Wu H., Sun B. (2010). Validation of ECMWF and NCEP-NCAR reanalysis data in Antarctica. *Advances in Atmospheric Sciences*, *27*, pp. 1151-1168.

Zhang Y., Wallace J. M., Battisti D. S. (1997). ENSO-like interdecadal variability: 1900-93. *Journal of climate*, *10*(5), pp. 1004-1020.

Zhong Z., Wang X., Lu W., Hu Y. (2010). Further study on the effect of buffer zone size on regional climate modeling. *Climate dynamics*, *35*(6), pp. 1027-1038.

Climatic data sets references

ERA40 and ERA-Interim Reanalysis data retrieved from:
European Centre for Medium-Range Weather Forecasts (ECMWF)
http://apps.ecmwf.int/datasets/data/interim-full-daily/

NCEP/NCAR-v2 Reanalysis data retrieved from:
National Oceanic and Atmospheric Administration (NOAA) | Earth System Research Laboratory (ESRL) | Physical Sciences Division (PSD)
http://www.esrl.noaa.gov/psd/data/gridded/data.ncep.reanalysis2.html

Monthly observational data from ground weather stations in Bolivia retrieved from:
The Latin American Climate Assessment & Dataset (LACA&D)
http://lacad.ciifen.org/

"Monthly Climatic Data for the World"
Sponsored by World Meteorological Organisation (WMO)
Published by National Climatic Data Center (NCDC)
Retrieved from: NCDC – Image and Publications System (IPS)
http://www.ncdc.noaa.gov/IPS/

Other references

NASA Earth Observatory
http://Earthobservatory.nasa.gov/

The Chacaltaya GAW Station
http://www.chacaltaya.edu.bo/

"Algorithm Theoretical Basis Document"
Published by the European Climate Assessment & Dataset (ECA&D)
http://lacad.ciifen.org/documents/atbd.pdf

Annexes

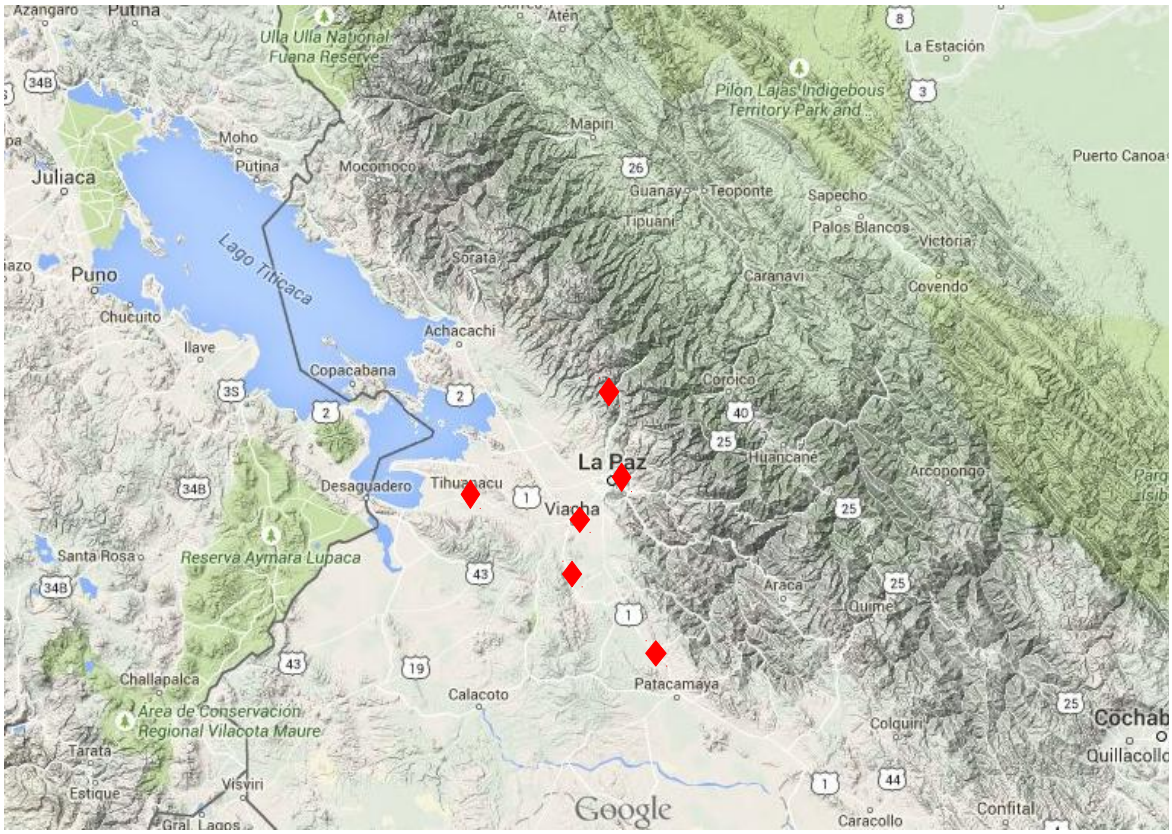

Figure 1: Topography of the study area. Each red point indicates the presence of a weather station. Source: *Google Maps (2015)*

Figure 2: Approximate location of the Ayo Ayo weather station.
Source: *Google Maps (2015)*

Figure 3: Approximate location of the Collana weather station.
Source: *Google Maps (2015)*

Figure 4: Approximate location of the Huarina Cota Cota weather station.
Source: *Google Maps (2015)*

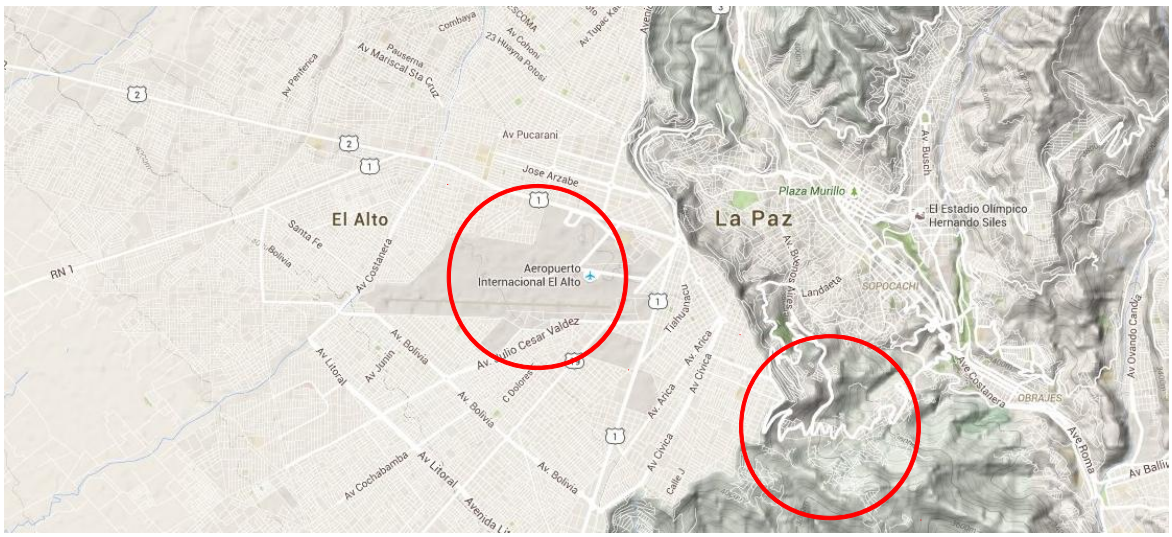

Figure 5: Approximate location of the El Alto (left circle) and La Paz (right circle) weather stations. Source: *Google Maps (2015)*

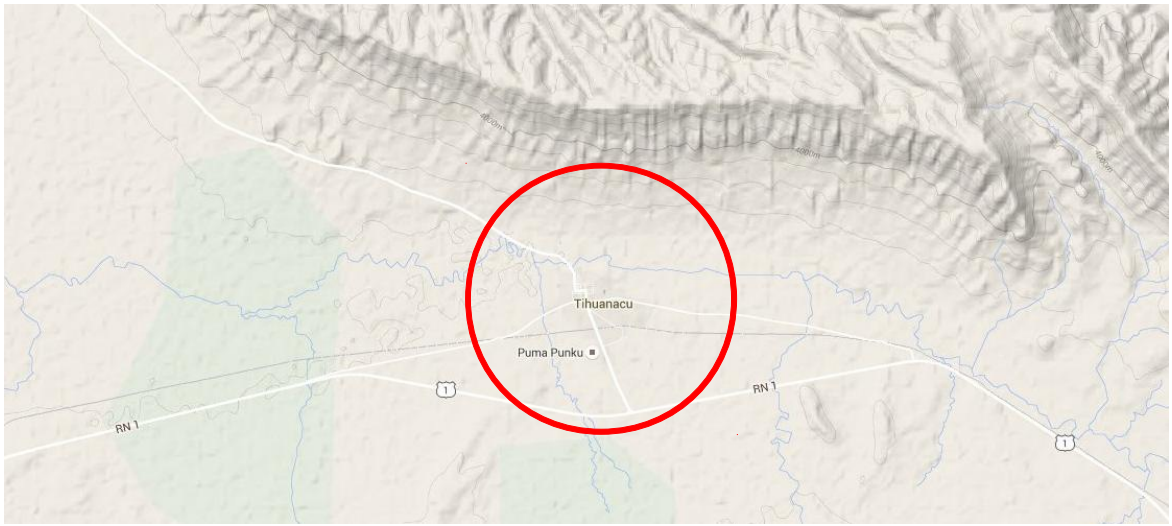

Figure 6: Approximate location of the Tiawuanacu weather station.
Source: *Google Maps (2015)*

Figure 7: Approximate location of the Viacha weather station.
Source: *Google Maps (2015)*